ELECTRONIC PROPERTIES OF MODIFIED GALLIUM ARSENIDE SURFACES AND INTERFACES

A THESIS
SUBMITTED TO THE
UNIVERSITY OF POONA

FOR THE DEGREE OF
DOCTOR OF PHILOSOPHY
IN PHYSICS

BY

Ms. VARDHIREDDY MANORAMA
M.Sc., M.Phil.

DEPARTMENT OF PHYSICS
UNIVERSITY OF POONA
PUNE - 411 007
INDIA

DECEMBER 1989

CERTIFICATE

Certified that the work incorporated in this thesis entitled "ELECTRONIC PROPERTIES OF MODIFIED GALLIUM ARSENIDE SURFACES AND INTERFACES" by Ms. VARDHIREDDY MANORAMA was carried out by the candidate under our supervision. The work incorporated in this thesis has not been submitted to this or any other University for the degree of Ph.D. or any other degree of academic award.

(S.V. BHORASKAR)

Guide

Reader in Physics

Department of Physics

University of Poona, Pune-7.

(V.J. RAO)

Co-Guide

Scientist,

National Chemical Laboratory

Pune-8.

DATE : September 1989.

ACKNOWLEDGEMENTS

Words are insufficient to express my deep sense of gratitude and thankfulness to my guides Dr. (Mrs) S.V. Bhoraskar, Reader, Department of Physics, University of Poona and Dr. V.J. Rao, Scientist, National Chemical Laboratory, Poona for all they have done for me. I am extremely indebted to them. Their constant encouragement and interest only, has made it possible for me to complete the task to the best of my ability and satisfaction. They also provided moral support as and when the need arose. They have instilled in me the confidence to work independently.

I am obliged to Prof. A.S. Nigavekar, Head, Department of Physics, University of Poona and Dr. R.A. Mashelkar, Director, National Chemical Laboratory for extending all the available facilities in the two institutes to me. I am extremely thankful to them.

I would like to sincerely acknowledge the help of Drs. S. Badrinarayan and A.B. Mandale Scientists, NCL, for their help in carrying out the ESCA experiments. Dr. Prabhat Singh's help in the TEM studies, Dr. S.T. Kshirsagar's assistance in the Raman Scattering studies and Dr. (Mrs) A.A.Belhekar for recording the FTIR spectra need to be specially acknowledged. I would like to thank Dr. S.M. Sathaye for his ungrudging help and encouragement during the growth and characterisation of the ZnSe films. Dr.C.S.Dorai's help in understanding the basics of chemistry, which was very useful in analysing the results, needs to be specially acknowledged. I am extremely grateful to them all for helping me in interpreting the different results.

Prof. Vikram Kumar, IISc, Bangalore and Dr. A.K. Srivastava, TIFR Bombay, need special thanks for their help in carrying out the photoluminescence measurements.

Prof. S.B. Ogale's help in carrying out the ion beam mixing of S:GaAs is duly acknowledged.

My special thanks are also due to Prof.B.Satyanarayana, Head, Department of Metallurgy, College of Engineering, Pune, for allowing us to use the SEM facility.

I would like to pen my appreciation for the assistance rendered and the congenial atmosphere provided by my colleagues R.S. Bhide, G.N.Chaudhari, Sandhya Moghe, Suvarna Dusane, Pratima Chaudhari, K. Madhukumar, Medha Katarki, Savita Pundalik and Priyamvada. It has been a memorable experience working with them. I wish to thank most warmly my friends Nitya Vittal, Dr. R.N. Prasad, Dr. Neelima Abhyankar, Milan Bannerjee and G. Srinivasa Rao for their esteemed company which proved very beneficial to me. Especially their help during the last stages of my thesis writing needs mention.

Constant moral support at all times from my father, brothers and friends who did without my company for several days during my work, made it possible for me to pursue my studies. There are no words in which I can express my gratefulness to them.

My thanks are also due to Mr. L.P.Kadam for making the manuscript into a beautifully typed thesis.

There are many more people whose names it is difficult to record who have helped me directly or indirectly during my tenure as a Ph.D. student. I sincerely thank them all.

Finally, I also acknowledge the financial assistance in the form of a Senior Research Fellowship offered by the Council of Scientific and Industrial Research, India.

I can only once more confirm my indebtedness to all and wish that these few words could go at least a small way in repaying them.

Manorama

September, 1989. (VARDHIREDDY MANORAMA)

C O N T E N T S

CHAPTER 1	: GENERAL INTRODUCTION		
	1.1	: Introduction to Gallium Arsenide	1
	1.2	: GaAs Crystal Structure	4
	1.3	: Surface Properties	5
	1.4	: Summary of the Thesis	8
CHAPTER 2A	: LITERATURE SURVEY		
	2A.1	: Sulphur and Phosphorous Passivation	10
	2A.2	: Na_2S and $(NH_4)_2S$ Passivation	11
	2A.3	: Photochemical Passivation	13
	2A.4	: AlN, SiN, SiO_2 and Al_2O_3 Dielectric Passivation	14
	2A.5	: H_2, N_2 etc. Plasma Passivation	15
	2A.6	: Other Passivants	16
	2A.7	: Techniques developed to Study Passivation	16
	2A.8	: Fermi level Pinning	17
	2A.9	: Heterojunction : GaAs/ZnSe System	18
CHAPTER 2B	: THEORETICAL BACKGROUND		
	2B.1	: Energyband Picture of an Ideal Metal Semiconductor Contact	20
	2B.2	: Energy Band Picture of a Metal Semiconductor Contact with Surface States	21
	2B.3	: Capacitance-Voltage Measurements of Metal-Semiconductor Junction	22
	2B.4	: Ohmic Contact on n-GaAs	23
	2B.5	: An Ideal Metal-Insulator Semiconductor Diode	24

2B.6 : Energy Band Diagram of an Ideal MIS Structure with Band Bending of the Semiconductor (n-type) 25
2B.7 : Electronic Properties 27
2B.7.1 : Current Voltage (I-V) Characteristics 27
2B.7.2 : Capacitance-voltage (C-V) Characteristics 28
2B.7.3 : Scanning Electron Microscope - Electron Beam Induced Current (SEM-EBIC) 29
2B.7.3a: SEM-EBIC, Diffusion Length `L' Measurement 30
2B.7.3b: SEM-EBIC, Surface Recombination Velocity `S' Measurement 32
2B.8 : Spectroscopic Techniques
2B.8.1 : X-Ray Photoelectron Spectroscopy 32
2B.8.2 : Laser Raman Spectroscopy 34
2B.8.3 : Photoluminescence Spectroscopy 38
2B.8.4 : X-Ray Fluroscence Analysis (XRF) 39
References 41
CHAPTER 3 : GaAS/POLYTHIOPHENE SYSTEM
3.1 : Introduction 52
3.2 : Experimental Details
3.2.1 : Thiophene 54
3.2.2 : Plasma Polymerisation System 54
3.2.3 : Deposition of Polythiophene by Plasma Polymerisation 55
3.3 : Metal Polythiophene GaAs (MIS) Structure 56
3.4 : Surface Properties
3.4.1 : Capacitance-Voltage : Barrier Height Measurement 56

3.4.2	: SEM-EBIC Diffusion Length Measurements	57
3.4.3	: SEM-EBIC Surface Recombination Velocity (SRV) Measurements	58
3.5	: Interfacial Properties	58
3.5.1	: Raman Scattering Studies	58
3.5.2	: Photoluminescence Studies	58
3.6	: Results and Discussion	
3.6.1	: Capacitance Voltage	59
3.6.2	: EBIC Studies	59
3.6.3	: Raman Scattering Studies	60
3.6.4	: Photoluminescence	60
	Possible Mechanism of Passivation of GaAs Surface by Polythiophene	61
	References	63
CHAPTER 4	: GaAs/S ION BEAM MIXING : AN ESCA STUDY	
4.1	: Introduction	
4.2	: Experimental	68
4.3	: Results	68
4.4	: Discussion	70
4.5	: Conclusions	72
	: References	73
CHAPTER 5	: GaAs/ZnSe SYSTEM	
5.1	: Introduction	76
5.2	: Theoretical Background	79
5.2.1	: Heterojunction Band Discontinuity	79
5.3	: Experimental Details	80
5.3.1	: Growth of ZnSe Films by Liquid Gas Interface	80

5.4 : Results 82

5.4.1 : Physical Properties 82

5.4.2 : X-Ray Fluoroscence Analysis for Composition Analysis 82

5.4.3 : Structural Analysis by TEM 83

5.4.4 : Chemical Analysis of GaAs/ZnSe Interface Using ESCA 84

5.4.5 : X-Ray Diffraction Analysis 86

5.4.6 : Growth Model for the ZnSe/GaAs Interface 87

5.4.7 : C-V Measurements 89

5.4.8 : Photoluminescence measurements 89

5.4.9 : Valence Band Discontinuity in ZnSe/GaAs Heterojunction 90

References 92

CHAPTER 6 : AMORPHOUS GaAs

6.1 : Introduction 94

6.2 : Experimental Details 97

6.2.1 : Deposition of Thin Films of a-GaAs 97

6.2.2 : Structure 98

6.2.3 : Morphology 99

6.2.4 : Hydrogen Passivation of a-GaAs 99

6.2.4A : Hydrogen Plasma Passivation 100

6.2.4B : Hydrogen Ion Bombardment 100

6.3 : Results and Discussion 101

6.3.2 : X-Ray Diffraction (XRD) 101

6.3.3 : Transmission Electron Microscopy (TEM) 102

6.3.4 : Fourier Transform Infrared Spectroscopy (FTIR) 103

		Conclusions	105
		References	106
APPENDIX	:	THERMALLY STIMULATED EXOELECTRON EMISSION	
		Introduction	109
A1	:	TSEE from - Irradiated Alkali Halides	111
A1.1	:	Experimental Details	111
A1.1.1	:	Experimental Setup	111
A1.1.2	:	Samples	111
A1.1.3	:	Experimental Procedure	112
A1.2	:	Results	112
A1.3	:	Discussion	113
A2	:	Energy Analysis of the Thermally Stimulated Exoelectrons Using a 127° CDA	116
A2.1	:	Experimental Details	117
A2.2		Results and Conclusions	118
		Conclusions	120
		References	121
		Concluding Remarks and Scope for Further Work	123

Chapter 1

General Introduction

1.1 Introduction to Gallium Arsenide:

The great advances in solid state technology can be traced to an unique combination of basic conceptual advances, the perfection of new materials and the development of new device principles. Ever since the invention of the transistor some forty years ago, we have witnessed a spectacular growth in silicon technology, leading to increasingly higher densities of devices and more complex functions. Over the past 25 years the silicon microelectronics has grown to a current status, during which the complexity of silicon integrated circuits has increased by a factor of 10^5; the speed by a factor of 10^3 and the cost has decreased by a factor of 10^6. The rate of advancement in silicon microelectronics shows no signs of slowing and within the next few years, application of specific silicon integrated circuits will appear with over one million transistors per chip.

However, notwithstanding the remarkable success of silicon microchip technology and its penetration into almost all aspects of electronic systems, there remain a number of significant areas of application in which silicon cannot serve. These are the highest frequency (microwave) electronic applications in the front end of systems such as radar, electronic warfare and microwave communications (including satellite) and optoelectronics for example light wave communications and optical signal processing. This is because the electron mobility and velocity in silicon cannot be as fast as required (See Table I). Thus there arises the demand for the high technology practical materials which can fulfil these requirements. This is where in particular, the 20th century material, gallium arsenide (GaAs) one of the III-V compound semiconductors comes into picture.

TABLE 1

Comparison of GaAs and Silicon

Property	GaAs	Si	Implication
1. Peak Electron Velocity (cms^{-1})	$2\text{-}3x10^7$	10^7	Higher speed Devices
2. Electron mobility ($cm^2V^{-1}S^{-1}$)	8000	1500	Higher speed devices
3. Band gap (eV)	1.43	1.12	Insulating substrates
4. Band gap type	Direct	Indirect	Good optoelect-ronic properties
5. Thermal conductivity	0.44	1.45	Power dissipa-tion limits.
6. Radiation resistance	Good	Poor	Military Applications.
7. Heterostructures	Yes	No	Optoelectronic integration.

Almost as revolutionary as the invention of the transistor in 1947 was the invention of the laser a decade later. The practical demonstration of an operating laser in 1960 suggested that light might one day replace electrical signals as the common carrier for information exchange because of its enormous information capacity. Thus concurrent with the electronics revolution, we have seen another technological breakthrough, the so called photonics revolution. What was lacking in the early years of photonic technology was a practical set of materials that could meet its technical demands.

The lasers that provide light wave communication systems are not made from silicon but from compound semiconductors. These are generally compounds of elements, and alloys of these compounds, from Group III of the periodic table such as Ga, Al and In, along with elements from group V, most notably As, P and Sb. This gives rise to a large family of materials with a wide range of properties well suited to electronic and optoelectronic applications. Some of these materials are GaAs, InP, GaSb, GaAlAs, InAsP, GaInAs etc.

GaAs is one member of this III-V family of compound semiconductors. Over the next 10-20 years we expect to see GaAs microchips advance in performance and decrease in cost. The result will be a major revolution in electronic systems technology and the emergence of significant new applications for electronic and optoelectronic systems. GaAs is sometimes hailed as the new microchip technology which will replace silicon that is now so widely used. This is entirely the wrong perception of the role of gallium arsenide, it will not replace silicon but will be used widely to complement it in very high speed and high frequency applications. The use of GaAs as a semiconductor is still in its infancy. But in comparison with silicon,

gallium arsenide has a number of interesting and useful properties that make it a versatile candidate for the above mentioned applications. Some of these include the following :

1. GaAs exhibits a bulk negative resistance property which is determined by the electronic band structure of the material and gives rise to its well known application as a microwave solid state power source, now used widely in a number of microwave system applications (the Gunn diode).

2. The energy gap separating the valence and conduction band extrema is larger in GaAs (1.42 eV) than in Si (1.08 eV). Thermal generation of carriers (electrons and holes) across this gap at 300 K thus produces lower steady state carrier densities in GaAs ($10^6 cm^{-3}$) compared to Si (10^{10} cm^{-3}), so more highly insulating materials and a superior device isolation capability are potentially available in GaAs. Further, the temperature at which thermal generation occurs across the bandgap overrides any particular carrier density, achieved by doping in devices, is higher in GaAs and a better temperature range of device functions ensues.

3. Since the conduction band varies much faster with wave vector (momentum) at the Γ point in GaAs than at the minimum point in Si, the effective electron mass is much lower in GaAs than in Si. The force on an electron in an electric field therefore accelerates electrons in GaAs much more quickly than electrons in Si and since scattering processes are of similar magnitude in the two materials, the mean drift velocity of low energy carriers is much higher in GaAs than in Si. Thus electrons in GaAs have a much higher velocity than in silicon and as a result GaAs transistors can operate as analogue devices at much higher frequencies and as digital devices at much

higher speeds than silicon. This is one of the major attractions for GaAs in electronic applications.

4. Substitutional impurity atoms from groups II, IV and VI will act as shallow donors and acceptors in the GaAs lattice, favouring an extra degree of freedom as compared to the situation in silicon or germanium.

5. In addition, GaAs and most other members of the III-V family emit and absorb light (normally in the infrared region of the spectrum) more efficiently than silicon, thus opening a vast range of applications for GaAs solid state devices in optoelectronic applications.

6. GaAs and other III-V compounds can be used in heterojunction structures in which a p-n junction is located at the interface between different materials of the III-V family for eg. GaAs/GaAlAs or InP/GaInAsP. Such structures offer extra degrees of flexibility in the design of semiconductor devices such as transistors, lasers, light emitting diodes and photodetectors.

When the whole family of III-V compounds is envisaged, including interperiodic compounds and alloys, the potential advantages over the group IV sequence are even more obvious. Thus the study of GaAs as a prototype is clearly justified in both an academic and an applied sense.

Table I compares the properties of GaAs and silicon and their possible implications.

GaAs crystal structure :

GaAs has a density of 5.3174 g cm^{-3} and crystallises into the zinc blende structure, which consists of two equivalent, interpenetrating face centred cubic lattices one containing Ga atoms

and the other As atoms (Fig.1). The two sublattices are separated by 2.44793 Å along the body diagonal of the unit cube whose side length is 5.65325 Å at 300 K. The lattice is broadly equivalent to that of silicon, which has a diamond structure, but the presence of dissimilar atoms with different valences makes GaAs polar. As a result, except for the <100> and <110> type axial direction, all other axes are polar i.e. with unequal Ga-As separations. This is most clearly seen in the <111> case (Fig.1). This gives rise to some significant differences in the crystal properties. A shift of valence charge from gallium to arsenic produces a mixed (ionic/covalent) bond compared to the covalent bond in silicon. This has very significant effects on the electronic band structure and increases the bond strength. The hardness of GaAs is between 4 and 5 on the Moh's scale and the degree of charge transfer of the bond is about 0.3e, where e is the charge of an electron. The symmetry of the GaAs crystal is lower than that of silicon and only the latter possesses a centre of symmetry, which makes the absorption of infrared radiation by optical phonons a forbidden process in silicon but allowed in GaAs. A further consequence of the presence of dissimilar atoms is a marked difference in the chemical activity of opposite (111) crystal faces in GaAs.

1.3 Surface properties :

The band structure and electronic properties of bulk GaAs have been studied for the last 25 years and by now understood in great detail, but not the surfaces, which pose problems. In spite of great efforts during the last few years, one is still far from complete understanding of the geometry and electronic properties of GaAs surfaces. As it is, surface properties are very different from the bulk which is well known from the study of monoatomic semiconductors

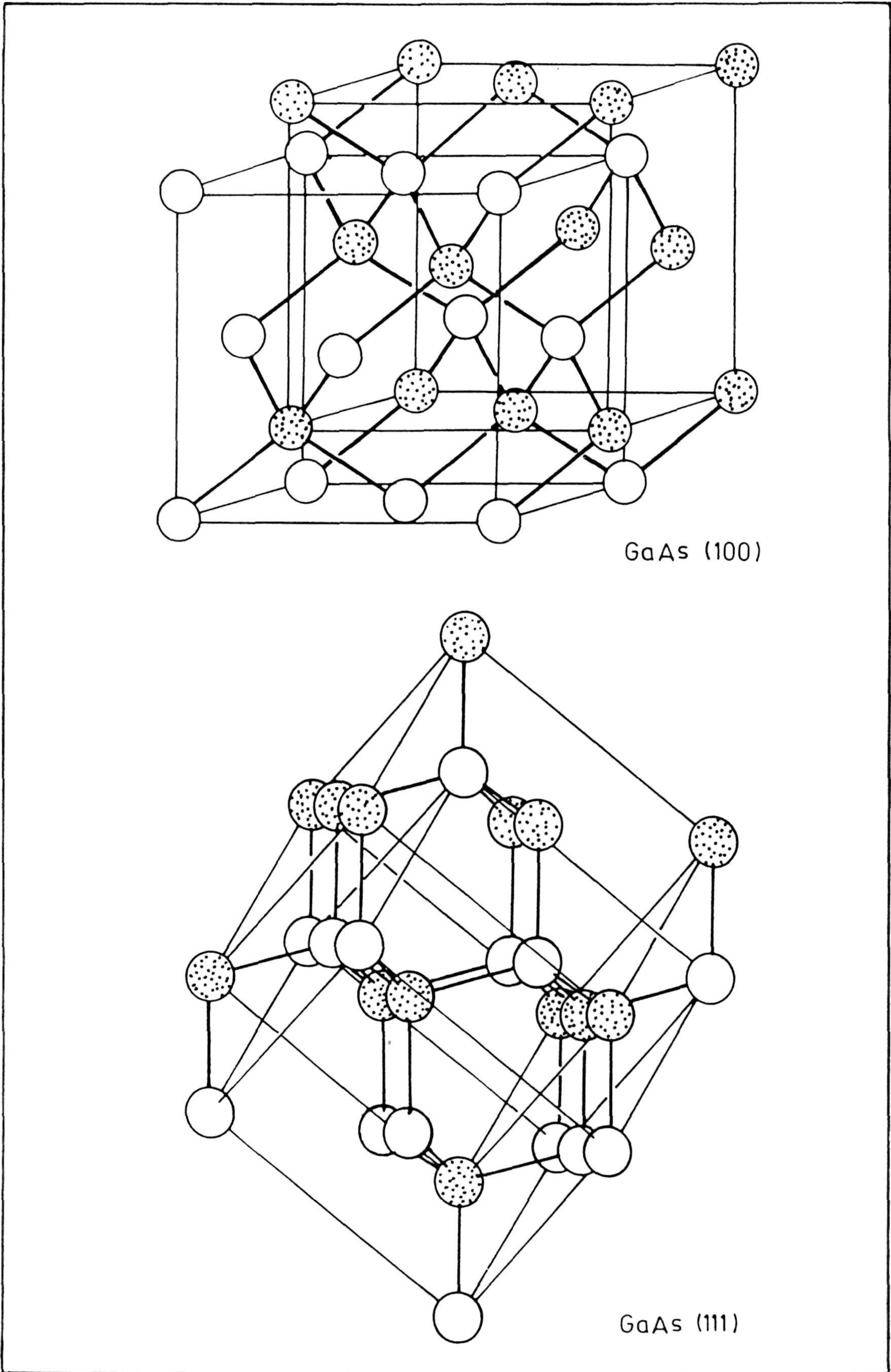

Fig.1. Crystal structure of GaAs.

such as silicon with diamond like structure, which is esentially the same as that of GaAs.

Firstly, if we consider the surface of elemental semiconductors like silicon, which is different from the bulk due to the presence of

- broken bonds
- dangling or unsatisfied bonds
- termination of the crystal periodicity.

The three dimensionally periodic potential in the crystal is abruptly terminated at the surface, and this introduces departures from the energy band structure appropriate inside the crystal. Furthermore, an oxide layer adsorbed on the surface can give rise to discrete energy levels, which influence the properties of the solid in a region near the surface. This results in a large density of localised quantum states in the badgap. Such levels are called surface states and their densities are typically of the order of $10^{23}/cm^3$, about one for each surface atom in the crystal.

These are some of the intriguing features of the surface of monoatomic silicon. In case of diatomic semiconductor like GaAs, in addition to these, less understood are

- the chemistry on the surface.
- partial ionic character of the bonds.
- Ga, As deficiencies leading to vacancies and interstitials, which in turn lead to new problems such as structural rearrangement of the surface atoms, high energy barriers due to Fermi level pinning at midgap and large density of states, which are characteristic of GaAs surfaces.

Several models suggest that surface oxides in the form of As_2O_3 and Ga_2O_3 together with elemental arsenic are reasons for the high

concentration of midgap defects associated with GaAs surface. Fig. 2 shows the schematic of the lattice and electronic structure of the GaAs (110) face after rearrangement (relaxation). The As surface atoms have taken up a p^3 bonding arrangement while the Ga has gone from the bulk sp^3 to a sp^2 arrangement. Since the p^3 bonding angles are more acute than the bulk sp^3 bonds, the As moves outward; conversely, the Ga moves inward. The movements are large (large fractions of an Å). This rearrangement moves the filled and surface states out of the band gap. These states which are responsible for the Fermi level pinning have prevented the development of a successful MISFET based on GaAs. Though ridding the GaAs surfae of oxides and excess free arsenic can result in dramatically improved surface properties, but in order to achieve long lasting benefits, it is necessary to passivate the surface of GaAs.

Surface passivation is also essential for the fabrication of devices using lithographic techniques. In case of silicon, the thermal oxide, SiO_2 provides a very good passivating and insulating layer which can be selectively etched during device fabrication. But unfortunately no such passivating agent is available for GaAs, which could serve as an insulator in GaAs MIS device processing. As will be seen from the review of the earlier work, it has been established that elements like sulphur, phosphorous, selenium etc. form very stable bonds with Ga and As and hence seem to be effective in reducing the dangling bond density on the surface of GaAs. Various compounds containing these elements have been reported to passivate the GaAs surface. In the present thesis attempts have been made to explore new materials, and novel methods for their deposition, for achieving this objective. More emphasis is laid on the characterisation of the

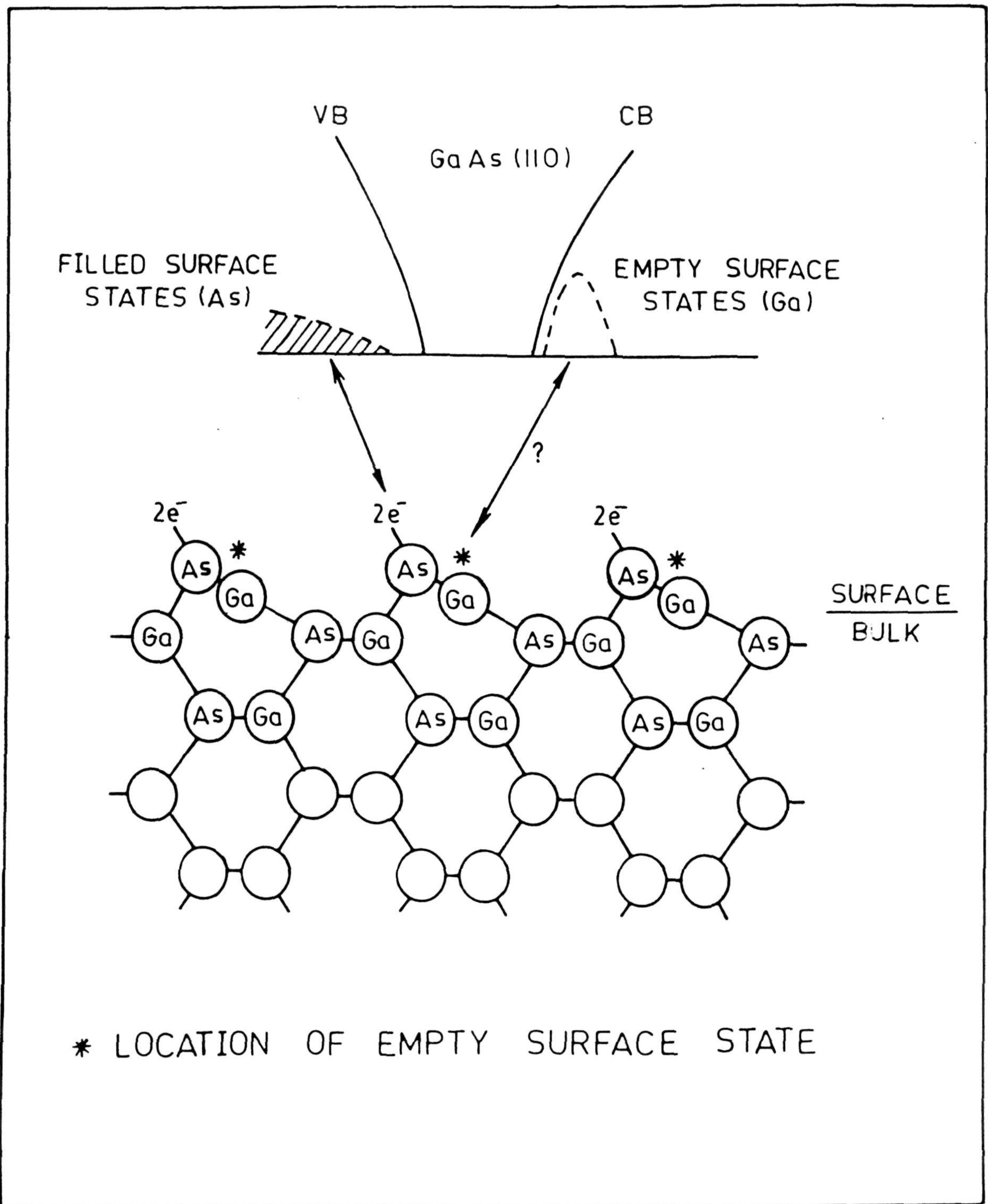

Fig.2. Schematic of the lattice and electronic structure of the GaAs (110) face after rearrangement.

passivated GaAs surface by a sulphur containing polymer and thin films of zinc selenide a II-VI compound which has some interesting properties.

1.4 Summary of the Thesis

The thesis consists of six chapters. A general introduction as decribed above forms the first chapter.

Chapter 2 deals with the survey of the work done in the area of GaAs surfaces and interfaces relevant to the present work. It also provides with some theoretical background of the various phenomena, and a brief description of the various techniques employed in the course of this study.

Chapter 3 concentrates on the passivation of GaAs with a thin film of plasma polymerised thiophene. The effect of passivation on the various electronic properties are discussed.

Chapter 4 describes the X-ray photoelectron spectroscopic study of the interfaces between GaAs and sulpher by ion beam mixing technique. The effect of ion bombardment on the GaAs surface is also included.

Chapter 5 presents the results of the study on the III-V/II-VI particularly GaAs and ZnSe heterostructure. The effect of annealing of this system on the various interface properties are described. XPS is used to study the chemical reactions taking place at the heterointerface and the effect of annealing on the valence band discontinuity.

Chapter 6 deals with the studies on amorphous gallium arsenide thin films deposited by flash evaporation and its characterisation by various techniques such as X-ray diffraction, Transmission Electron Microscopy etc. The studies include the effect of different kinds of

post hydrogenation treatments on the a-GaAs films studied by Fourier Transform Infrared Spectroscopy.

The Appendix is concerned with one of the major research contributions of the author. It deals with the setting up of an experimental facility for Thermally Stimulated Exoelectron Emission measurements (TSEE) to study the defects in solids. The energy analysis of these exoelectrons was carried out using a laboratory made 127° Cylindrical Deflector Analyser (CDA).

Finally, some concluding remarks on the work done, followed by some ideas regarding the scope for futher studies in this particular area of GaAs surfaces and interfaces is mentioned.

This part of Chapter 2 gives an account of the various attempts by different researchers in this field of GaAs surface passivation and related phenomena.

The presence of interface traps for various anodic and pyrolytic dielectrics on GaAs has prevented the development of a MOS technology for GaAs. In fact, the oxidation of GaAs appears to result in Fermi level pinning at the GaAs surface. Also the high surface recombination at GaAs surfaces exposed to air at room temperature has been shown to cause surface current to dominate bulk current [1]. These problems suggest that the oxidation procedures which are so useful for silicon may not be suitable for adaptation to the III-V compounds as surface passivants or as insulators for MOS or MIS devices.

2A.1 Sulphur and phosphorous passivation :

The problem of passivation of GaAs surface to improve the intrinsic material properties has been approached by different routes. Elemental sulphur [2] and phosphorous as the passivants have been tried for GaAs and other III-V compounds like InP. The use of liquid and gas phase sulphur pretreatment of the surface of InP [3] as a way to form a near ideal passivated surface prior to chemical deposition of SiO_2 has been studied and improvements in the FET characteristics have been observed. Passivation of the GaAs surface is made possible by an overlayer provided that physical and chemical continuity take place at the interface in order to minimize the intrinsic lattice defects that pin the Fermi level. Amorphous phosphorous [4-6] was tried as the suitable candidate. It is known that the network of a-P is of polymeric nature with a layer like local order when deposited at substrate temperatures below $200^{o}C$ [4]. The polymeric microscopic structure leads to a small number of dangling bonds. The arrangement

of the P atoms in the layers closely mimics the atomic pattern of the III-V surfaces and it provides a natural physical continuation of the GaAs surface. This a-P has shown excellent interfacial properties with the InP surface [7], producing a low density of states near the conduction band [8].

Recently the concept of a group V containing dielectric P_3N_5 [9] to prevent and compensate loss of phosphorous in InP was used to improve the semiconductor insulator interface. The root cause of arsenic segregation lies in the presence of oxygen that is always present in a minute amount [10,11]. Therefore the success of any passivating technique hinges on choosing a species that makes the surface repel approaching oxygen and at the same time has a higher heat of formation than Gallium oxide. Excellent candidates that meet the two requirements are phosphorous compounds since the heat of formation of phosphorous oxide is higher than that of Ga_2O_3. Best results were obtained by first etching in $NH_4OH:H_2O_2:H_2O$ mixture [12] and then dipping in solutions of PCl_3 and P_2S_5 dissolved in NH_4OH [13] which resulted in stable passivation properties even after several days of treatment.

2A.2 Na_2S and $(NH_4)_2S$ passivation :

Compounds of sulphur like Na_2S and $(NH_4)_2S$ have been routinely tried and they have been shown to impart long lasting improvements to the GaAs surface properties like surface recombination velocity (SRV) which degrades the material and thereby the device. Heterostructures of GaAlAs/GaAs have been found to be the solution to this problem. The SRV at the interface between $Na_2S,9H_2O$ and GaAs begins to approach that of nearly ideal GaAlAs/GaAs interface [14]. Subsequently, this interfacial system has been employed on GaAs heterojunction bipolar

transistors (HBT) to improve the current gain by sixty fold [15]. Reduction in SRV by sulphide regrowth leads to an AlGaAs/GaAs HBT with near ideal transport properties [16]. The reduction in SRV which gives rise to the increase in HBT current gain has been observed by transient photoconductivity [14], photoluminescence [17] and Raman Scattering [18].

The effect of Na_2S and $(NH_4)_2S$ edge passivation treatments have been investigated on the dark I-V characteristics of GaAs p-n homojunction diodes [19]. Comparable reduction in 2KT edge recombination current was observed. There are results existing which show that while the surface recombination rate of the GaAs surface may certainly have been reduced by the sulphide treatment, as evidenced by the PL yield increase, this does not imply Fermi level unpinning. A possible model which accounts for this effect is based on the change in band bending brought on by the surface treatments [20]. Hence an increase in band bending implies an increase in PL yield without reducing the recombination centres. Photoemission was also used to study this band bending [21,22].

Though the detailed structure of the interface between GaAs and these sulphides has not yet been determined, it seems almost certain that sulphide termination of the III-V compounds is crucial in obtaining surfaces of high electronic quality. There is a model proposed to explain the effective passivation of the GaAs surfaces by $(NH_4)_2S_x$ treatment [23]. This is supported by the X-ray photoelectron spectroscopy studies on these systems. The results reveal that after sulphide reaction the GaAs is free of native oxides and the surface becomes terminated with arsenic sulphur bonds [24]. The effect of aging on the sulphide treated samples has been studied by XPS which

shows that, as the surface becomes oxidised, As-oxide is peferentially drawn to the surface relative to Ga-oxide [25] and the sulphur coverage is independent of the ammonium sulphide concentration although the relative amount of arsenic decreases as the sulphide concentration increases. The effect of metal on the Schottky barrier formation on $(NH_4)_2 S_x$ treated GaAs was studied. The barrier height was observed to change remarkably with the type of metals, which is predicted in the case of low interface state density [26]. Samples which have undergone the $(NH_4)_2S$ treatment show a reduced pinning of the Fermi level at the surface and hence Schottky barriers which are more sensitive to the metal work function [27] are formed.

2A.3 Photochemical Passivation :

The simplest technique to get rid of the oxides on the GaAs surface is by spinning ultrapure water in the presence of laser light illumination. The photoluminescence from GaAs surface, passivated by photowashing or coating with $Na_2S,9H_2O$ are shown to be sensitive to the gas ambient [28]. Both water vapour and oxygen must be present in order to obtain a large PL signal. The effects are activated by measuring the Laser light [29]. XPS was used to investigate the effects of deionised water on chemically etched GaAs surfaces [30]. It is shown that running water can remove the oxide film, formed in the static condition as well as oxidised layer due to air exposure. This photochemically unpinned GaAs surface has also been characterised [31]. This unpinning is seen in the PL and SRV measurements [32], of photochemical surface passivation and on Reverse current in Ti-GaAs Schottky diodes [33].

A rigorous theoretical analysis of the surface recombination and PL intensity was made and a correlation between PL and surface state

density on GaAs surfaces was established. It is shown that the increase of PL intensity cannot be explained by reduction of N_{SS} but by the generation of a negative fixed charge on the surface [34].

2A.4 AlN, SiN, SiO_2, Al_2O_3 etc dielectric passivation :

These are used as protective coverings to prevent exposure of GaAs surfaces to ambients and also as capping materials. AlN seemed suitable because its bandgap is 6.2 eV and its thermal expansion coefficient is almost the same as GaAs. Sputter deposited AlN was used as a passivation film for GaAs FETs [35] and for annealing after ion implantation into GaAs [36]. Better passivation characteristics were also observed on plasma CVD AlN films which create less damage on III-V compounds than sputtering [37,38]. Photo CVD deposited SiN was also shown to be a suitable candidate for GaAs MESFET passivation [39]. Low temperature MOCVD growth of AlN and GaN has also been used for high quality surface passivation of III-V semiconductors [40,41]. The characteristics and thermal stability of the AlN/GaAs MIS diodes are improved by pretreatment conditions. The pretreatment is expected to control the stoichiometry and the atomic structure of the GaAs surface [42]. Barrier height enhancement at elevated temperatures is observed for all refractory metal nitride/GaAs contacts which were investigated. The cause is attributed to the incorporation of nitrogen into the GaAs substrate. They serve as suitable gate materials for self aligned GaAs MESFET processing [43]. MIS structures were also prepared by plasma oxidation of aluminium layers on GaAs and their properties were studied [44].

Superstructures were also observed by grazing incidence X-ray diffraction at the AlN/GaAs interface fabricated by MOCVD [45]. Improvements in GaAs/plasma deposited SiN interface was observed by

predeposition surface treatment and post deposition annealing [46].

2A.5 H_2, N_2 etc Plasma passivation :

When starting from the surface covered with its native oxide, the oxide has to be removed or transformed. In the past, promising results were obtained by treating the surface in a mixed oxygen and freon (CF_4) [38,11] plasma. The results obtained were very irreproducible and the passivating layer very sensitive to atmospheric contamination. A number of authors [47] have suggested nitridation as a possible solution to this problem. In this case it is necessary to remove entirely the native oxide before building up a nitride-GaAs interface in a controlled manner. Thus multipolar plasma containing a high proportion of atomic species (nitrogen and hydrogen) yield very sharp interfaces and good electrical properties [48,49]. RF sputter cleaning in H_2 and N_2, despite being more energetic than a multipolar plasma, in conjunction with a plasma deposited Ga oxide is shown to effectively depin the Fermi level at the Ga oxide/ GaAs interface [50].

Hydrogen plasma treatment is shown to passivate [51-53] the electrically active centres and deep level defects in GaAs [54]. This hydrogen plasma treated GaAs clearly shows the presence of silicon related hydrogen complexes in case of n-GaAs doped with silicon as seen in the IR [55] and PL spectra [55].

The hydrogen also neutralises the donor (Si) [57] and carbon acceptors [58]. Raman studies also indicate hydrogen related complexes [59]. HCl gas and H_2 mixture cleaning prior to MBE growth was investigated as a means of reducing the carrier depletion at the interface [60]. The effect of H_2 on minority carrier recombination at dislocations and subboundaries is also studied [61].

2A.6 Other passivants :

Good electrical properties of antimony passivated, air exposed and regrown interfaces were also obtained by depositing elemental antimony using molecular beams [62]. Chemisorbed Ruthenuim has also shown a reduction in SRV [63]. Polyimide [64], Langmuir Blodgett films [65], heteropolyanions [66] on GaAs have shown passivating properties.

Substrate heating of GaAs produces Ga oxide which also acts as a passivating layer [67]. The interfacial properties of fluoride-GaAs have been shown to be improved by post growth annealing [68,69]. The structure and bonding at the CF_2/GaAs interface is also studied [70]. Some of the other passivants tried are polythiophene deposited by electropolymerisation [73] and LaB_6 [74]. Surface states on GaAs are also shown to be reduced by plasma growth of oxyfluorides [75]. Germanium (oxy) nitride based surface passivation has also been applied to GaAs [76].

2A.7 Techniques developed to study passivation :

Raman scattering (RS) has proved to be a potential technique to study the passivation of semiconductor surfaces [77]. By observing the longitudinal optical (LO) mode in the Raman spectra the extent of passivation can be very simply estimated [78]. These experiments yield information similar to that obtained from photoemission and photovoltage measurements, but they can also be carried out on surfaces which are contaminated or even covered with partially transparent layers such as metallic films [79-82]. RS has also been used to determine the free carrier concentration and width of the surface space charge layer [83]. Surface band bending on clean and oxidised surfaces of GaAs have also been studied by RS [84,85].

Electronic RS with below band gap excitation was used to access residual shallow acceptors in undoped GaAs with different degrees of compensation [86]. It has also been used to monitor the progress of pulsed dye laser annealing of high dose ion implanted GaAs [87] . Photoluminescence [78, 88-90] is also widely used to estimate the extent of passivation. It throws light on the recombination centre density. This information can also parallely be obtained from the surface recombination velocity (SRV) measurement [91], using the scanning electron microscope [92]. Passivation was also observed by a low SRV on Si and Ge surfaces [93]. The recombination lifetimes mediated by defects is also studied on GaAs epilayers grown by different methods [94].

Some of the other techniques are picosecond transient reflectivity, used to study unpinned GaAs surfaces [95] and EXAFS in total reflection and dispersive mode to study the buried interface of silicon nitride / GaAs [96].

Investigation of "real" surfaces of GaAs by pulsed field effect techniques and surface photovoltage spectroscopy revealed the presence of two states with discrete energy positions 0.7 and 0.9 eV below the conduction band [97]. Deep level transient spectroscopy (DLTS) is especially apt to study the interface states [98].

2A.8 Fermi level pinning :

Until quite recently, nearly all investigations of GaAs interfaces supported the existence of a pinned surface potential which has been attributed to surface states of various possible origins. These midgap states are known to increase the non radiative recombination centres [99]. In one widely accepted model, proposed by Spicer et al [100-104] the surface states are derived from inherent

defect vacancy sites. Other models such as that of Wooda and co-workers [105], attributed pinning to surface impurity states consisting of arsenic metal or arsenic oxide films with midgap states. Regardless of the model, the practical effect is to make it difficult to change the interface potential. This provides a formidable problem in development of high efficiency GaAs devices. Although a clear understanding of interface formation is crucial to the development of reliable FET technologies,such an understanding has thus far remained elusive. The arsenic and metal induced interface states [106] responsible for pinning of Fermi level near midgap have been studied by low energy cathodoluminescence.

There have been several attempts to understand the Fermi level pinning due to oxygen adsorption [107-108] and cleaving in UHV and then exposing to molecular oxygen etc and studying by UPS [109]. The correlation between heavily damaged semiconductors [110], metallic character in silver overlayers on GaAs [111] and the fermi level pinning has been studied. A theory for the surface pinning of E_F developed by Bardeen was used to explain the concept of neutral level of the surface. The theory was used to explain the effect of surface structure on the Schottky barrier height [112]. By depositing monolayers of silver on freshly cleaned GaAs surface the E_F is pinned at 0.45 eV $\pm$ 0.05 eV above valence band maximum (VBM) for p-GaAs and 0.65 $\pm$ 0.05 eV above VBM for n-GaAs due to the formation of midgap electronic states [113]. Many other theories exist which try to explain the Fermi level pinning in these semiconductors [114-116].

2A.9 Heterojunctions : GaAs/ZnSe System :

Semiconductor heterojunction structures are becoming an increasingly important element in the design of advanced solid state

electronic devices. The valence band and conduction band discontinuities ΔE_V and ΔE_C have been predicted using quantum mechanical calculations [117-127]. Photoemission techniques have been recently applied to determine ΔE_V [124-130]. X-ray photoelectron spectroscopy has been shown to be particularly useful for the direct determination of E_V [127, 131-133]. One of the principal results of these XPS studies was to demonstrate that interface properties can significantly influence ΔE_V. Thus in the Ge-GaAs, GaAs-CuBr, Ge-CuBr series of heterojunctions, it was shown that ΔE_V is not a transitive property [134]; for GaAs-AlAs heterojunctions, ΔE_V was found to depend on the growth sequence [135]. Low energy electron diffraction and Auger electron spectroscopy was also used to characterise the GaAs-ZnSe heterointerface [134].

In particular the GaAs-ZnSe system grown by different techniques like vapour phase epitaxy (VPE) [135, 136], Organometallic Chemical Vapour Deposition (OMCVD) [137], Molecular Beam Epitaxy [138-140] etc have been widely studied. ZnSe-GaAs heterojunctions and superlattices are now candidate materials with practical use in optoelectronics [141]. Their application in integrated optics [142] and relevant superlattice design have also been reported. The band structure of this superlattice has been studied with a semiempirical tight binding technique [143].

Though much efforts are concentrated on these heterojunctions, less attention has been given to the effects that these II-VI compound overlayers can exert on the properties of the III-V surfaces such as barrier height, fermi level pinning and recombination velocity.

The ZnSe is a possible passivant for GaAs surfaces. It has been shown that growth of ZnSe on GaAs improves the electronic properties of GaAs [144,145].

Chapter 2B

Theoretical Background

This section of chapter 2 is concerned with a brief theoretical background of the various phenomena and the techniques employed during the course of study. This is relevant to the understanding of GaAs surfaces and interfaces. For the sake of completion and continuity the section starts with the energy band diagrams and then proceeds to describe the different techniques.

2B.1 Energy band picture of an ideal Metal-Semiconductor contact:

When a metal is making intimate contact with a semiconductor, the Fermi levels in the two materials must be coincident at thermal equilibrium. The two limiting cases are shown in Figs. 1 and 2. Fig.1 shows the electronic energy relations in an ideal contact between a metal and an n-type semiconductor in the absence of surface states.

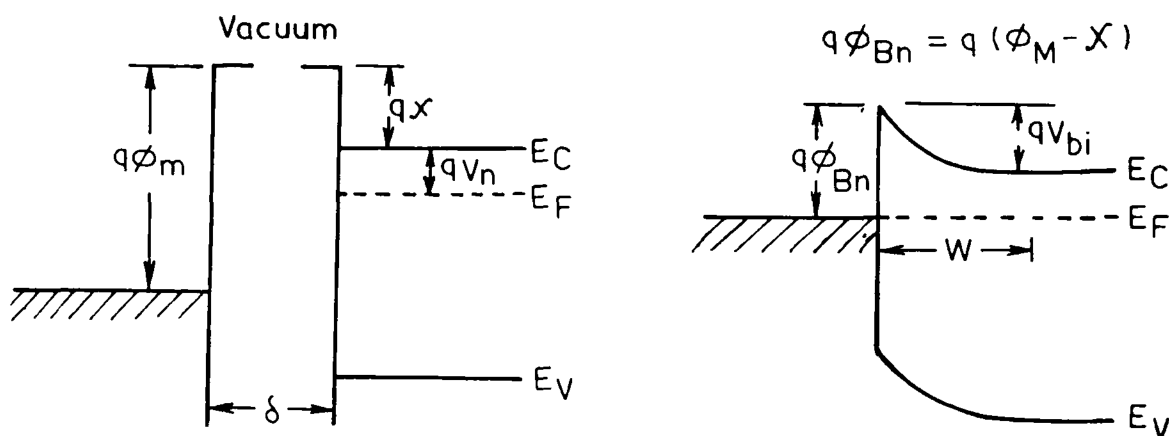

Fig.1

Relative to the Fermi level in the metal, the Fermi level in the semiconductor is lowered by an amount equal to the difference between the two work functions. The work function is the energy difference between the vacuum level and the Fermi level. This quantity is denoted by $q\,\phi_m$ for the metal, and equal to $q\,(\chi + V_n)$ in the semiconductor, where $q\,\chi$ is the electron affinity measured from the bottom of the

conduction band E_c to the vacuum level, and q V_n is the energy difference between E_c and the Fermi level. The potential difference $q\phi_m - q(\chi + V_n)$ is called the contact potential. As the distance between the metal and semiconductor decreases, an increasing negative charge is built up at the metal surface. This implies that an equal and opposite (positive) charge must exist in the semiconductor. Because of the relatively low carrier concentration, this positive charge is distributed over a barrier region near the semiconductor surface. When is small enough to be comparable with interatomic distances, the gap becomes transparent to electrons, and we obtain the limiting value of barrier height $q\phi_{Bn}$ given by

$$q\phi_{Bn} = q\ (\phi_m - \chi) \qquad 1$$

2B.2 Energy band picture of a metal semiconductor contact with surface states :

This case is shown in Fig.2 where a large density of surface states is present on the semiconductor surface. The figure shows equilibrium between the surface states and the bulk of the semiconductor but non-equilibrium between the metal and the semiconductor. In this case, the surface states are occupied to a level E_F. When the metal semiconductor system is in equilibrium, the Fermi level of the semiconductor relative to that of the metal must fall an amount equal to the contact potential and, as a result, an electric field is produced in the gap. If the density of the surface states is sufficiently large to accommodate any additional surfaces resulting from diminishing without appreciably altering the occupation level E_F, the space charge in the semiconductor will remain unaffected. As a result, the barrier height is determined by the

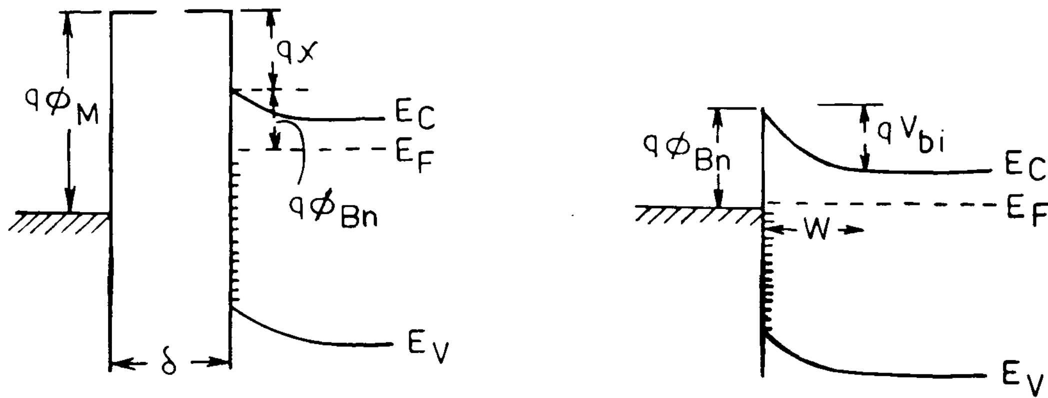

Fig. 2

property of the semiconductor surface and is independent of the metal work function.

2B.3 Capacitance-Voltage measurements of Metal-Semiconductor junction:

It is clear from the above discussion that when a metal is brought into intimate contact with a semiconductor, the conduction and valence bands of the semiconductor are brought into a definite energy relationship with the Fermi level in the metal. Once this relationship is known, it serves as a boundary condition on the solution of the Poisson equation in the semiconductor. Under abrupt approximation

$- q\ N_D$ for $x < W$ and $p \simeq 0$, $dV/dx = 0$ for $x > W$.

where W is the depletion width.

The space charge Q_{sc} per unit area of the semiconductor and the depletion layer capacitance C per unit area are given by

$$Q_{sc} = q\ N_D W = 2q\ \epsilon_s N_D\ [V_{bi} - V - (kT/q)]\quad C/m^2 \qquad 2$$

$$C = Q_{sc}/dV = (q\epsilon_s\ N_D)/\ 2(V_{bi} - V - kT/q) = \epsilon_s/W\quad F/cm^2 \qquad 3$$

This can be written in the form

$$1/C^2 = 2(V_{bi} - V - kT/q)/q\ \epsilon_s N_D \qquad 4$$

This expression can be used to determine the barrier height. When a small ac voltage is superimposed upon a dc bias, charges of one sign are induced on the metal surface and charges of the opposite sign in the semiconductor. From the intercept on the voltage axis, the barrier

height can be determined

$$\varnothing_{Bn} = V_i + V_n + (kT/q) - \varnothing \qquad 5$$

where V_i is the voltage intercept and V_n the depth of the Fermi level below the conduction band, which can be computed if the doping concentration is known.

2B.4 Ohmic contacts on n-GaAs:

An ohmic contact is defined as metal semiconductor contact that has a negligible contact resistance relative to the bulk or spreading resistance of the semiconductor. A satisfactory ohmic contact should not significantly perturb device performance, and it can supply the required current with a voltage drop that is sufficiently small compared with the drop across the active region of the device.

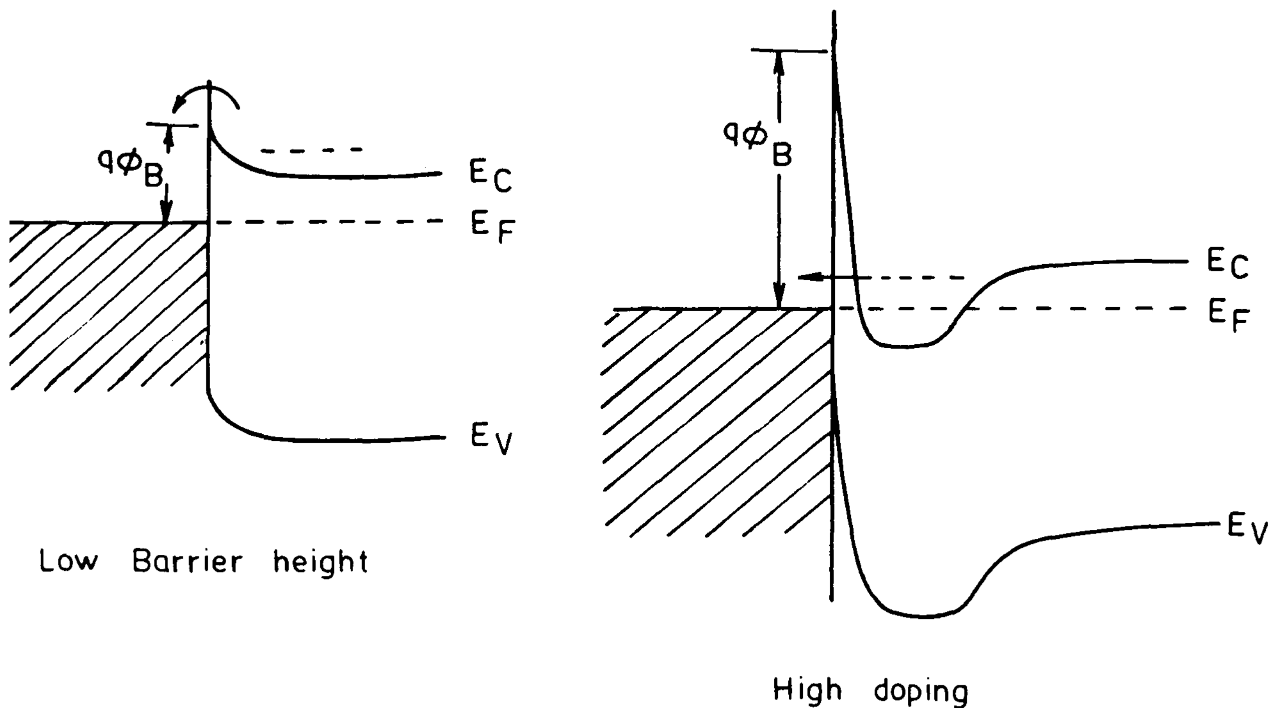

Fig. 3

Fig. 3 shows the low barrier height or high doping condition which are the alternatives to obtain an ohmic contact. It is difficult to make ohmic contacts on wide gap semiconductors. A metal does not

generally exist with a low enough work function to yield a low barrier. In such cases the general technique for making an ohmic contact involves the establishment of a heavily doped surface layer such as metal-n^+-n contact by various methods, such as shallow diffusion, alloy regrowth, indiffusion of a dopant contained in the contact material, double epitaxy and ion implantation. For GaAs and other III-IV compound semiconductors, various technologies have been developed for the ohmic contacts. We have used a method wherein Ni-Ge-Au are evaporated one above the other and this n-GaAs-Ni-Ge-Au system is annealed at 440°C for 30 seconds in nitrogen atmosphere. The Germanium in the alloy forms an n^+ layer on the n-GaAs which enables the formation of a high doping essential for ohmic contact formation.

2B.5 An Ideal Metal-Insulator-Semiconductor Diode:

The Metal-Insulator-Semiconductor (MIS) diode is the most useful device in the study of semiconductor surfaces. Since the reliability and stability of all semiconductor devices are intimately related to their surface conditions, an understanding of the surface physics with the help of MIS diodes is of great importance to device operations. The MIS structure is shown in Fig.4 where d is the insulator thickness

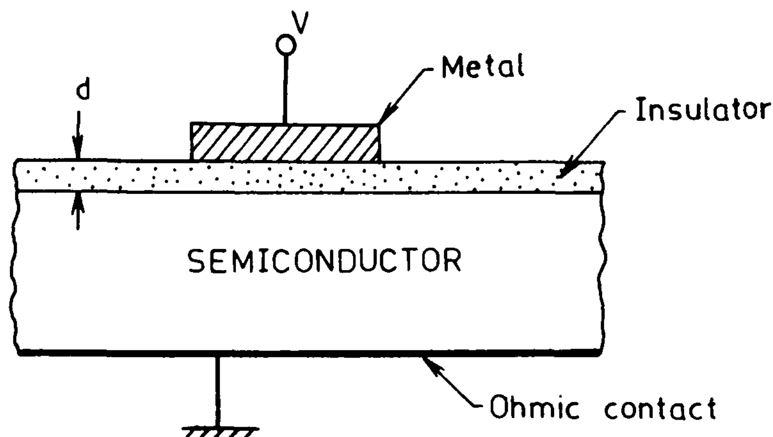

Fig.4

and V is the applied voltage on the metal field plate. The energy band diagram of an ideal MIS structure for V = 0 is shown in Fig.5.

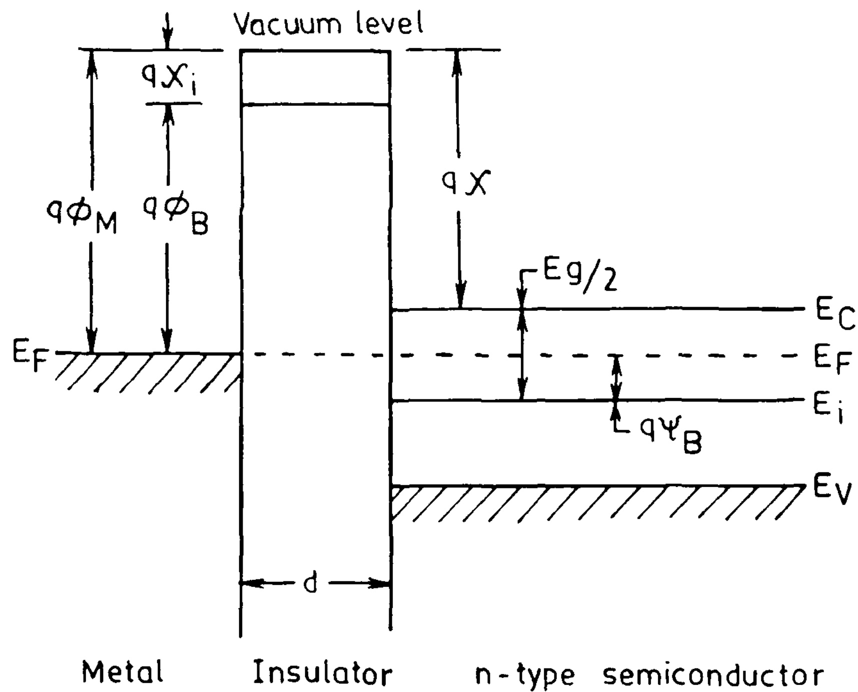

Fig.5

2B.6 Energy band diagram of an Ideal MIS structure with the band bending of the semiconductor (n-type):

Fig. 6 shows the energy band diagram of an ideal MIS structure.

There are several studies reported on the interface trapped charge also called interface states, fast states or surface states. These exist within the forbidden gap due to the interruption of the periodic lattice structure at the surface. Measurements on clean surfaces in ultra high vacuum conditions have also confirmed that this charge is very high of the order of the density of surface atoms (~ 10^{15} atoms/cm^2). This interface trapped charge can be neutralised by different processes, like in silicon, growing of a thermal oxide SiO_2 on the silicon surface neutralises most of the trapped interface charge. This is also known as passivation. A surface state is

considered a donor if it can become neutral or positive by donating an

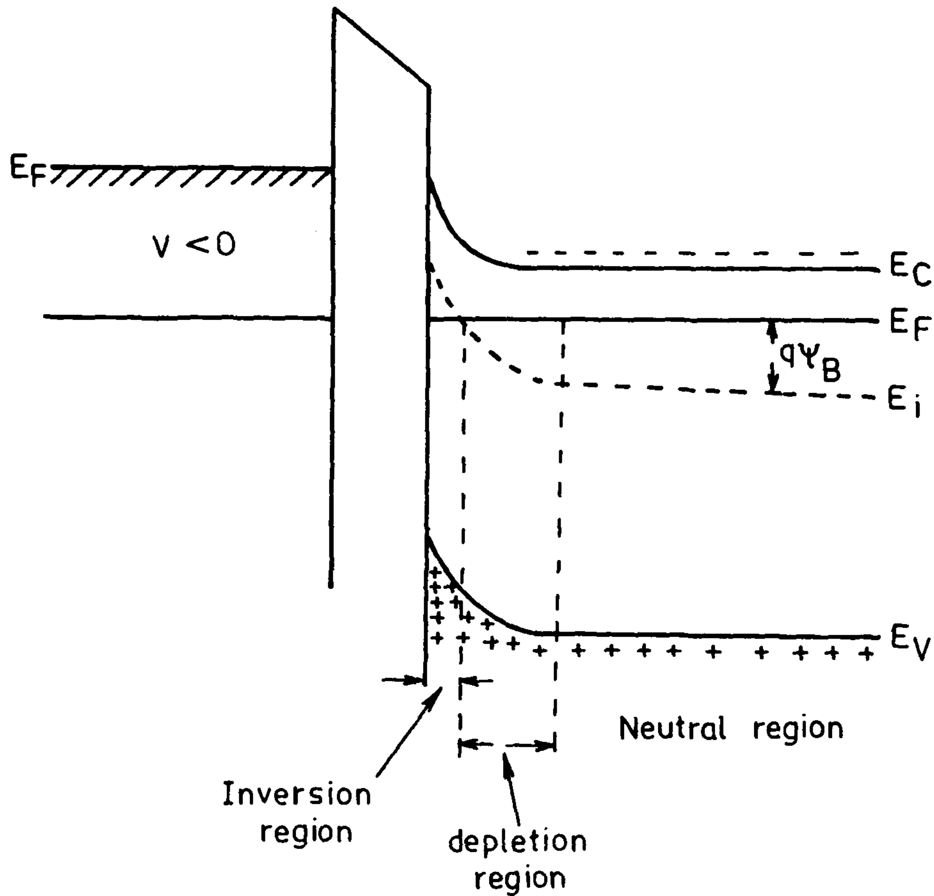

Fig.6

electron. An acceptor interface trap can become neutral or negative by accepting an electron.

When a voltage is applied, the interface trap levels move up or down with the valence and conduction bands while the Fermi level remains fixed. A change of charge in the interface trap occurs when it crosses the Fermi level. This change of charge contributes to the MIS capacitance and alters the ideal MIS curve.

On exposure to air, semiconductor surfaces invariably form an oxide on the surface. In case of silicon, SiO_2 formed itself acts as a protective layer and prevents further oxidation. Air exposed GaAs surfaces in particular always have a layer containing oxides of gallium and arsenic, free arsenic and arsenic vacancies. These create

states in the gap at particular energy levels as shown in Fig.2 of Chapter 1. This makes the Fermi level immobile and results in what is known as `Pinning of Fermi level' near midgap. These high density of surface states are responsible for the large number of recombination centres which degrade the material. If it would be possible to passivate or chemically tie up the dangling bonds and physically protect the GaAs surface it would be possible to depin the Fermi level and improve the intrinsic material properties of this semiconductor.

Deposition of an insulating layer in between the metal and semiconductor results in an MIS diode which is a very convenient device to study the properties of the semiconductor. This MIS configuration is used to estimate the diffusion length and surface recombination velocity by SEM-EBIC, barrier height by I-V and C-V characteristics etc.

2B.7 ELECTRONIC PROPERTIES:

2B.7.1 Current voltage (I-V) characteristics :

Obtaining dc I-V curves appears to be a very routine procedure. It is so when the values of current and voltage are in a certain range. (Current in milli-amperes or micro-amperes and voltage in volts). However when the current is in the range of nano-amperes, the internal resistance of the measuring instrument becomes significant and cannot be ignored. The resistance of the diodes with thicker insulator layers, in Metal Insulator Semiconductor (MIS) configuration is as high as and often higher than the internal resistance of the voltmeter. Fig.7 gives a schematic of the setup used for obtaining the I-V characteristics under these conditions.

The current I is the true value (only limited by the instrument, the ammeter), and the voltage across the diode can be found by $V-I\Upsilon$

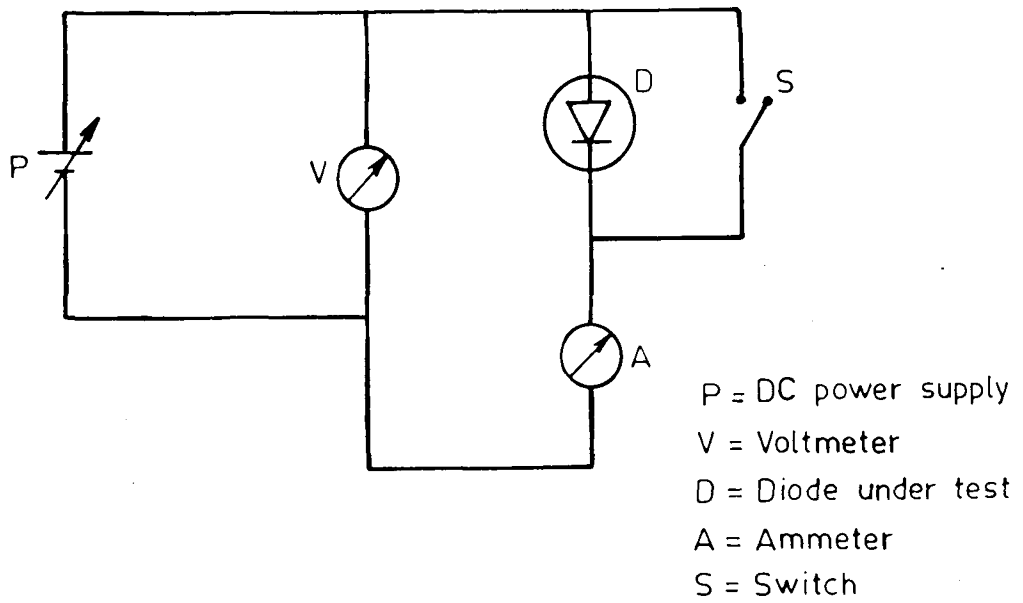

Fig. 7

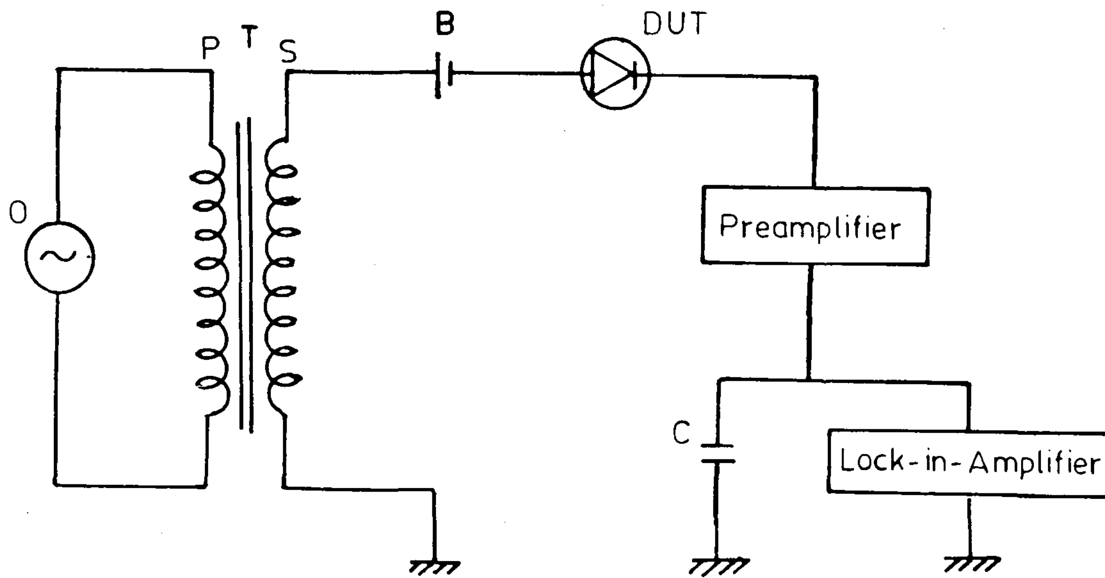

O : Oscillator

T : Isolation transformer

B : Voltage bias

DUT : Diode under test

C : Capacitor

Fig. 8

where `V' is the voltmeter reading, `I' is the ammeter reading and `r' is the internal resistance of the ammeter. This `r' can be obtained by closing the switch `S' and noting the corresponding ammeter reading I' and voltmeter reading V' ($r = V'/I'$).

Sze [146] has shown that the forward current density J, of the Schottky barrier junction for $V > 3kT/q$ is approximately given by

$$J = A^{*} T^{2} \exp(-qV_{Bi}/kT) \exp(qV/nkT) \quad 6$$

where A^{*} is the effective Richardson constant

T is the junction temperature in K

k is the Boltzman constant

n is the ideality factor

V is the applied forward bias voltage.

The current density J is the forward current per unit area of the diode (Amp/cm^2).

The extrapolated value of the current density to zero bias voltage gives the saturation current density

$$J_{sat} = A^{*} T^{2} \exp(-qV_{Bi}/kT) \quad 7$$

The barrier built in voltage is then given by

$$V_{Bi} = (kT/q) \ln (A^{*}T^{2}/J_{sat}) \quad 8$$

and the ideality factor of the diode

$$n = (q/kT) (\partial V/\partial \ln J) \quad 9$$

where $(\partial V/\partial \ln J)$ is the slope of ln J vs V characteristics.

2B.7.2 Capacitance-Voltage (C-V) measurements of MIS diodes:

The schematic of the experimental setup used for the C-V measurements is shown in Fig.8. The Schottky barrier height, $\emptyset_B$ is estimated from the intercept on the X-axis of the $1/C^2$ versus V plot.

2B.7.3 Scanning Electron Microscope - Electron Beam Induced Current (SEM-EBIC) :

The recombination properties of the minority carriers constitute the basic electronic properties of semiconductors and essentially control the performance of numerous types of devices. The scanning electron microscopy technique is widely used for the study of excess carriers and their recombination characteristics [147]. The excess carriers excited by the electron beam diffuse to a potential barrier (Schottky or p-n junction) where the electrons and holes are separated and a current is generated reflecting the amount of excess carriers; this current is referred to as the Electron Beam Induced Current (EBIC). Simplified but useful models have been developed to analyze EBIC [147,148]. EBIC is widely used to detect recombination inhomogeneities resulting from compositional or structural defects [149-152]. Quantitative analysis of the EBIC makes possible the determination of the diffusion length [153] and the surface recombination velocity [154] with high spatial resolution, by utilising the high resolution

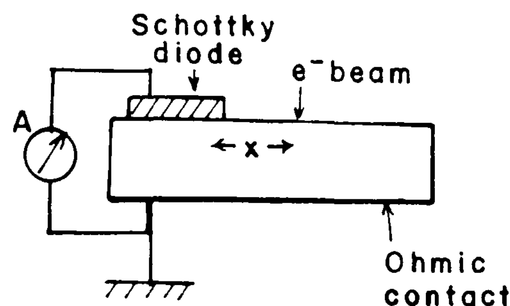

Fig. 9

capability of the SEM and the three dimensional profiling by the precise control of the electron beam energy.

The configuration used for the measurement of the diffusion length L and surface recombination velocity S is shown in Fig.9. The geometry is such that the incident electron beam is perpendicular to the charge collecting barriers.

2B.7.3a SEM-EBIC Diffusion length `L' measurement:

The diffusion length `L' is defined as the average distance, a carrier generated travels before it recombines. As the number of recombination or defect centres decrease the diffusion length is expected to increase. In this technique of SEM-EBIC, the electron beam is slowly scanned across an edge marking the limits of the Schottky barrier contact on the surface of the semiconductor (Fig.9). The generated electron hole pairs will diffuse into the high field region near the contact and some will recombine before being collected. The further the generation region from the edge of the electrode, the larger the proportion lost by recombination. A measurement of the EBIC as a function of distance of excitation measured perpendicular to the edge and parallel to the specimen surface, enables the determination of the minority carrier diffusion length. For distances large compared to the diffusion length `L', the EBIC decreases with distance from the junction `d' according to a simple exponential [155].

$$I(d) \propto \exp(-d/L) \text{ and } \qquad 10$$

L is determined from the slope of a plot of ln I against `d'.

2B.7.3b SEM-EBIC, Surface recombination velocity, S measurement:

The recombination properties of the minority carriers constitute the basic electronic properties of semiconductors and essentially control the performance of numerous types of devices. The SEM is

widely used for the study of excess carriers and their recombination characteristics. The recombination of the electron beam induced excess carriers is far more effective on the surface than in the bulk. This is due to the presence of surface states and other recombination centres. The recombination on the surface introduces an additional recombination rate effect to the bulk lifetime of carriers near the surface. This reduction of the excess carriers (due to surface recombination) can be taken as an apparent reduction of the generation rate. Accordingly we can use the concept of an effective generation rate, G_{eff}.

Then for surface excitation ($\xi = 0$) where ξ is the excitation depth

$$(\partial/\partial\xi)\,(\ln G_{eff})\Big|_{\xi=0} = S/D \qquad 11$$

where S is the surface recombination velocity and D is the diffusion constant.

The excitation depth is taken as one third of the penetration depth. The penetration depth R of an electron beam with particular energy can be calculated from the Range- Energy relation given by Young[156]

$$R = (1/\rho)\ 4.0 \times (E)^{1.75} \times 10^{-6}\ \text{um} \qquad 12$$

where ρ is the density of the material

E is the energy of the electron beam in keV

1.75 is the empirical exponent given for insulators and semiconductors.

The range vs energy curve is plotted for GaAs in Fig.10.

Since the electron beam induced current (EBIC) is proportional to the excitation strength

$$I = K\, G_{eff} \qquad 13$$

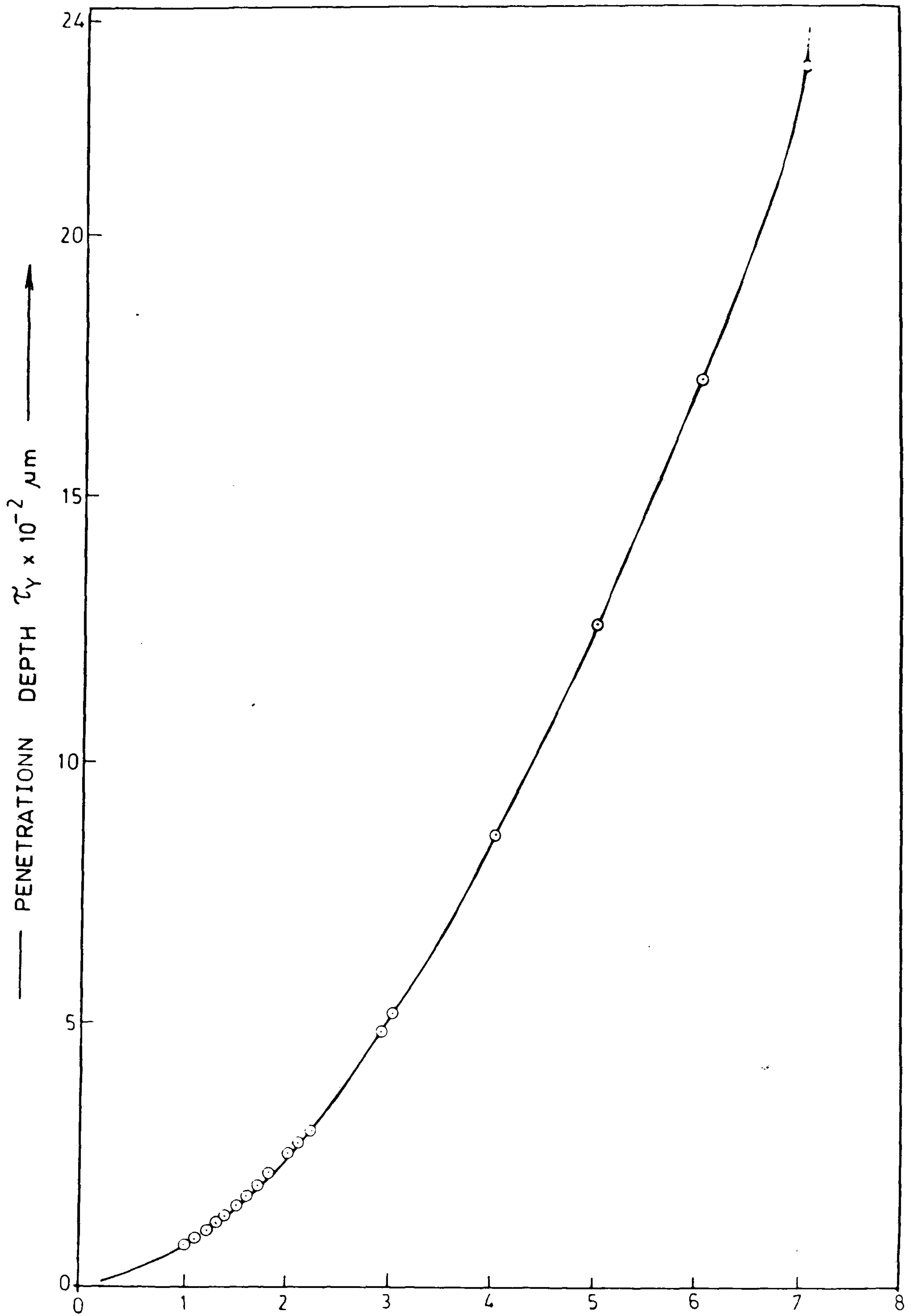

Fig. 10 : Range-Energy curve for GaAs

where K is the constant of proportionality which depends on the geometry of the junction and the surface.

The current change for excitations near the surface is then given by

$$(\partial/\partial\xi) \ln I\Big|_{\xi=0} = S/D \quad 14$$

$$S = D\,(\partial/\partial\xi) \ln I\Big|_{\xi=0} \quad 15$$

The above expression provides a convenient method for the determination of the surface recombination velocity. The slope of the tangent at $\xi = 0$ of the ln I versus ξ curve gives a measure of S.

2B.8 SPECTROSCOPIC TECHNIQUES:

2B.8.1 X-ray Photoelectron Spectroscopy :

It has been shown that photoelectron spectroscopy can yield values for the binding energies of all the electrons in an atom or molecule. The basic principle involves an absorption process, where the electron is excited by absorption of electromagnetic radiation from a lower to a higher energy level. If the energy of the electromagnetic radiation is greater than the difference between the initial electronic energy level and any higher energy level, the electron will actually leave the atom or molecule and travel in free space with a velocity determined by the energy difference between the initial energy level and the energy of the electromagnetic radiation.

If electromagnetic radiation is in the X-ray range, say the MgKα or AlKα radiation is used, all the core orbital electrons as well as the valence orbital electrons could be ejected to give photoelectrons of different energies. This type of photoelectron spectroscopy is called X-ray photoelectron spectroscopy (XPS) or Electron Spectroscopy for Chemical Analysis (ESCA). Once the kinetic energy of the ejected electrons has been measured in the spectrometer,

the binding energy can be obtained using the following equation

$$K.E. \text{ (ejected electron)} = h\nu - B \qquad 16$$

B is the energy of the electronic energy level from which the electron was ejected measured as a binding energy.

The recoil energy of the atom or molecule is negligible and hence ignored. In the case of solid materials the attachment of the sample to the holder will give rise to a contact potential equal to the difference in the work function between the sample and the sample holder. This gives

$$K.E. = h\nu - B + \phi_{cpd} - \phi_{sp} \qquad 17$$

putting B on scale with respect to the Fermi level, B', rather than with respect to the vacuum level, where

$$B = B' + \phi_{cpd} \qquad 18$$

$$K.E. = h\nu - B' - \phi_{sp} \qquad 19$$

In addition, the sample charging effect has also to be considered each time. Once the binding energy of a particular electron is obtained using the above equation useful chemical information is obtained.

The case of core orbitals is different. If the element exists in its free state it gives a single peak for the photoelectrons ejected. But if this element is bonded to some other species then the binding energy is either less than or greater than the original value depending on whether the species is more electropositive or more electronegative than the element. Thus the binding energies of core electrons give rise to a chemical shift. If both the free element and the bonded species co-exist then, this gives rise to two peaks.

In fact chemical shifts can be observed for the core electrons of all elements except hydrogen (whose single electron is involved in all compounds involving hydrogen and is thus always a valence electron).

This means that the photoelectron spectroscopy of core electrons is a very powerful technique for investigating the structure and bonding in chemistry. In addition, since the core electron binding energies are characteristic of a particular type of atom, the atomic constituent of a compound can be readily determined, and further, the area under the peaks corresponds to the number of atoms present. It is these two features that lead to the name ESCA.

2B.8.2 Laser Raman Spectroscopy :

Raman spectroscopy is a contactless and non destructive technique to obtain valuable information about semiconductor surfaces and interfaces. In Laser Raman analysis, a laser beam is bounced off a sample surface and the energy of the scattered light is measured relative to that of the laser beam. The resulting Raman spectrum is a record of the intensity of the scattered light corresponding to specific shifts in energy from the laser line. Because these energy shifts are related to the molecular and structural characteristics of the scattering medium, they offer a unique source of analytical information. Raman spectroscopy can also provide insight into process induced strain, dopant levels, the optimum composition of III-V semiconductor alloys, and the nature of crystalline interfaces which affect the overall electrical properties of finished devices. The salient parameters of a semiconductor Raman spectrum are the peak position and the line shape of the crystal lattice modes designated longitudinal optic (LO) and transverse optic (TO).

The conservation of momentum plays a very important role in the understanding of the spectra of solids. First the frequency of a phonon either in the acoustical or optical modes, varies with momentum throughout the Brillouin zone (the maximum $k = 2\pi/q$ where q is the

crystal lattice constant). For example, Fig. 11 shows how the frequency varies with momentum for two acoustical modes and two optical modes. With a visible source of light, where $|k| = \nu/c \cong 10^5$ cm^{-1}, a 90^0 scattering will create or destroy with $|k| \cong 10^5$ cm^{-1}; in the scale of Fig.11 this $|k|$ is very small so we often refer to the Raman effect measuring the $|k| \cong 0$ phonon. Let us examine the

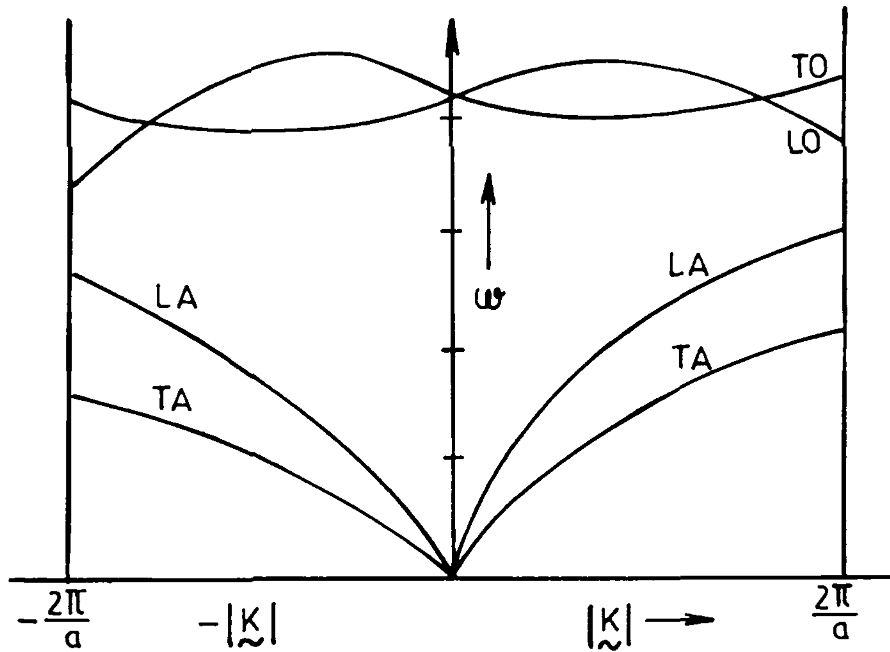

Fig. 11

influence of this conservation of momentum in another case. In case of solids which have a doubly degenerate phonon of symmetry E which is both Raman and IR active. When IR active in the X direction its polarizability tensor components xz and zx are different from zero. On the other hand, when the phonon is polarized in the y direction the yz and zy polarisability components are different from zero. Imagine that we are looking at the xz polarizability component of this E, line; if the light is incident in the z direction and the observation is made along the y direction, by conservation of momentum, a phonon is produced in the yz plane with z polarisation (since we are measuring

the xz component of the tensor). So this phonon has a propagation direction perpendicular to its polarisation and is a transverse optical phonon (TO). If, still measuring the xz spectrum, the light is incident in the z direction and the observation is in the x direction we produce a phonon in the xz plane with x polarisation. This observed phonon is both transverse (propagation ⊥ to polarisation) and longitudinal (LO). Since the transverse and longitudinal phonons have different frequences we observe two lines. So in the z (xz) y spectrum we see only one line, the TO phonon, while in the z (xz)x spectrum we see two E, lines, the TO and LO phonons.

Our Raman scattering studies are concerned with the surface depletion layer at etched GaAs surfaces before and after passivation or other surface treatment. It is known that at the surface of III-V semiconductor compounds a space charge layer may exist in which the density of charge carriers is different from that in the bulk. The width and character of this layer depends on the carrier density and the location of the surface Fermi level. For example, at real surfaces of n- and p-type GaAs there are depletion layers with widths as small as 100 A. In the general case, for optical penetration depths larger than the depletion widths, the Raman spectra will show the bands of the coupled modes from the bulk as well as the uncoupled LO phonon band from the depletion layer. The intensity of the LO phonon band from the depletion layer has been shown to depend on the width of the layer and the penetration of the incident light.

The selection rules for first order Raman scattering by the optical phonons of the zinc blende structure III-V compounds are obtained from the raman tensors tabulated by Loudon [157]. Scattering by LO phonons is allowed in back scattering spectra from (100) and

(111) surfaces and forbidden in those from the cleavage (110) surfaces. For incident photon energies in resonance with the Eo, Eo + Δo, E_1 and E_1 + ΔE_1 optical energy gaps, scattering by LO phonons is also observed in backscattering from (110) surfaces. Thus, in the case of degenerate III-V compounds, a surface of arbitrary orientation can be studied by surface Raman spectroscopy of LO phonons and their coupled modes. In the backscattering configuration used, Raman scattering by TO phonons is allowed and is independent of the electric field. There is an increase of the LO phonon intensity with the occurence of a surface electric field and there is always a LO phonon like peak present even at flat band conditions.

A quantitative analysis, as described below, allows us to determine in each case the band bending in the GaAs depletion layer. This gives us an independent technique for evaluating the contribution of changes in band bending to Schottky barrier formation.

Mills [158] has given a theoretical discussion of LO phonons in a surface space charge region of doped polar semiconductors. He found that in the depletion layer there are well defined modes with frequency w_{LO}, identical to that of LO phonons in the undoped crystal. Further into the sample, where the local carrier density approaches that in the bulk, the mode becomes exponentially damped. On the basis of these results we are going to assume, for the quantitative analysis, that Raman scattering by the LO phonons in the depletion layer is similar that in an undoped crystal.

For a doped opaque semiconductor with a penetration depth D and a depletion width δ, such that $\delta < D$, the intensity I (LO) of the LO phonon is given by

$$I\ (LO) - I_o\ (LO)\ (1 - e^{-2\delta/D}), \qquad 20$$

where I_o (LO) is the LO phonon intensity of the undoped semiconductor. Similarly, it is possible to write for the intensity I (TO) of the TO phonon peak. This TO or in some cases the L^- phonon-plasmon peak is used as a reference. It does not depend on the surface electric field.

$$I\ (TO) = I_o\ (TO)\ e^{-2\delta/D} \qquad 21$$

where I_o (TO) would be the intensity of the TO peak if there were no depletion layer. Taking the ratio of eqn 20 and 21 gives

$$[I(LO)/I(TO)] = [I_o(LO)/I_o(TO)]\ [(1 - e^{-2\delta/D})/(e^{-2\delta/D})] \qquad 22$$

For the untreated GaAs it is possible to calculate the ratio I_o (LO)/I_o(TO) from the experimentally determined ratio I(LO)/I(TO). In equations (1) to (3), excludes the 50 A transition region between the depletion layer and the bulk, such that $\delta = \delta_o - 50$ Å and δ_o is given by

$$\delta_o = [(\epsilon_o K \phi_B)/(2\pi n e^2)]^{1/2} \qquad 23$$

where ϵ_o is the permittivity of free space

K is the dielectric constant of GaAs

ϕ_B is the barrier height

n is the carrier density

e is the electronic charge

Using equations (3) and (4), ϕ_B can be calculated from the ratio of I(LO)/I(TO).

2B.8.3 Photoluminescence Spectroscopy (PL):

Photoluminescence spectroscopy is another effective method for obtaining information critical in the production of semiconductor devices. Like Raman scattering, PL offers the advantages of a non-contact and non-destructive technique. It is superior to commonly used methods like Hall effect and resistivity measurements, because these techniques are difficult to employ with high resistance materials

because of instrumental limiations, sample preparation and data interpretation.

Basically the phenomenon of PL involves exciting the sample with a laser light and then analysing the emission with a spectrometer equipped with an appropriate detector. The energy of the excitation should be greater than the bandgap of the sample. An argon ion laser with line at 488 nm and 10-100 mW power over a 1 mm diameter spot is normally used. The method gives information both on intrinsic and extrinsic semiconductor properties.

The PL process can generally be considered as comprising of three distinct events in sequence. First, an electron hole pair is excited, usually by the absorption of a photon. Second, the electron and hole relax down in energy by emitting a series of phonons and usually end up in band edge localised states. Finally, there is a recombination, either by luminescence or by some non radiative mechanism. Various aspects of the luminescence experiment explore each of these different events. Some of the characteristics of the PL spectrum are that, at low temperature there is usally an intense emission. When temperature is increased, the luminescence intensity decreases and the peak moves to lower energy. In addition the peak is most intense in samples in which the defect density is lowest, which implies that intrinsic states are involved.

2B.8.4 X-Ray fluorescence Analysis (XRF) :

A schematic of the processes leading to X-ray fluorescence is shown in Fig.12a. The continuous radiation (Bremstrahlung) emitted from the anode of high power X-ray tube is incident on the sample. The energy rich X-ray quanta excite the atoms of the sample by raising the electrons out of the inner shells (K,L) into higher orbits or by

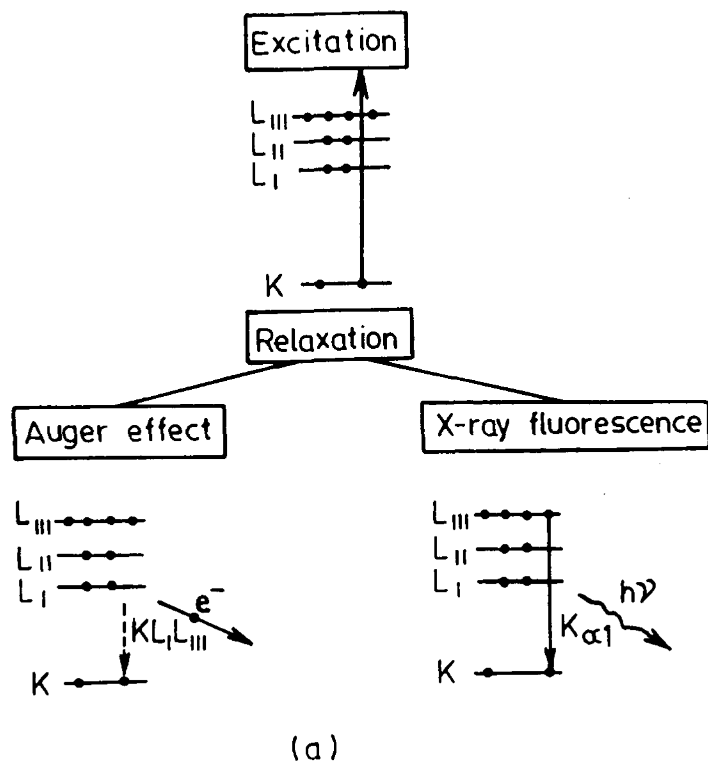

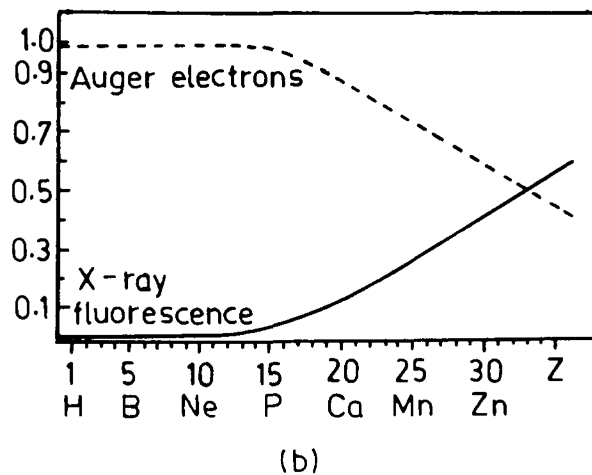

Fig.12(a): Schematic of the processes leading to XRF and Auger effect.

(b): Excitation probabilities of XRF and Auger electrons if the primary excitations occured in the K-shell.

filled by electrons from the outer shells; thus, X-ray line spectra (K,L,M) are emitted which are characteristic of that particular atom type. This process is termed fluorescence. The fluorescence produced in the sample is detected by

- wavelength dispersive means or
- energy dispersive means

From this, information regarding

- qualitative analysis : position of energy of spectra
  = type of element.
- quantitative analysis : number of pulses
  = amount of element under investigation

  can be obtained.

Some of the advantages of this technique are

-it is free of any interference

-can be easily automated

-high sensitivity of detection (1-100 ppm)

-possesses high degree of accuracy

Some of the disadvantages are

-elements with atomic number less than 6 cannot be detected and

-elements with $Z < 12$ detected but with low sensitivity.

Fig.12b shows the excitation probabilities of XRF if the primary ionisation occured in the K shell. Similar curves can be obtained for other excitations.

By taking this probability factor and the peak height corresponding to the particular element, the concentration of the element in the compound can be established. This also gives an idea of the stoichiometric ratios of the different elements in the compound.

REFERENCES

1. C. H. Henry, R. A. Logan, F. R. Merritt, J. Appl. Phys. **49,** 3530 (1978).
2. N. Barbouth, Y. Berthier, J. Oudar, J. M. Moison, M. Bensoussan, J. Electrochem Soc. 133, 1663 (1986).
3. R. Iyer, R. R. Chang, D. L. Lile, Appl. Phys. Lett. **53,** 134 (1988).
4. D. J. Olego, R. Schacter, J. Baumann, Solid State Commu. **53,** 90 (1985).
5. D. J. Olego, R. Schacter, J. Baumann, J. Vac. Sci. Technol. B, **3,** 1097 (1985).
6. D. J. Olego, R. Schacter, J. A. Baumann, Appl. Phys. Lett. **45,** 1127 (1984).
7. R. Schacter, D.J. Olego, J.A. Baumann, L.A. Bunz, P.M. Raccah, W.E. Spicer, Appl. Phys. Lett. **47,** 272 (1985).
8. R. Schacter, D.J. Olego, J.A. Baumann, C.G. Michel, M.A. Kuck, L.G. Polgar, P.M. Raccah, W.E. Spicer, Proc. of the 17th Int. Conf. on the Physics of semiconductors, San Francisco.
9. Y.H.Jeong, S.Takagi, F.Arai, T.Sugano, J.Appl.Phys. **62,** 2370 (1987).
10. C.O. Thermond, G.P. Schwartz, C.W. Kammlot, B. Schwartz, J. Electrochem. Soc. **127,** 1366 (1980).
11. E. Capasso, G.F. Williams, J. Electrochem. Soc. **129,** 921 (1982).
13. S.D. Mukherjee, D.W. Woodard, Gallium Arsenide (Wiley, New York) Chap. 4 (1985).
14. E. Yablonovitch, C.J. Sandroff, R. Bhat, T. Gmitter, Appl. Phys. Lett. **51,** 439 (1987).

15. C.J. Sandroff, R.N. Nottenburg, J.C. Bischoff, R. Bhat, Appl. Phys. Lett. **51**, 33 (1987).

16. R.N. Nottenburg, C.J. Sandroff, D.A. Humphrey, T.H. Hollenbeck, R. Bhat, Appl. Phys. Lett. **52**, 218 (1988).

17. B.J. Skromme, C.J. Sandroff, E. Yablonovitch, T. Gmitter, Appl. Phys. Lett. **51**, 2022 (1987).

18. L.A. Farrow, C.J. Sandroff, M.C. Tamargo, Appl. Phys. Lett. **51**, 1931 (1987).

19. M.S. Carpenter, M.R. Melloch, M.S. Lundstorm, S.P. Tobin, Appl. Phys. Lett. **52**, 2157 (1988).

20. R.S. Besser, C.R. Helms, Appl. Phys. Lett. **52**, 1707 (1988).

21. C.J. Spindt, R.S. Besser, R. Cao, K. Miyano, C.R. Helms, W.E. Spicer, Appl. Phys. Lett. **54**, 1148 (1989).

22. E. Yaltonovitch, B.J. Skromme, R. Bhat, J.P. Harbison, T.J. Gmitter, Appl. Phys. Lett. **54**, 555 (1989).

23. Y. Nannichi, Jia-Fa-Fan, H. Oigawa, A. Koma, Jap. J. Appl. Phys. **27**, L2367 (1988).

24. C.J. Sandroff, M.S. Hegde, L.A. Farrow, C.C. Chang, J.P. Harbison, Appl. Phys. Lett. **54**, 362 (1989).

25. B.A. Cowans, Z. Dardas, W.N. Delglass, M.S. Carpenter, M.R. Melloch, Appl. Phys. Lett. **54**, 365 (1989).

26. Jia-Fa-Fan, H. Oigawa, Y. Nannichi, Jap. J. Appl. Phys. **27**, L2125 (1988).

27. M.S. Carpenter, M.R. Melloch, T.E. Dungan, Appl. Phys. Lett. **53**, 66 (1988).

28. C.W. Wilmsen, P.D. Kirchner, J.M. Woodall, J. Appl. Phys. **64**, 3287 (1988).

29. J.M. Woodall, G.D. Petit, T. Chappell, H.J. Ho, J. Vac. Sci. Technol. **16**, 1389 (1979).

30. J. Massies, J.P. Contour, Appl. Phys. Lett. **46**, 1150 (1985).

31. C.W. Wilmsen, P.D. Kirchner, J.M. Woodall, J. Vac. Sci. Technol. B, **6**, 1180 (1988).

32. S.D. Offsey, J.M. Woodall, A.C. Warren, P.D. Kirchner, T.I. Chappell, G.D. Petit, Appl. Phys. Lett. **48**, 475 (1986).

33. Z. Meglicki, B.D. Nena, K. Prasad, H.S. Sharda, L. Faraone, A.G. Nassibian, Jpn. J. Appl. Phys. **27**, L290 (1988).

34. H. Hasegawa, T. Saitoh, S. Konishi, H. Ishi, H. Ohno, Jap. J. Appl. Phys. **27**, L2177 (1988).

35. E.Y. Chang, G.T. Cibuzai, J.M. Vanhove, R.M. Nagarajan, K.P. Pande, Appl. Phys. Lett. **53**, 1638 (1988).

36. S. Okamura, H. Nishi, T. Inada, H. Hashimoto, Appl. Phys. Lett. **40**, 689 (1982).

37. F. Hasegawa, T. Takahashi, K. Kubo, S. Ohnari, Y. Nannichi, T. Arai, Jpn. J. Appl. Phys. **26**, L1448 (1987).

38. B. Bayraktaroglu, R.L. Johnson, J. Appl. Phys. **52**, 3515 (1981).

39. R. Padmanabhan, B.J. Miller, G. Tam, Mats. Res. Soc. Symp. Proc. **101**, 379 (1988).

40. M. Mizuta, S. Fujieda, Y. Matsumoto, T. Kawamura, Jpn. J. Appl. Phys. **25**, L945 (1986).

41. S. Fujieda, M. Mizuta, Y. Matsumoto, Jpn. J. Appl. Phys. **26**, 2067 (1987).

42. S. Fujieda, M. Mizuta, Y. Matsumoto, Jpn. J. Appl. Phys. **27**, L296 (1988).

43. L.C. Zhang, S.K. Cheung, C.L. Liang, N.W. Cheung, Appl. Phys. Lett. **50**, 445 (1987).

44. E. Pincik, B. Matako, J.Bartos, I. Thurzo, M. Grendel, V. Nadazzly, M. Zubekova, M. Morvik, Phys. Stat. Sol. (a) **106,** 659 (1988).

45. K. Akimoto, I. Hirosawa, J. Mizuki, S. Fujieda, Y. Matsumoto, J. Matsui, Jap. J. Appl. Phys. **27,** L1401 (1988).

46. M.D. Clark, C.L. Anderson, J. Vac. Sci. Technol. **21,** 453 (1982).

47. R.P.H.Chang, J.J.Coleman, A.J.Polac, L.C.Feldman, C.C.Chang, Appl.Phys.Lett.**34,**237 (1979).

48. S.Gourrier,A.Mircea,M.Bacal, Thin. Sol. Films,**65,** 315 (1980).

49. P.Friedal, J.P.Landesman, Phil. Mag. B, **55,** 711 (1987).

50. A. Callegari, P.D. Hoh, D.A. Buchanan, D. Lacey, Appl. Phys. Lett. **54,** 332 (1989).

51. C.E. Dube, S. P. Tobin, J.I. Hanoka, IEEE 19th Photovoltaic Spec. Conf, 1516 (1987).

52. S.J. Pearton, C.S. Wu, M. Stavola, F. Ren, J. Lopata, W.C. Dautremont-Smith, S.M. Vernon, V.E. Haven, Appl. Phys. Lett., **51,** 496 (1987).

53. B. Pajot, R.C. Newman, R. Murray, A. Jalil, J. Chevallier, R. Azoulay, Phys. Rev. B **37,** 4188 (1988).

54. W.C. Dautremont-Smith, J.C. Nabity, V. Swaminathan, M. Stavola, J. Chevallier, C.T. Tu, S.J. Pearton, Appl. Phys. Lett. **49,** 1098 (1986).

55. A. Jalil, J. Chevallier, J.C. Pesant, R. Mastefaolier, B. Pajot, P. Murawala, R. Azoulay, Appl. Phys. Lett. **50,** 439 (1987).

56. Jorg Weber, S.J. Pearton and W.C. Dautremont-Smith, Appl. Phys. Lett. **49,** 1181 (1986).

57. J. Chevallier, W.C. Dautremont-Smith, C.W. Tu, S.J. Pearton, Appl. Phys. Lett. **47,** 108 (1985).

58. N. Pan, S.S. Bose, M.H. Kim, G.E. Stillman, F. Chambers, G. Devane, C.R. Ito, M. Feng, Appl. Phys. Lett. **51**, 596 (1987).

59. Y.A. Aleshchenko, L.K. Vodopyanov, E.M. Omeljanovsky, A.V. Pakhomov, A.Y. Polyakov, Solid State Commu. **70**, 123 (1989).

60. J. Saito, K. Nanbu, T. Bhiwara, K. Kondo, Jpn. J. Appl. Phys. **27**, L202 (1988).

61. A. Djemel, J. Castaing, J. Chevallier, Rev. Phys. Appl. **23**, 1337 (1988).

62. T.M. Kerr, P.C. Peacock, C.E.C. Wood, J. Appl. Phys. **63**, 1494 (1988).

63. R.J. Nelson, J.S. Williams, H.J. Leamy, B. Miller, H.C. Casey Jr. B.A. Parkinson, A. Heller, Appl. Phys. Lett. **36**, 76 (1980).

64. Hsu Jung Kuei, Lau Kei Mary, J. Appl. Phys. **63**, 962 (1988).

65. M. Tabib Azar, A.S. Dewa, W.H. Ko, Appl. Phys. Lett. **52**, 206 (1988).

66. P. Allongue, H. Cachet, M. Fournier, N.A. Yao, Electrochim Acta **33**, 693 (1988).

67. J.P. Contour, J. Massies, H. Fronius, K. Ploog, Jap. J. Appl. Phys. **27**, L167 (1988).

68. K.H. Kim, H. Ishiwara, T. Asano, S. Furukawa, Jpn. J. Appl. Phys. 27, L2180 (1988).

69. H. Ishiwara, K.H. Kim, K. Tsuti, T. Asano, S. Furukawa, Proc. Electrochem. Soc. **88**, 278 (1988).

70. Y. Yamada, M. Oshima, T. Waho, T. Kawamura, S. Maeyama, T. Miyahere, Jpn. J. Appl. Phys. **27**, L1196 (1988).

71. H. Hasegawa, H.L. Hartnagel, J. Electrochem. Soc. **123**, 713 (1976).

72. R.J. Nuzzo, B.R. Zegarski, L.H. Dubois, J. Am. Chem. Soc. **109**, 734 (1987).

73. Xu Zhigang, G. Horowitz, F. Garnier, J. Electroanal. Chem. Interfacial Electrochem. **246**, 467 (1988).

74. S. Takatani, Y. Uchida, T. Yakotsuka, H. Nakeshima, Jpn. J. Appl. Phys. **26**, L1770 (1987).

75. R.K. Ahrenkiel, L.L. Kazmerski, P.J. Ireland, O. Janjaum, P.E. Russel, D. Dunlavy, R.S. Wagner, S. Pattilo, T. Jervis, J. Vac. Sci. Technol. **221**, 434 (1982).

76. B. Bayraktaroglu, R.L. Johnson, D.W. Langer, M.G. Mier, The Physics of MOS Insulators ed. G. Lucovsky, S.T. Pantelides and F.L. Galeener, Oxford Pergamon Press (pp 207-11) (1980).

77. L.A. Farrow, C.J. Sandroff, Proc. SPIE-Int. Soc. Opt. Eng. 822 (1987).

78. Vardhireddy Manorama, S.V. Bhoraskar, V.J. Rao, S.T. Kshirsagar, To appear in Appl. Phys. Lett. Oct. 1989.

79. A. Pinczuk, E. Burstein, Phys. Rev. Lett. **21**, 1073 (1968).

80. R. Tsu, H. Kawamura, L. Esaki, Solid State Commu. **15**, 32 (1974).

81. V.I. Zemski, E.L. Ivchenko, D. Mirlin, I.I. Reshi, Solid State Commu. **16**, 221 (1975).

82. A. Pinczuk, A.A. Ballman, R.E. Nahory, J.M. Worlock, J. Vac. Sci. Technol. **16**, 1168 (1979).

83. H. Shen, F.H. Pollack, R.N. Sacks, Appl. Phys. Lett. **47**, 891 (1985).

84. H.J. Stolz, G. Abstreiter, Solid State Commu. **36**, 857 (1980).

85. H.J. Stolz, G. Abstreiter, J. Vac. Sci. Technol. **19**, 380 (1981).

86. J. Wagner, H. Seelewind. J. Appl. Phys. **64**, 2761 (1988).

87. H.D. Yao, A. Compaan, E.B. Hale, Solid State Commu. **56**, 677 (1985).

88. T. Suzuki, M. Ogawa, Appl. Phys. Lett. **31**, 473 (1977).

89. D. Guidotti, E. Hasan, H.J. Hovel, M. Albert, Appl. Phys. Lett. **50**, 912 (1987).

90. H. Venghaus, J. Lumin. **16**, 331 (1978).

91. V.J. Rao, Vardhireddy Manorama, S.V. Bhoraskar, Appl. Phys. Lett. **54**, 1799 (1989).

92. L. Jastrezebski, J. Lagowski, H.C. Gatos, Appl. Phys. Lett. **27**, 537 (1975).

93. E. Yablonovitch, D.L. Allara, C.C. Chang, T. Gmitter, T.B. Bright, Phys. Rev. Lett. **57**, 249 (1986).

94. E. Yablonovitch, R. Bhat, J.P. Harbison, R.A. Logan, Appl. Phys. Lett. **50**, 1197 (1987).

95. S. M. Beck, J.E. Wessel, Appl. Phys. Lett. **50**, 149 (1987).

96. E. Dartyge, A. Fontaine, A. Jucha, G. Tourillon, J.F. Peray, R. Jouband, P. Alnot, J. Phys. Colloq. (C8 Vol.1) 1986.

97. T.M. Valahas, J.S. Sochanski, H.C. Gatos, Surf. Sci. **26**, 41 (1971).

98. W.Platen, H.J.Schmutzler, D.Kohl, K.A.Brauchle, K. Wolter J.Appl.Phys. **64**, 218 (1988).

99. D.E. Aspnes, Surf. Sci. **132**, 406 (1983).

100. W.E. Spicer, P. W. Chye, P.R. Skeath, C.Y. Su, I. Lindau, J. Vac. Sci. Technol. **16**, 1427 (1979).

101. W.E. Spicer, I. Lindau, P.R. Skeath, C.Y. Su, J. Vac. Sci. Technol. **17**, 1019 (1980).

102. W.E. Spicer, I. Lindau, P.R. Skeath, C.Y. Su, P.W. Chye, Phys. Rev. Lett. **44**, 420 (1980).

103. N. Newman, W.E. Spicer, T. Kendelewicz, I. Lindau, J. Vac. Sci. Technol. B 4, 931 (1986).

104. W.E. Spicer, T. Kendelelwicz, N. Newman, R. Cao, C McCants, K. Miyano, I. Lindau, Z. Lillienthal-Weber, E.R. Weber, Appl. Surf. Sci. 33/34, 1009 (1988).

105. J.M. Woodal, J.L. Freeouf, J. Vac. Sci. Technol. **19**, 794 (1981).

106. R.E. Viturro, J.L. Shaw, L.J. Brillson, J.M. Woodal, P.D. Kirchner, G.D. Pettit, S.L. Wright, J. Vac. Sci. Technol. B, **6**, 1397 (1988).

107. V.L. Berkovits, V.A. Kiselev, T.A. Minashvilli, V.I. Safarov, Solid State Commun. **65**, 385 (1988).

108. A.Ismail, J.M. Palau, J. Appl. Phys. **60**, 1730 (1986).

109. K. Stiles, D. Mao, A. Kahn, J. Vac. Sci. Technol. B. **6**, 1170 (1988).

110. W. Walukiewicz, Phys. Rev. B. **37**, 4760 (1988).

111. K. Stiles, A. Kahn, Phys. Rev. Lett. **60**, 440 (1988).

112. X. Zhang, Bandoti Xuebao **8**, 643 (1987).

113. T.T. Chiang, C.J. Spindt, W.E. Spicer, I. Lindau, R. Browning, J. Vac. Sci. Technol. B **6**, 1409 (1988).

114. H.H. Weider, J. Vac. Sci. Technol. **14**, 1498 (1978).

115. G.P. Schwartz, G.J. Guattieri, J. Electrochem. Soc. **133**, 1266 (1986).

116. A.M. Cowley, S.M. Sze, J. Appl. Phys. **46**, 3212 (1965).

117. M.L. Cohen, Adv. Electron. Electron Phys. **51**, 1 (1980).

118. J. Pollman, Festkorperprobleme, **20**, 117 (1980).

119. M. Schluter, Festkorperprobleme, **18**, 155 (1978).

120. W.E. Pickett, S.G. Louie, M.L. Cohen, Phys. Rev. B **17**, 815 (1978).

121. W.E. Pickett, M.L. Cohen, Phys. Rev. B **18**, 939 (1978).

122. J. Ihm, M.L. Cohen, Phys. Rev. B **20**, 729 (1979).

123. A. Madhukar, J. Delgado, Solid State Commun. **37**, 199 (1981).

124. G. Margaritondo, N.G. Stoffel, A.D. Katani, H.S. Edelman, C.M. Bertoni, J. Vac. Sci. Technol. **18**, 784 (1981).

125. A.D. Katani, R.R. Daniels, Te-Xiu Zhao, G. Margaritondo, J. Vac. Sci. Technol, **20**, 662 (1982); G. Margaritondo, Bull. Am. Phys. Soc. Ser. II, **27**, 140 (1982).

126. P. Perfertti, D. Denley, K.A. Mills, D.A. Shirley, Appl. Phys. Lett. **33**, 667 (1978).

127. E.A. Kraut, R.W. Grant, J.R. Waldrop, S.P. Kowalzyk, Phys. Rev. Lett. **44**, 1620 (1980).

128. R.S. Bauer, J.C. McMenamin, J. Vac. Sci. Technol. **15**, 1444 (1978).

129. R.W. Grant, J.R. Waldrop, E.A. Kraut, J. Vac. Sci. Technol, **15**, 1451 (1978); Phys. Rev. Lett. **40**, 656 (1978).

130. W. Monch, R.S. Bauer, H. Gant, R. Murschall, J. Vac. Sci. Technol. **21**, 498 (1982); W. Monch, Bull. Am. Phys. Soc. Ser. II 27, 141 (1982); W. Monch, H. Gant, J. Vac. Sci. Technol. **17**, 1094 (1980).

131. J.R. Waldrop, R.W. Grant, Phys. Rev. Lett. **43**, 1686 (1979).

132. J.R. Waldrop, S.P. Kowalczyk, R.W. Grant, E.A. Kraut, D.L. Miller, J. Vac. Sci. Technol. **19**, 573 (1981).

133. S.P. Kowalczyk, W.J. Schaffer, E.A. Kraut, R.W. Grant, J. Vac. Sci. Technol. **20**, 705 (1982).

134. D.W. Tu, A. Kahn, J. Vac. Sci. Technol. **A2**, 511 (1984).

135. M.R. Czerniak, P. Lilley, J. Cryst. Growth, **59**, 455 (1982).

136. P. Lilley, M.R. Czerniak, J.E. Nicholls, J.J. Davies, J. Cryst. Growth, **59**, 161 (1982).

137. F.A. Ponce, W. Stutius, J.G. Werthen, Thin Sol. Films, **104**, 133 (1983).

138. R.N. Bhargava, J. Crys. Growth, **86**, 873 (1988).

139. J.Petruzello, B.L.Greenberg, D.A.Cammack, R.Dalby, J. Appl. Phys. **63**, 99 (1988).

140. Y.Hishida, K.Yoneda, N.Matsunami, N.Itoh, J. Appl. Phys. **62**, 4460 (1988).

141. P. Besomi, K. Christianson, B.W. Wessels, Thin Sol. Films, **55**, 113 (1981).

142. P.L. Jones, D. Moore, D.R. Cotton, J. Cryst. Growth, **59**, 183 (1982).

143. D. Shen, K. Zhang, R. Fu, Appl. Phys. Lett. **53**, 500 (1988).

144. D.J. Olego, Appl. Phys. Lett. **51**, 1422 (1987).

145. S.K.Gandhi, S.Tyagi, R.Venkatasubramanian, Appl.Phy.Lett.**53**, (1988).

146. S.M.Sze, Physics of semiconductor devices, 2nd Edn. (Wiley,New York) p.393, (1981).

147. O.C.Wells, Scanning Electron Microscopy New York:McGraw Hill, p.238, (1974).

148. F.Berz, H.K.Kuiken, Solid State Electron. **19**, 437 (1976).

149. H.K.Kuiken, Solid State Electron. **19**, 447 (1976).

150. A.J.R.de Kock, Appl.Phys.Lett.**27**, 313 (1975).

151. D.B.Holt, R.Ogden, Solid State Electronics, **19**, 37 (1976).

152. H.Menninger,H.Raidt, and G.Voigt, Phys.Stat.Sol.(a), **35**,639 (1976).

152. W.Czaja, J.Appl.Phys.**37**,4236 (1966).

153. C.van.Opdorp, R.C.Peters, M.Klerk, Appl.Phys.Lett. **24**,125 (1974).

154. M.Watanabe, G.Actor, H.C.Gatos, IEEE Trans. Electron Devices, **ED-24**, 1172 (1977).

155. W.H.Hackett, J.Appl.Phys. **43**,1649 (1972).

156. J.R.Young, J.Appl.Phys. **28**, 524, (1957).

157. R.Loudon, Adv. Phys. **13**, 423 (1964).

158. D.L.Mills,Vijnana Parishad Anusandhan Patrika **14**, 115 (1971).

Chapter 3

GaAs / Polythiophene System

3.1 INTRODUCTION

The development of high speed electronic devices based on III-V semiconductors has been hampered by problems encountered in proper passivation of the semiconductor surfaces. The pinning of energy levels at surface defects and instability of native oxides require solutions that are different from those of silicon based devices. The oxides of gallium and arsenic and the presence of elemental arsenic on the surface have been shown to be responsible for the large density of states in the gap. The high energy barriers due to Fermi level pinning around midgap, large surface recombination velocity (SRV) and high surface state density are characteristics of GaAs surfaces [1-3]. These properties continue to limit the performance of certain minority carrier devices such as bipolar transistors, by providing channels for surface recombination. Because of its important impact on insulated gate field effect devices, surface passivation has been approached by depositing amorphous dielectrics (like Al_2O_3, SiO_2, Si_3N_4 etc.) [4-6] or epitaxial growth of high resistivity semiconductors (AlGaAs) [7], for metal insulator semiconductor field effect transistors (MISFETs). More recently the notion of a group V element containing dielectric (P_3N_5) [8] to prevent loss of the volatile group V element from the semiconductor surface was applied to improve the semiconductor insulator interface.

There were several attempts in the past to passivate the surface of GaAs with overlayers of amorphous phosphorous or sulphur or compounds of sulphur like Na_2S, $(NH_4)_2S$ etc. Particularly sulphur is known to be a versatile element with regard to GaAs and it forms many compounds with both Ga and As. The chalcogenides have been cited on several occassions for being able to lower the surface density of

states in GaAs, a result presumably of a strong affinity between S and GaAs. But as yet no completely successful scheme has been established, which passivates the GaAs interface both electronically and chemically while permitting the growth of an insulating barrier.

Some of the other specifications to be met with by the passivating material include :

i) It should serve as a protective layer and thereby prevent reaction between the GaAs surface and the outside atmosphere.

ii) It should chemically satisfy the dangling bonds responsible for the high density of states in the gap.

iii) It should be a good insulator for use in GaAs MISFETs.

iv) It should stand appreciably high temperatures which are unavoidable during device fabrication and processing (typically >300 ^{o}C).

v) It should itself be stable and not degrade with time or other treatments.

vi) It should be selectively etchable.

This chapter deals with the passivation of the GaAs surface made possible by an overlayer provided by a thin film of a polymer. Plasma chemical vapour deposition (PVCD) method was adopted for the deposition of this polymer. By this technique good quality thin adhesive layers of polymers can be deposited onto any substrate in a flawless and uniform manner using a completely pure and dry phase process. The polymer is deposited on the substrate while being polymerised by free radical recombination. The sulphur content of the polymer and the technique of deposition make plasma polymerised thiophene a favourable candidate for the GaAs passivation studies.

The effects of polymer overlayer on the intrinsic properties of GaAs surface have been investigated by means of SEM-EBIC, on the diffusion length and surface recombination velocity. Capacitance - voltage measurements were used to probe the density of states at the GaAs-polymer interface. Spectroscopic techniques like Raman scattering and Photoluminescence also supported our results of the passivation of the GaAs surface.

3.2 EXPERIMENTAL DETAILS

3.2.1 Thiophene:

It is a heterocyclic five membered ring carbon compound with sulphur as one of its constituents. It has a chemical formula C_4H_4S with structural formula

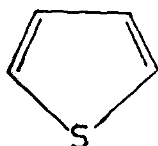

At room temperature it is a colourless liquid with a pungent odour. It has a boiling temperature of $63^{o}C$. Polythiophene is the polymer of this monomer thiophene.

3.2.2 Plasma polymerisation system :

The plasma polymerisation system basically consists of three main parts, namely, the high vacuum pump, the discharge reactor (plasma chamber) and the rf power generator. Except the rotary pump and rf generator all other accessories were fabricated in the laboratory itself. The high vacuum pump includes a mercury diffusion pump backed by a rotary and three liquid nitrogen traps at different stages. The main part of the system is a capacitively coupled discharge reactor. A cylindrical glass dome, having a diameter of 0.18 m and a height of 0.19m, is placed vertically on the base plate with a rubber gasket. The base flange is connected to the vacuum system and it also has

provision for electrical feedthroughs for rf supply, thermocouple and heater connections. A flange similar to the base plate with provision for monomer/gas inlets is placed on the top of the dome. Inside the dome, there are two parallel plate electrodes made of stainless steel, each of 0.15m diameter placed 0.05 m apart. Vacuum of about 10^{-5} torr can be achieved in this system. The rf power supply is a radio frequency transmitter type T1154B of Marconi, USA. This operates only at 4 MHz and 10 MHz. A schematic of the setup is shown in Fig.1 and a photograph of the system is shown on the next page.

3.2.3 Deposition of polythiophene by plasma polymerisation :

The monomer Thiophene obtained from Fluka AG, was distilled before use. The distillation was carried out in dry nitrogen atmosphere by heating the monomer in a water bath. The boiling point of the monomer was monitored by a thermometer held in its vapour.

The system used for the deposition is already described in the previous section. The substrates were placed on the lower plate of the capacitively coupled electrodes. The system was maintained under dynamic vacuum conditions. Initially, the system was evacuated to a low pressure and hydrogen was flushed into the system. Plasma was then excited at a frequency of 10 MHz. This red coloured hydrogen plasma was maintained for about 5 minutes. This H_2 plasma treatment was done to ensure a chemically clean GaAs surface of the substrates. The monomer bulb was then connected to the system via a precision controlled needle valve. The valve was kept open and the monomer frozen using liquid nitrogen and all residual gases in the bulb were evacuated. The monomer warmed up gradually and started boiling at low pressure. the vapours of the monomer thereby entered the chamber to obtain a monomer plasma. The monomer pressure in the chamber was

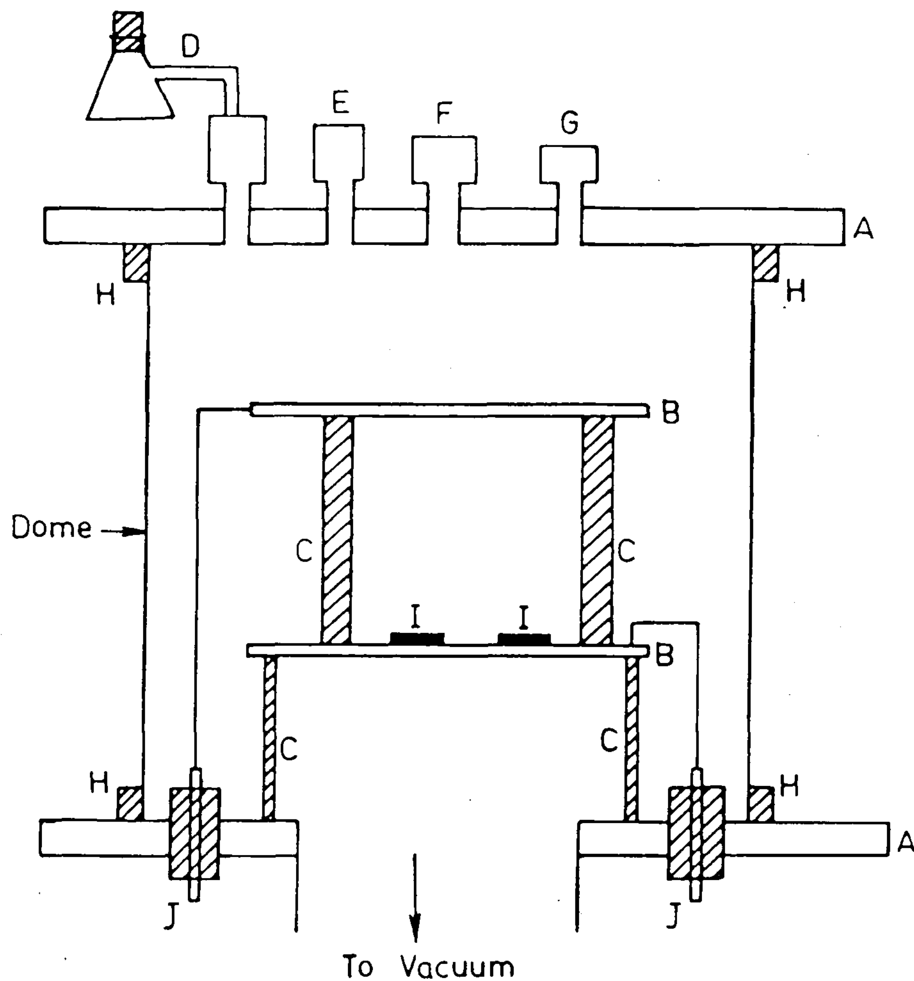

Schematic of the plasma polymerisation chamber

A : Flanges
B : Steel plates
C : Teflon supports
D : Needle valve (monomer inlet)
E : Gas inlet
F : Thermocouple gauge head
G : Leak valve
H : Rubber gaskets
I : Substrates
J : Leads to the rf generator

Fig. 1

maintained at 0.5 Torr. The thiophene plasma was easily distringuished because of its peculiar yellowish brown colour. The monomer thiophene polymerises into polythiophene and gets deposited on the plates and thereby on the GaAs substrates. The deposition was thus carried out for about 15 minutes to obtain a thickness of about 400-500 Å. These films were yellowish brown in colour and very uniform. After the deposition is stopped the system was pumped for further 15 minutes to exhaust any residual monomer vapours.

3.3 METAL POLYTHIOPHENE GaAs (MIS) STRUCTURE :

The GaAs wafers were (100) n type with carrier concentration ~ $10^{17}/cm^3$). These wafers were polished on one side. Prior to any application the wafers were degreased in boiling transene and chemically etched with a solution of 1:1:4:: $H_2O_2:H_2O:H_2SO_4$ and thoroughly rinsed in deionised water. Ohmic contacts were provided by vacuum evaporating Nickel, Germanium and Gold onto the unpolished side of the GaAs wafer and sintering at 440°C for 5 minutes in hydrogen atmosphere. The polished surfaces were then etched with a mild etchant (1:8:500 :: $H_2SO_4:H_2O_2:H_2O$) and rinsed in deionised water prior to polythiophene deposition. After deposition of polythiophene as described in detail in the previous section, the MIS diodes were completed by vacuum evaporation of silver or palladium dots of 0.01 cm diameter. The diodes were tested by observing their current voltage (I-V) characteristics on a tracer. Those diodes which showed ideal Schottky behaviour were used for further characterisation.

3.4 SURFACE PROPERTIES

3.4.1 Capacitance - Voltage : Barrier height measurement :

The effect of surface passivation of GaAs surfaces can be very effectively observed by studying the capacitance-voltage

characteristics of GaAs Schottky diodes with and without the polythiophene passivation layer. In the air exposed GaAs surfaces, there exists a large density of surface states which are responsible for pinning the Fermi level around midgap and thereby a high value for the barrier height is measured. The effect of passivation is to reduce the surface states and effectively the barrier height. A reduction of barrier height by deposition of polythiophene can be easily seen when the capacitance-voltage characteristics at sufficiently high frequencies shift towards lower reverse bias thereby indicating a reduction in barrier height.

The C-V measurements were performed using a Lock in amplifier (Model : EG & G 5204). The values of $1/C^2$ were plotted against V of the n-GaAs/Ag system before and after polythiophene deposition.

3.4.2 SEM-EBIC diffusion length measurements :

The technique of SEM-EBIC to estimate the diffusion length of carriers is already described in section 2B.7.3a. This parameter diffusion length is an important electronic property when studying semiconductor surfaces. It gives an idea of the density of defects on the surface, may be dangling bonds, vacancies etc which are effective in reducing the induced current and thus the collection efficiency of the device. The results of the diffusion length measurements in the study of passivation of GaAs surfaces is important because any reduction in the defect density should show itself in an increase in the diffusion length. As has already been explained in section 2B.7.3a the diffusion length L is obtained from the reciprocal of the slope of ln I versus d straight line. The ln I versus d for the diodes on air exposed GaAs surface and the GaAs surface with polythiophene overlayer were plotted and L was estimated.

3.4.3 SEM-EBIC surface recombination velocity (SRV) measurements :

The SRV is a very versatile electronic property and [9] gives a measure of the recombination centres. The surface of GaAs is plagued by a very high SRV which is detrimental to device operation. The effect of deposition of an overlayer as a passivant should clearly reflect in a decrease of the SRV. The variation of the electron beam induced current I with penetration depth at the surface gives an estimate of the SRV as described in section 2B.7.3b.

$$S = D \, \partial \ln I / \partial \xi \quad , \text{at } \xi = 0$$

where S is the surface recombination velocity cm/sec

I is the EBI current

ξ is the penetration depth

D is the diffusion constant

The ln I versus ξ curves for air exposed and polythiophene deposited n GaAs (100) samples were plotted, and the SRV's were calculated using the above equation.

The EBIC measurements were performed on a scanning Electron Microscope (SEM) (Model: Cambridge 9000) and the EBI current was measured on an electrometer amplifier (Model: EA 815).

3.5 INTERFACIAL PROPERTIES

The Interfacial properties of GaAs/polythiophene were studied using spectroscopic techniques like Raman scattering and photoluminescence. The 400 Å thick layer of polythiophene on the GaAs was most ideal for these studies because the Argon ion laser of wavelength 5145 Å has a penetration depth of about 1053 Å in GaAs which is more than the estimated space charge layer of 500 Å.

3.5.1 Raman Scattering Studies :

The Raman scattering from the GaAs surface were recorded in the

back scattering geometry in which the propagation direction of the incoming and outgoing photons make an angle of 60° between the Laser beam and GaAs surface. The scattered light was analysed with a SPEX 1403 spectrometer and detected with a GaAs photomultiplier. The spectra for the air exposed GaAs surface and GaAs surface with polythiophene overlayer were recorded. The spectra are interpreted on the basis of the explanation given in section 2B.8.2 and the barrier heights for the two cases were calculated using equation 23 these results were compared with those of the barrier height measurements obtained from the C-V measurements.

3.5.2 Photoluminescence (PL) studies :

The PL measurements were performed in the back scattering geometry in which the incident and reflected photons are normal to the front surface of the sample. These spectra were recorded on a Midac PL system at 4.2 K.

3.6 RESULTS AND DISCUSSION

3.6.1 Capacitance - Voltage :

The results of the C-V studies are presented in Fig.2. It gives a plot of $1/C^2$ vs V of the n-GaAs/Ag system before and after the polymer deposition. The reduction in the barrier height from 0.8 to 0.3 eV is a clear indication of the GaAs surface passivation.

3.6.2 EBIC studies :

The results of the EBIC measurements on n-GaAs/Ag surface barrier diodes before and after passivation are shown in Fig.3 and 4 respectively. The curve (a) in both the figures is for GaAs surface which was chemically etched, rinsed in deionised water and then nitrogen dried. The measured L was 5.25 µm and corresponding S was 2.8×10^4 m/s. Curve (b) also measured as in (a) shows the effect of

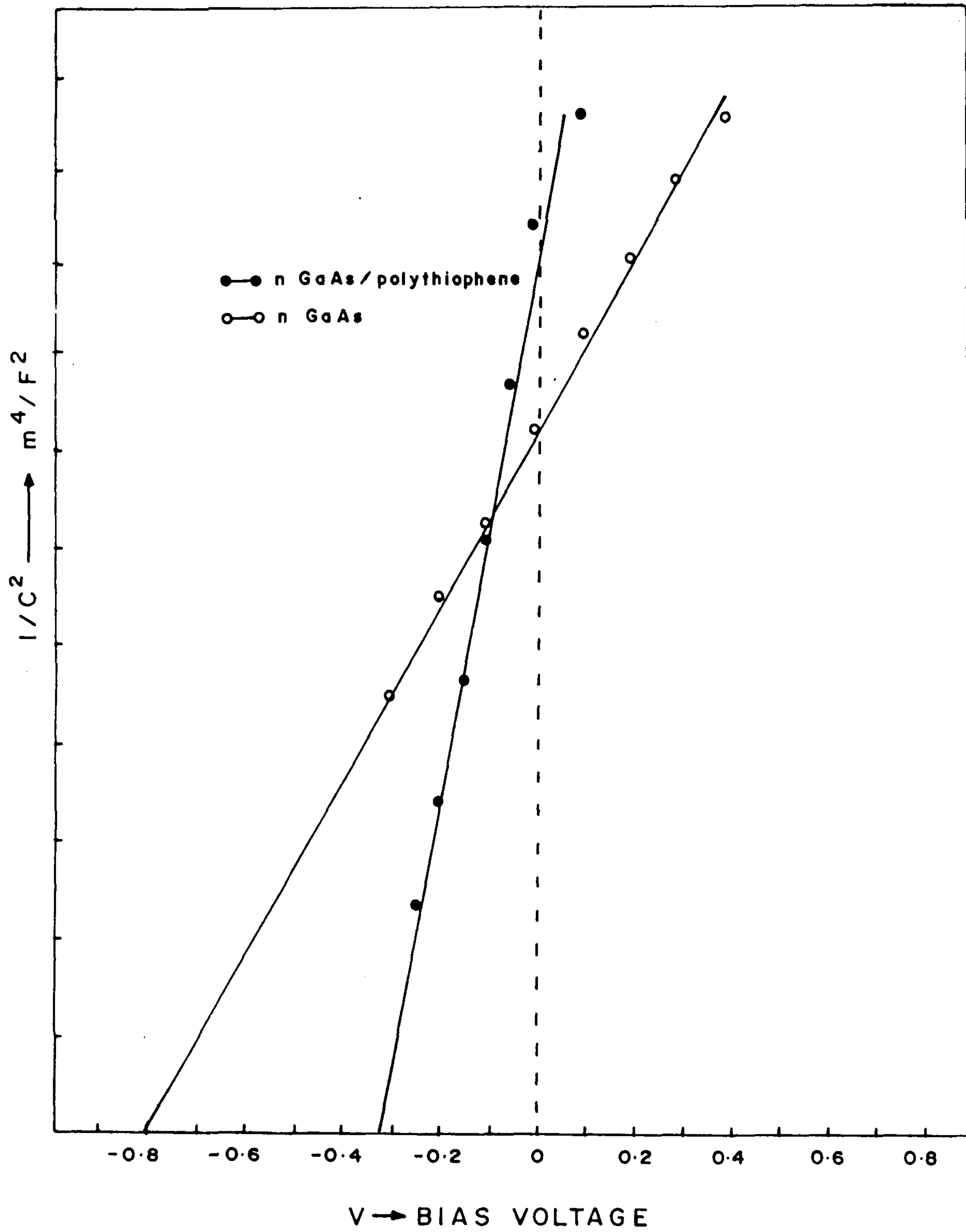

Fig.2. Plot of $1/C^2$ vs V for n-GaAs/Pd system before and after passivation with polythiophene.

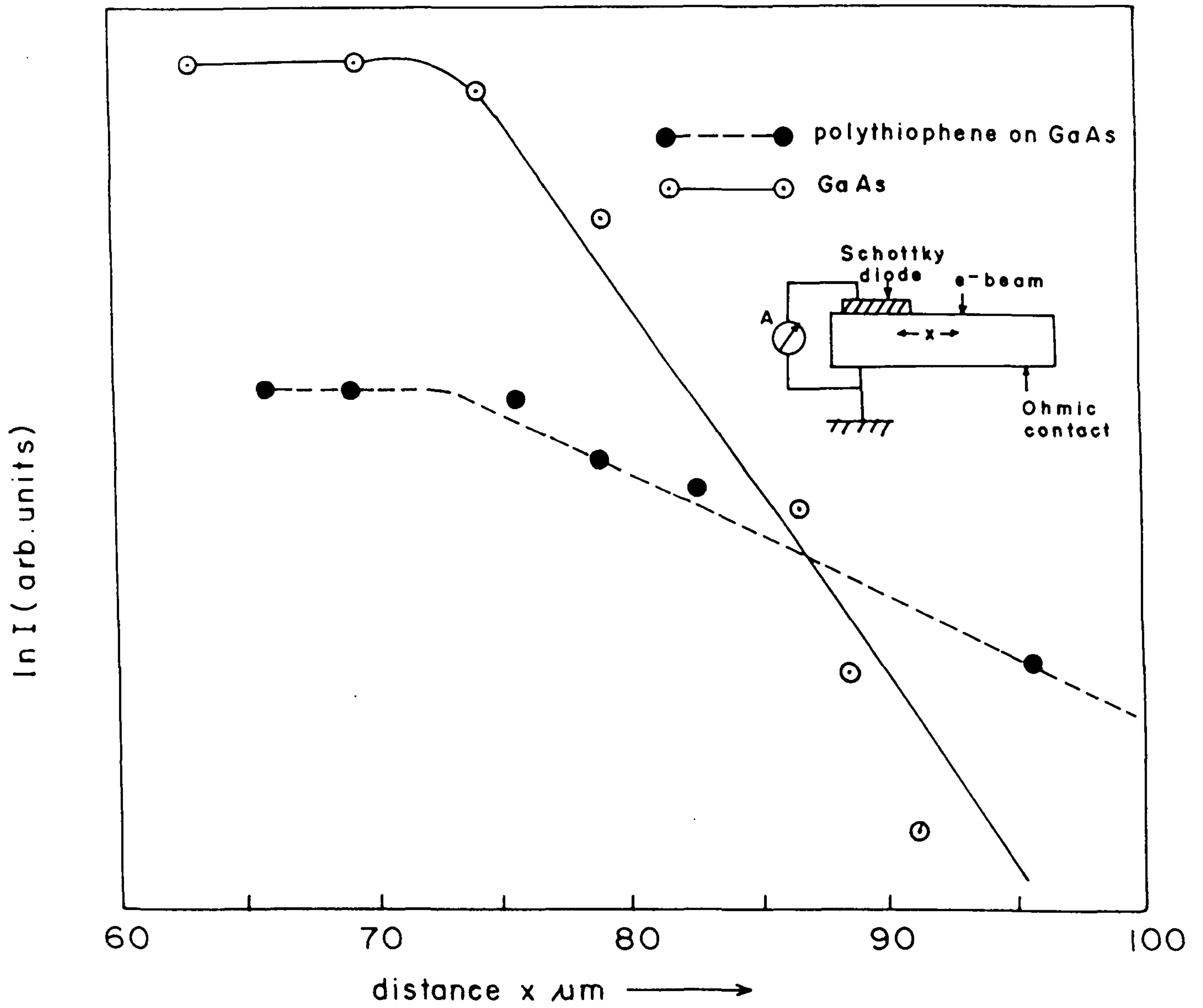

Fig.3. Variation in ln I as a function of distance before and after passivation of n-GaAs with polythiophene.

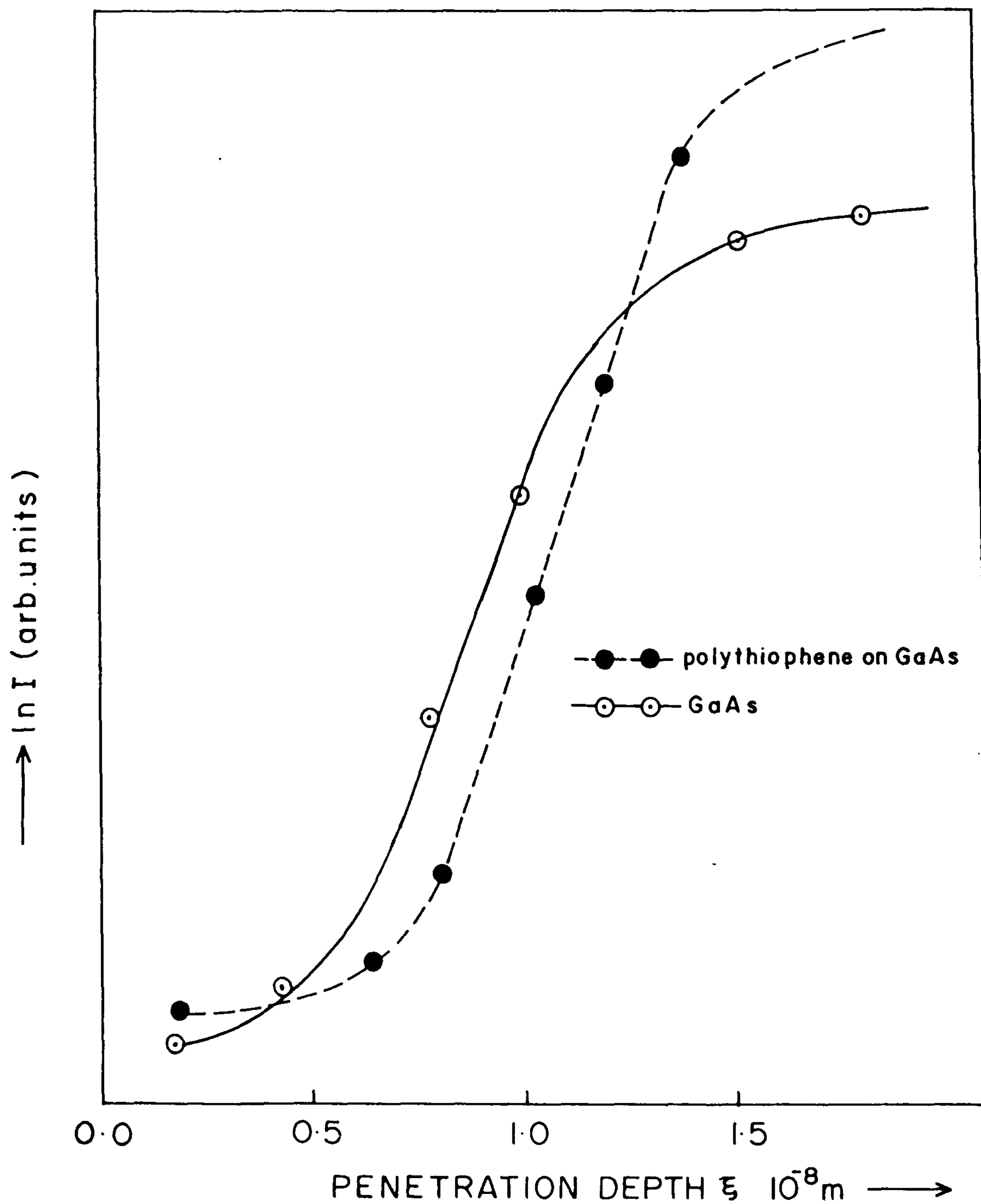

Fig.4. Variation of ln I as a function of penetration depth before and after passivation of n-GaAs with polythiophene.

deposition of thin film of polymer, polythiophene on GaAs surface. As a result of the polymer film L was seen to increase to 15.86 μm and S was found to be reduced to 1.2×10^3 m/s.

3.6.3 Raman scattering studies :

Fig.5 displays the first order Raman spectra of GaAs. The Raman band ~ 271 cm^{-1} corresponds to scatterng by transverse optical (TO) phonons. The line at ~ 291 cm^{-1} is due to scattering by the unscreened longitudinal optical (LO) phonons of the space charge layer. Changes in the LO intensity directly reflects variations of barrier height. The TO line intensity does not depend on E_S, the surface electric field and is used as an internal reference. The spectra of Fig.5 show a reduction in the ratio I (LO)/I(TO) when the polythiophene layer is present. Therefore, the measured reduction of LO intensity indicates a weakening of E_S and a lowering of $\emptyset_B$. Using eqn.22 and 23 $\emptyset_B$ was calculated. In air exposed surfaces of GaAs with n ~ 2×10^{17} cm^{-3} the barrier height $\emptyset_B$ was 0.8 eV as measured on the Schottky diodes by C-V measurements. The effect of polymer overlayer has been to reduce $\emptyset_B$ to 0.3 eV $\pm$ 0.1 eV. The potential estimated from the Raman studies indicated a value of 0.15 $\pm$ 0.05 eV for the polymer deposited surface. Within the experimental accurary the two values are in close agreement to each other. The reduction in the barrier height is a clear indication of the GaAs surface passivation.

3.6.4 Photoluminescence :

The lowering of the barrier of GaAs, as shown by the Raman studies, should be accompanied by an unpinning of the fermi levels at energies closer to the conduction band and consequently, a reduction in the density of midgap states. The results of the PL measurements on the same surfaces for which the Raman spectra of Fig.5 were taken,

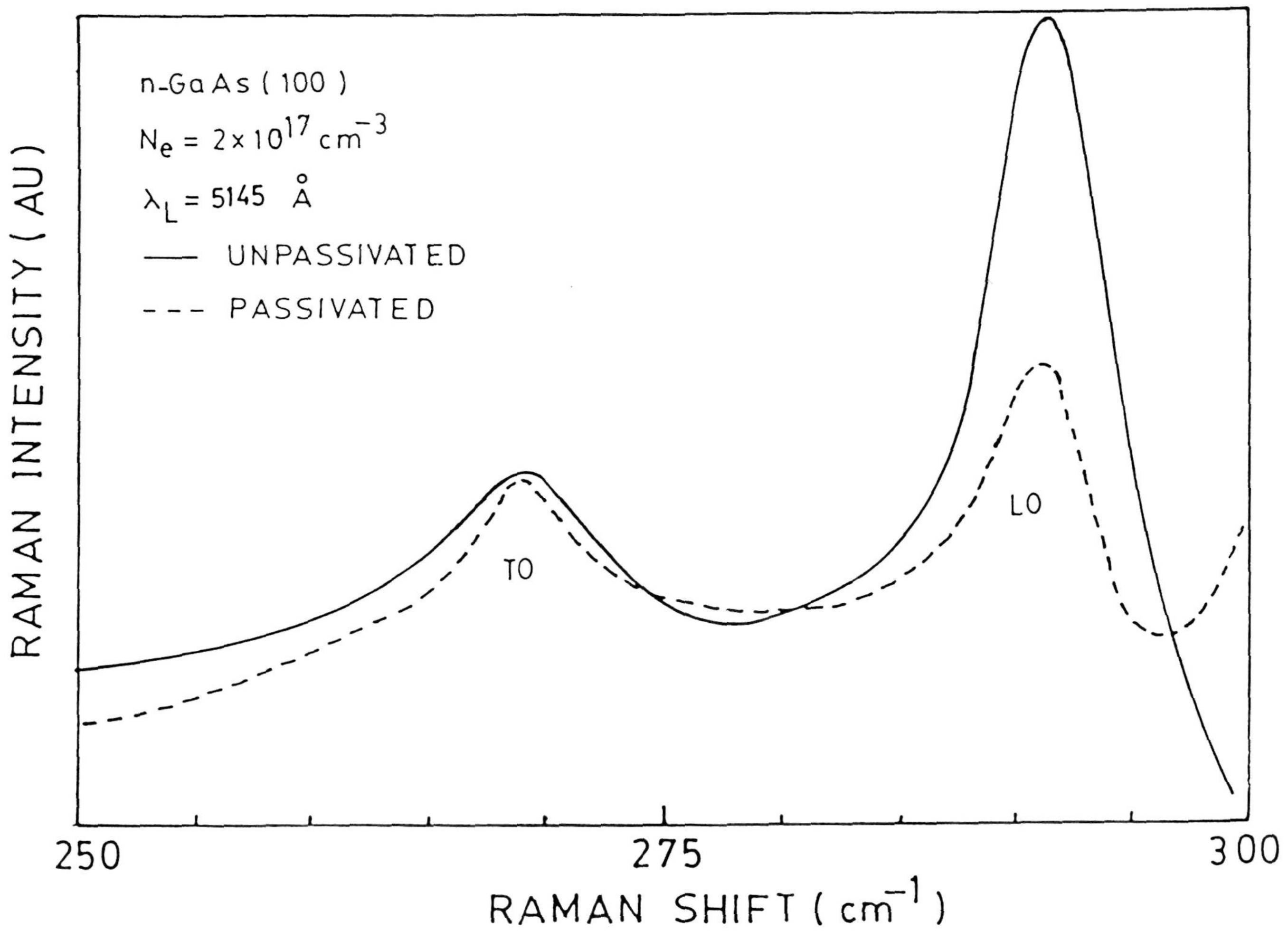

Fig.5. Raman scattering spectra of unpassivated and polythiophene passivated n-GaAs(100) surfaces.

confirm that this is indeed the case. PL spectra of GaAs with and without the polymer overlayer are displayed in Fig.6. The measured line shape is characteristic of heavily doped semiconductors. The striking feature of the results shown in Fig.6 is the increase in the PL peak intensity by a factor of 3 when the polymer is present. This effect is due to the decrease in the surface recombination velocity S. Another interesting point to be noted is that the polythiophene overlayer does not give rise to any PL peaks of its own but only enhances the characteristics of the GaAs peaks; thereby clarifying that the observed PL intensities are only due to the interface between the GaAs and the polymer.

Possible mechanism of passivation of GaAs surface by polythiophene :

We now comment briefly on the mechanism of the polythiophene passivation treatment. There have been a good number of reports on the passivation of GaAs surface by sulphide solution treatments. Essentially different effects for the sulphides Na_2S, $(NH_4)_2S$, $(NH_4)_2Sx$ etc have been observed. The passivation is observed on an inert surface free from adatoms by an increase in photoluminescence intensity and a reduction in the surface interface state density. Orientation of the crystal also has a significant role to play. But, since we have not gathered sufficient data to give a complete picture of this parameter, we confine our discussion to the (100) plane.

Several models [10-14] suggest that the surface oxide, in the form of As_2O_3 and Ga_2O_3 together with elemental As are responsible for the high concentration of midgap defects associated with the GaAs surface. Group VI elements have been reported to confer improved electronic quality to the GaAs surface, particularly relevant to the present is the electronic measurement of the barrier height lowering

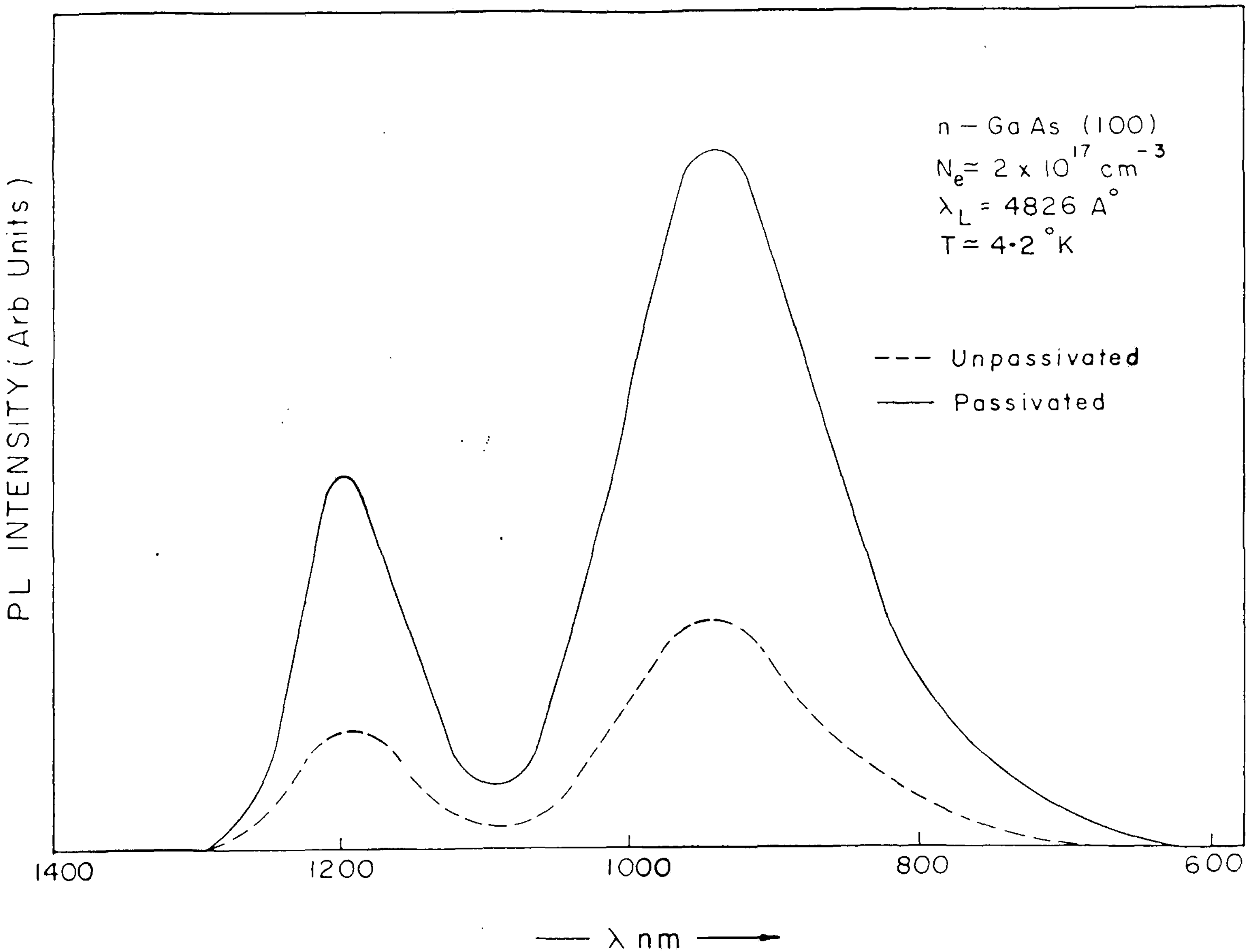

Fig.6. Photoluminescence spectra of **unpassivated** and passivated n-GaAs(100) sufaces.

of GaAs after reaction with H_2S at elevated temperatures. The barrier height reduction to ~ 0.4 eV in that study is remarkably closer to the value of 0.3 eV ± 0.1 eV reported here.

Thiophene is a heterocyclic compound in which there is a sulphur in a five membered carbon ring. Sulphur is a versatile element with regard to GaAs and it is known to form many compounds with both Ga and As. In fact the chalcogenides [13-15] have been cited on several occassions for being able to lower the surface density of states in GaAs, a result presumably of a strong affinity between sulphur and GaAs.

It seems likely in this context, that sulphur in Thiophene having a lone pair of electrons might react with Ga and As to form some of the many complexes. To rationalise the long lasting electronic benefits of polymer films deposited on GaAs, we speculate that a robust chemically bonded sulphur layer forms on the surface. The question is whether sulphur combines with Ga or As or both. It has been observed by means of LEELS [16] that an adsorption free surface is attained on both (111)A and (111)B planes as well, which implies that sulphur can combine with both Ga and As. It is also observed that the sulphur combines more strongly with Ga [17] than with As because the sulphur on the (111)A plane was more resistant to thermal liberation than that on the (111)B plane. This fact is also supported by the heats of formation of Ga and As sulphides which gives the more probable of the species that can be formed on the GaAs surface.

In our case it thus seems plausible to suggest that sulphur would bond with surface Ga atoms. the most efficient use of sulphur, which also leaves the surface free of dangling bonds, could have a sulphur atom bridging two surface Ga atoms.

REFERENCES

1. W.E. Spicer, P.W. Chye, P.R. Skeath, I. Lindau, J. Vac. Sci. Technol. **16**, 1422 (1979).
2. C.R. Zeisse, L.J. Messick, D.L. Like, J. Vac. Sci. Technol. **14**, 957 (1977).
3. T.E. Kazior, J. Lagowski, H.C. Gatos, J. Appl. Phys. **54**, 253 (1983).
4. T.Kobayashi, Y.Shinoda, J.Appl.Phys.**53**, 3339 (1982).
5. L.G.Meiners, D.L.Lile, D.A.Collins, J.Vac.Sci.Technol. **16**, 1458 (1979).
6. L.G.Meiners, J.Vac.Sci.Technol. **15**, 1402 (1978).
7. H.C.Casey, Jr., A.Y.Cho, D.V.Lang, E.H. Nicollian, P.W.Foy, J.Appl. Phys. **50**, 3484 (1979).
8. Y.Hiroto, T.Kobayashi, J.Appl.Phys. **53**, 5037 (1982).
9. M. Watanabe, G. Actor, H.C. Gatos, IEEE Trans. Electron Devices **ED-24**, 1172 (1977).
10. D. Liu, E.C. Larkins, T. Zhang, T.T. Chiang, R.A. Lakue, T. Sigmon, W.E. Spicer, J.S. Harris, Jr. Presented at the 15th Int. Conf. on GaAs and related compounds.
11. W.E. Spicer, T. Kendelewicz, N. Newman, R. Cao, C. McCants, K. Miyano, I. Lindau, Z. Lillienthal-Weber, E.R. Weber, Appl. Surf. Sci. 33/34, 1009 (1988).
12. W.E. Spicer, Z. Lillienthal-Weber, E. Weber, N. Newman, R. Cao, C.McCants, P. Mahowald, K. Miyano, T. Lindau, J. Vac. Sci. Technol. **B6**, 1245 (1988).
13. R.J. Nelson, J.S. Williams, H.J. Leamy, B.I. Miller, H.C. Casey, Jr. B.A. Parkinson, A. Heller, Appl. Phys. Lett. **38**, 76 (1980).

14. Massier, J. Chaplart, M. Larirow, N.T. Linh, Appl. Phys. Lett. **38**, 693 (1981).

15. G. Horowitz, P. Allongue, A. Cachet, J. Electrochem. Soc. **131**, 2563 (1984).

16. Y.Nannichi, Jia-Fa Fan, H.Oigawa, A.Koma, Jap.J.App.Phys. **27**, L2367 (1988).

17. E. Yablonovitch, C.J. Sandroff, R. Bhat, T. Gmitter, Appl. Phys. Lett. **57**, 439 (1987).

Chapter 4

GaAs/S Ion beam mixing: An ESCA study

4.1 INTRODUCTION

It has been made clear in chapter I that much of the interest in obtaining a better understanding of the fundamental properties of GaAs surface has been linked to the role that the empty and filled surface states play for the Fermi level pinning position and Schottky barrier height [1-7], since this aspect is important in attempts to achieve better passivation properties. One of the problems of the processing of GaAs and other III-V compounds is that there is no good insulating or passivating film, therefore, the GaAS MISFET has not been successful even though tremendous efforts have been made to make good insulating films [8-16]. Moreover the oxides of gallium and arsenic are very much unstable and so they by themselves cannot provide the much needed insulating layer.

As is indicated in chapter II it is also well known that sulphur forms many stable binary compounds with both Ga and As. GaS, Ga_2S_3 and As_2S_3 for example are well known layered semiconductors [17-19], the latter having better glass forming properties. The importance of covalently bonded sulphur in the passivation mechanism was suggested from Auger analysis of GaAs substrates which had been treated with sulphide at room temperature. Earlier reports also suggest that a very high quality electronic interface was obtained when GaAs was exposed to chalcogenide compounds [20,21].

The results in the previous chapter indicate the successful passivation of GaAs surface using a sulphur containing polymer which improved intrinsic properties of GaAs [14,15]. We observed a definite reduction in surface recombination velocity, barrier height and surface density of states and an increase in the diffusion length of carriers in the semiconductor. However, no experiment was carried out

to investigate the reaction at the interface leading to the formation of the sulphur compounds with Ga or As. Present chapter reports the experiments which were carried out and purposely planned to study the reaction of free sulphur with the surface of GaAs. In order to avoid the sublimation of sulphur from the reacted surface and to achieve better homogeneous reaction ion beam mixing was carried out.

During the last few years, ion beam mixing has emerged as a powerful technique for microalloying and mixing of the successively deposited thin layers of component materials and for modifying the surface properties of semiconductors [22-25]. This technology has attracted attention recently as a means of fabricating shallow and low resistive MOS and MISFET source and drain regions [26,27]. The main reasons for this trend is the precise controllability and high flexibility that ion implantation technology provides. The inprocess monitoring of ion implantation energy and dose facilitates high accuracy in fabricating very shallow junctions. Moreover ion implatation technology makes it possible to reduce the lateral spread of impurity as compared with conventional diffusion technology. Using this technique of atomic mixing, it is possible to surface the limits of solid solubility imposed by Hume-Rothery rules and to produce compositional and structural metastability [28].

As such, this method of impact surface processing offers newer probabilities of obtaining novel structures in the surface layers with interesting and technologically useful physical properties.

Ion-beam induced atomic mixing can be considered as a fast quenching process similar to the vapour-liquid quenching techniques. However, the atomistic details differ substantially in these cases. In ion-beam induced mixing, the high kinetic energy of the incident heavy

ions (typically 100-400 KeV) produces almost instantly (i.e. within a time scale of 10^{-10} - 10^{-12} sec.) highly disordered and kinetically active zone across interface making rapid transient atomic motion possible. This can lead to alloying of the elements in deposited layers under highly non-equilibrium conditions, which results in the formation of amorphous or metastable crystalline surface alloys. Such metastable structures pass through various states of transformations at different energies leading finally to the precipitation of equilibrium phases. In order to understand the whole sequence of events leading to `equilibration' and also to bring out the basic features underlying the ion-beam induced interface phenomena, it is essential to charactarize the beam mixed materials at various stages using a suitable experimental probe. A variety of techniques such as Rutherford Back Scattering (RSB), X-ray diffraction, electrical resistivity measurements etc. have been used to study the reactions occuring at the interface. However, these methods cannot yield information regarding important microscopic aspects such as local atomic environments, atomic motions of modified material etc. An interesting possibility of carrying out such a study is offered by X-ray photoelectron spectroscopy (XPS).

With this aim in view we have studied the X-ray photoelectron spectroscopy of n-GaAs:S subjected to an argon ion bombardment treatment. This results in mixing of species present at the interface. The present chapter carries the results of our studies on these systems. This has been done also with a view to explore the possibilities and effects of ion bombardment induced sulphur passivation of GaAs surfaces. In this chapter we report the XPS studies on the reactions occuring at the S:GaAs interface as a

consequence of ion-beam mixing at different energetic ion beams.

4.2 EXPERIMENTAL

The single crystals of n-GaAs (100) were first degreased in boiling transene 100 and then chemically etched in a solution of $H_2SO_4:H_2O_2:H_2O::4:1:1$. They were finally rinsed in deionised water and then dried. The polished surface of the wafers was exposed to a Hydrogen plasma to etch and thereby get rid of any remanent impurities which may still be present and then sulphur was deposited in situ by the technique of vacuum evaporation at a pressure of about $1x10^{-6}$ Torr.

The freshly prepared samples of n-GaAs:S were subjected to argon ion bombardment with an energy of 75 KeV and ion fluences of $4x10^{15}$ ions/cm^2 and $8x10^{15}$ ions/cm^2 to induce ion beam mixing at the interface. Ion bombardment was carried out by using an instrument developed in our department. The beam current was maintained in the range of 1-2 $\mu A/cm^2$ to avoid heating of the sample during bombardment.

One n-GaAs without any ion bombardment treatment and the above mentioned two samples were studied with X-ray photoelectron spectroscopy. The XPS measurements were recorded on ESCA-3, MK II model Electron spectrometer from VG Scientific UK using an AlK_α X-ray (1486.6 eV) source at a pressure less than 10^{-9} Torr. All the samples were given an in situ mild etching with an argon ion gun to get rid of adsorbed surface impurities. Spectra were then analysed using least square fitting for gaussian function.

4.3 RESULTS

The XPS spectra obtained were corrected using a linear background to account for the baseline correction and the charging effects were accounted for by considering the C 1s peak at 285 eV as reference.

Each figure consists of three spectra `a' is the virgin GaAs `b' is the GaAs:S bombarded with a dose of $4x10^{15}$ ions/cm^2 and `c' is the GaAs:S composite subjected to $8x10^{15}$ ions/cm^2 dose of argon ion bombardment.

Figure 1 shows the Al-K_α photoelectron spectrum of Ga 3p in GaAs and that after sulphur deposition followed by an ion bombardment with Ar ions with $4x10^{15}$ and $8x10^{15}$ ions/cm^2. Figure 1(a) has been fitted to three pairs of gaussian peaks, the pairs arising due to Ga $3p_{3/2}$ and Ga $3p_{1/2}$ levels. The spectra are recorded after cleaning the surface with Ar ion bombardment. The peaks are designated as 1,2 and 3 and the corresponding B.E. values for Ga $3p_{3/2}$ level are 103, 104 and 105.6 eV. On comparison with the literature values, the peak 1 was designated to free gallium, peak 2 to gallium bonded to arsenic and peak 3 to gallium oxide (Ga_2O_3). In addition, we observed a single peak at 102 eV which is attributed to Si. This peak appears only after ion bombardment. Silicon is a dopant in n-GaAs, it precipitates and is enriched on the surface after ion bombardment.

Figure 1b (GaAs-S ion dose $4x10^{15}$ ion/cm^2) shows a very broad Ga 3p level which is now resolved into 4 pairs of peaks in addition to single peak at 102 eV. We observed the presence of free gallium (peak-1, BE-104.0 eV) in addition to GaAs (peak 2), Ga_2O_3 (peak 3) and Ga_2S_3 (peak 4).

Experiments carried out with higher ion dose ($8x10^{15}$ ions/cm^2), Ga3p showed peaks similar to figure 1 (b); but with varying relative concentration of various species on the surface.

Fig. 2 shows the XPS of arsenic 3p level. Fig. 2(a) is the spectrum obtained from fresh GaAs surface, after argon ion cleaning in the spectrometer. We observe three pairs of As 3p levels. On binding

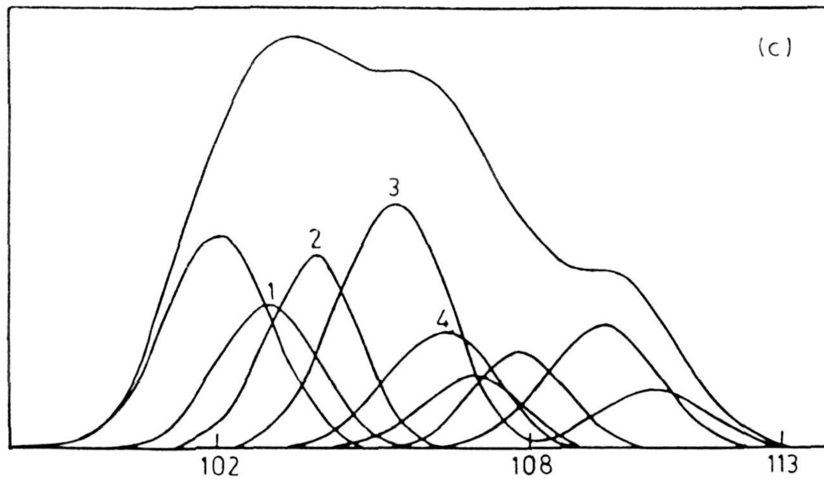

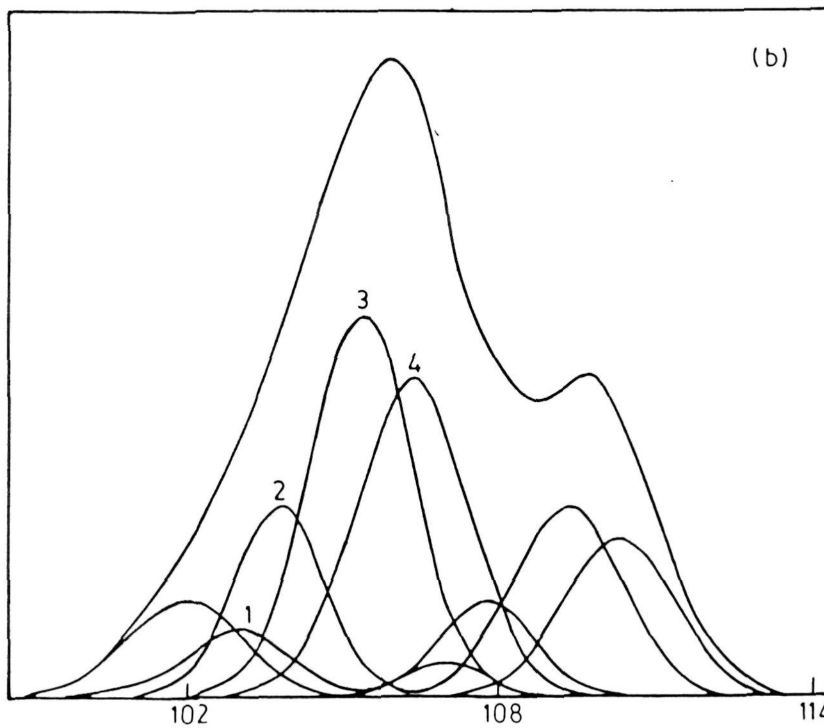

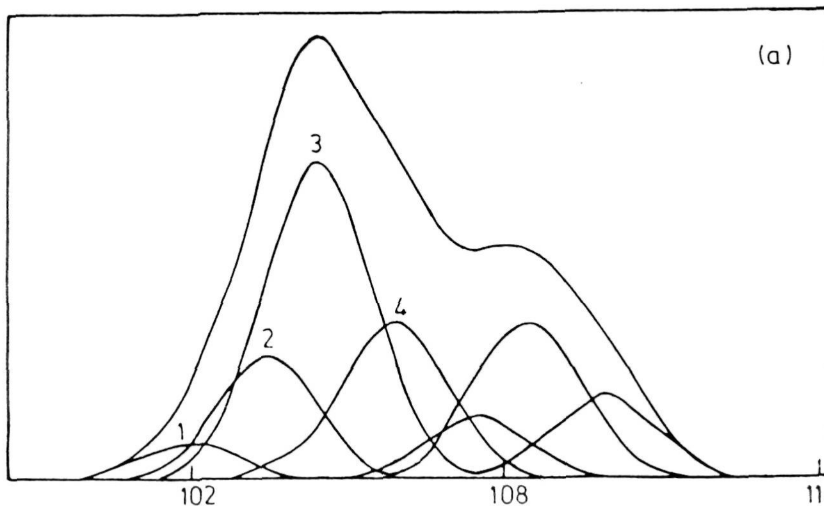

Fig.1 XPS of Ga 3p ; (a) Cleaned GaAs; (b) Ion bombardment with 4×10^{15} ions/cm^2; (c) Ion bombardment with 8×10^{15} ions/cm^2.

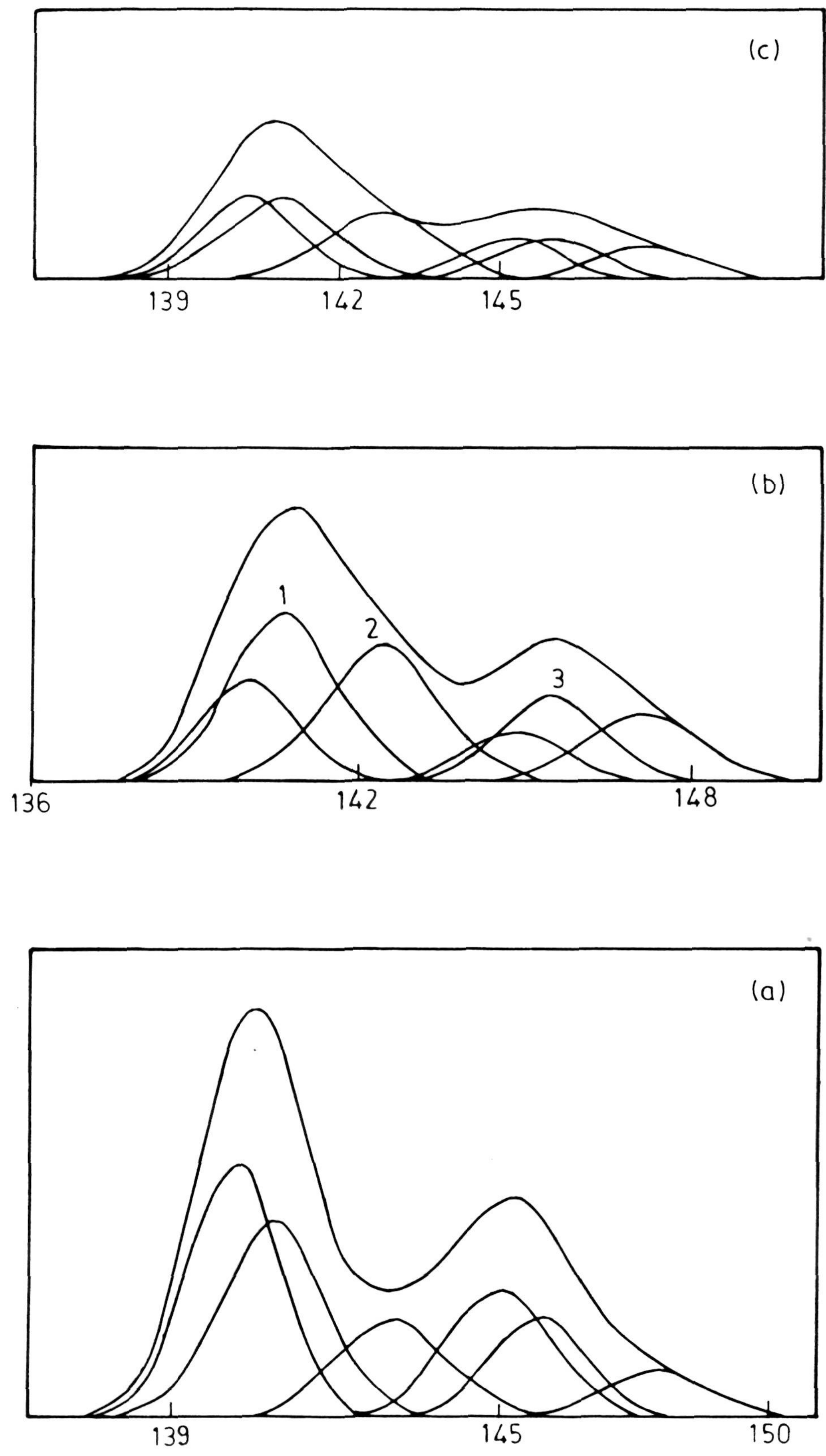

Fig.2 XPS of As 3p; (a) Cleaned GaAs; (b) Ion bombardment with 4×10^{15} ions/cm^2; (c) ion bombardment with 8×10^{15} ions/cm^2.

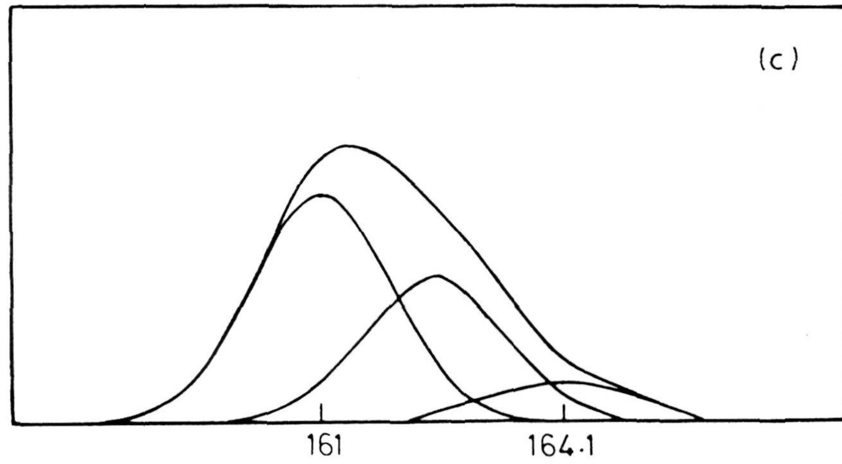

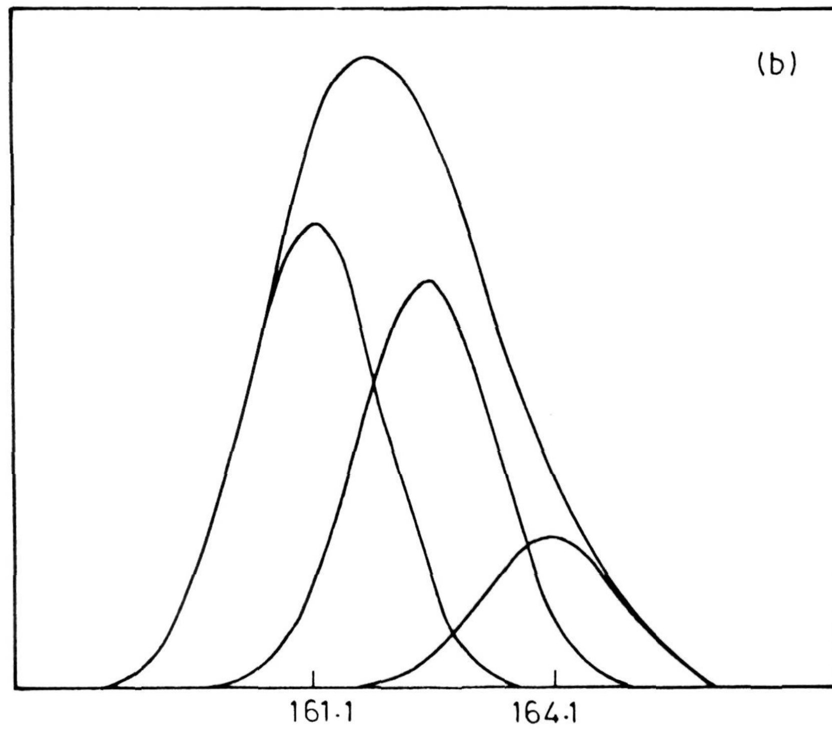

Fig.3 XPS of S 2p; (b) Ion bombardment with 4×10^{15} ions/cm^2; (c) Ion bombardment with 8×10^{15} ions/cm^2.

energy consideration, the first peak is assigned to As on GaAs surface, the second to free arsenic and the third to As_2O_3.

Fig. 2(b) shows the arsenic 3p spectrum in GaAs:S subjected to an argon ion dose of $4x10^{15}$ ions/cm^2. It consists of 3 pairs of subspectra. 1 is assigned to arsenic in GaAs, 2 is for free arsenic and 3 to arsenic sulphide. Peak 2 suggests the presence of excess elemental arsenic at the interface.

Fig. 2(c) is for GaAs:S with a dose of $8x10^{15}$ ions/cm^2. It is similar to 2(b) except that here the peak 2 height is reduced and has become comparable to peak 1 which shows that the surface is being depleted of free arsenic. There is an overall definite reduction in all the three peak heights suggesting an effect of sputtering.

Figure 3 shows the XPS spectrum of sulphur 2p. The spin orbit splitting is not resolved so we see only one set of sulphur 2p peaks. Figs. 3(b) and 3(c) clearly show three subspectra. 1 is due to free sulphur and 2 and 3 are assigned to gallium and arsenic sulphide respectively. As the dose of ion bombardment is increased all the species get sputtered and hence result in a reduction of all the three peak heights as seen in Fig. 3(b).

4.4 DISCUSSION

GaAs surface subjected to argon ion cleaning in the spectrometer, showed the presence of free gallium, free arsenic, and oxides of gallium and arsenic (Ga_2O_3 and As_2O_3). Even though it is not expected, it is surprising to see the presence of both free Ga and As, which can be explained as follows. It is well known that the surface of GaAs is rich in arsenic. The free gallium can be attributed to the preferential sputtering by the argon ion bombardment which is also supported by the fact that the heat of sublimation of Ga is lower than

that of As. The heat of sublimation of Ga is 270880 J/mol-cal, of As is 334107 J/mol-cal and of S is 238229 J/mol-cal. Since a long time sputtering leads to preferential enrichment of the surface, we have not attempted to remove all the oxide species from the surface. The peak at 102 eV is attributed to the precipitation of the dopant Si in n-GaAs on the surface, the intensity of which is found to increase with the increase in the duration of the sputtering as well as with higher doses of Ar ion bombardment. After deposition, sulphur on GaAs and after subjecting this to Ar ion bombardment, both Ga_2S_3 and As_2S_3 were formed. However, ion bombardment also leads to sputtering, we observed an increase in free gallium and arsenic. This is possible because from Ga_2S_3 and As_2S_3, sulphur can be preferentially sputtered leaving behind Ga and As. A slight oxygen contamination further leads to the formation of Ga_2O_3.

The intensities of the Ga3p, As3p and S2p peaks are used to calculate the ratio of the number of Ga atom to As atom, Ga atom to S atom and As atom to S atom using the relation[28],

$$n_1/n_2 = I_1/I_2 \times (E_{k2}/E_{k1})^{0.71} \times \sigma_2/\sigma_1$$

where I is the intensity of the peak,

σ is the photoelectron cross section

E is the corresponding kinetic energy

The following values are used to calculate the atomic ratios:

$\sigma_{Ga} = 2.1$, $\sigma_{As} = 2.7$, $\sigma_S = 1.1$,

$E_{k_{Ga}} = 1380$ eV, $E_{k_{As}} = 1346$ eV, $E_{k_S} = 1324$ eV

The calculated ratios are as follows:

Ga/As = 0.96, Ga/S = 0.51 and As/S = 0.5. The ratio of Ga/As is very nearly equal to the expected values of 1. However, the ratios of Ga/S and As/S are less than 0.66 which one would expect for Ga_2S_3 and

As_2S_3, but closer to these values.

4.5CONCLUSIONS:

Ion-beam induced atomic mixing in a interface GaAs and S is studied by employing the technique of interface sensitive XPS. A number of interesting features regarding the interface were observed in the as deposited and ion-beam mixed samples and their trasformations.It has been demonstrated that the recovery of the ion-beam mixed interfaces exhibits distinctly different features as compared to those in the case of the as deposited samples.

REFERENCES

1. A surface in which the Fermi level is "pinned" is one in which the surface state density is sufficiently high that it determines the Fermi level position.

2. J.Bardeen,
   Phys.Rev.**71**,717(1974).

3. V.Heine,
   Phys.Rev.A **138**,689(1965).

4. J.Tersoff,
   Phys.rev.B **38**,6968(1985);Phys.Rev.Lett. **52**,465(1984).

5. J.L.Freeouf and J.M.Woodall,
   Appl.Phys.Lett. **39**,727(1981).

6. W.E.Spicer,P.W.Chye,P.R.Skeath,C.Y.Su and I.Lindau,
   J.Vacuum Sci. Techn. **16**,1427 (1979); **17** 1019 (1980); Phys.Rev.Lett. **44**, 420 (1980).

7. Subsequent work has made it clear that defects must be near to but not at the surface to be effective in "pinning" the Fermi level when metals are deposited .See,for example ,ref.[8].

8. T.E.Kazior,J.Lagowski,H.C.Gatos,
   J.Appl.Phys. **54**, 2533 (1983).

9. W.E.Spicer,P.W.Chye,P.R.Skeath,C.Y.Su and I.Lindau,
   J.Vacuum Sci. Techn. **16**, 1422 (1979).

10. B.M.Arora and A.M.Narsale,
    Thin Solid Films **56**, 153 (1979).

11. D.J.Olego, R.Schacter and J.Baumann,
    J.Vacuum Sci. Techn. B3, 1097 (1987).

12. C.J.Sadroff,R.N.Nottenburg, J.C.Bischoff and R.Bhat, Appl.Phys Lett. **51**,33 (1987).

13. E.Yablonovitch, C.J.Sandroff, R.Bhat and T.J.Gmitter, Appl.Phys.Lett. **51**, 439 (1987).

14. V.J.Rao, V.Manorama and S.V.Bhoraskar, Appl.Phys.Lett. **54**, 1799 (1989).

15. V. Manorama, S.V. Bhoraskar, V.J. Rao and S.T. Kshirsagar, Appl. Phys. Lett. **55**, 1641 (1989).

16. H.Hasegawa,T.Saitoh, S.Konishi,H.Ishii and H.Ohno, Jap.J.Appl.Phys. **27**, L2177 (1988).

17. R.J.Nelson, J.S.Williams, H.J.Leamy, B.I.Miller, H.C.Casey, B.A.Parkinson and A.Heller, Appl.Phys.Lett. **28**, 76 (1980).

18. J.Massier,J.Chaplort,M.Larirow and N.T.Linh, Appl. Phys.Lett. **38**, 693 (1981).

19. G.Horowitz, P.Allongue and A.Catchet, J.Electrochem. Soc. **131**, 2563 (1984).

20. D.J.Olego, J.Vacuum Sci. Techn. **B6**, 1193 (1988).

21. S.K.Gandhi,S.Tyagi and R.Venkatasubramanian, Appl.Phys.Lett. **53**, 1308 (1988).

22. B.Y. Tsaur, Z.L. Liau and J.W. Mayer, Appl. Phys. Lett., **34**, 168 (1979).

23. B.Y. Tsaur, Z.L. Liau and J.W. Mayer, Phys. Lett. **A-71**, 270 (1979).

24. B.Y. Tsaur, S.S. Lau, L.S. Hung and J.W. Mayer, Nucl. Instrum. Methods 182/183, 67 (1981).

25. B.M. Paine, M.A. Nicolet, R.G. NewCombe and D.A. Thompson
Nucl. Instrum. Methods 182/183, 115 (1983).

26. G.Carter, W.A.Grant,
Ion implantation of Semiconductors, London,Edward Arnold (1976).

27. G.Dearnaley, J.H. Freeman,R.S. Nelson and J.Stephan,
Ion implatation ,Amsterdam, North Holland (1973).

28. J.W. Mayer and S.S. Lau,
Surface modification and alloying by Laser, ion and Electron beams, edited by J.M. Poate, G. Foti and D.C. Jacobson (Plenum, New York, 1983), pp. 241-258.

29. Z.Steiner,H.Hocht,W.Steffen and S.Hufner,
Z.Physik B 38, 191 (1980).

Chapter 5

GaAs / ZnSe System

5.1 INTRODUCTION

Two schemes of passivation to upgrade the surface properties of GaAs were described in the last two chapters. In both these schemes sulphur, was chosen as the passivating element (because Ga is known to form stable chemical compounds with second group elements). However the matrix through which sulphur approached the GaAs was different in these cases. The polymer gave a completely amorphous structure to the interface, wherein introduction of sulphur through ion beam mixing provided a random network at the interface.

Apart from fulfilling the requirements of ionic bonding for surface passivation, the strain at the interface should also be minimised in order to reduce the misfit defects, requires the graph of a passivating layer such that its lattice constant is very close to that of GaAs. One of the interesting compound fulfilling both the requirements is ZnSe, a II-VI compound, with a band gap of 2.7 eV. The lattice mismatch between GaAs and ZnSe is obtained from f = a (GaAs) - a (ZnSe), where `a' is the corresponding lattice constant. Its value is 0.00265 which is very small. Resistivities in excess of 10^9 Ωcm can be routinely obtained in ZnSe. Thermal coefficients of expansion also closely match with each other. Due to the close lattice matching and wide direct band gap, GaAs/ZnSe is a well known heterostructure. In addition since selenium is known to form stable compounds with Ga as well as As, zinc selenide is a prospective candidate for blue LED in GaAs/ZnSe MIS structure. In addition since selenium (also from group VI like sulphur) is known to form stable compounds with Ga as well as As. It is therefore expected that a lattice matched overlayer of ZnSe on GaAs will provide interesting control of deep levels and therefore help in unpinning of Fermi level on GaAs surface.

The properties of GaAs/ZnSe heterostructures are comparable to well known GaAlAs/GaAs heterostructure having good interface properties useful for solar cells and lasers. Besides the obvious technological importance of compound semiconductor heterostructure in light wave devices there has been an interest in such materials for their electronic properties, because of the higher electron mobilities available. Apart from this, many studies of the surface properties of GaAs have shown that its surface recombination velocity (SRV) is very high, approximately 4×10^6cm/s. The GaAlAs/GaAs heterostructure has been found to have good interface properties with decreased SRV's of 1×10^3 to 1×10^4 cm/s.

One of the drawbacks of GaAlAs/GaAs heterostructure is the instability of Al containing GaAlAs and the relatively low band gap; which limits the use of this structure. In contrast ZnSe thin films are chemically more stable when exposed to air, reactive atmosphere than those of Ga_{1-x} Al_x As with large values of x. In addition GaAlAs needs sophisticated techniques like Molecular Beam Epitaxy (MBE) and / or Metalloorganic chemical vapour deposition (MOCVD). Whereas in ZnSe can be grown by simple techniques, using chemical decomposition.

With this background we have undertaken the study of ZnSe/GaAs heterostructures where in ZnSe was grown by simple and novel technique of Liquid Gas Interface Reaction growth (LGIR). This technique was developed for the first time in our laboratory.

Different aspects of the interface were studied. In the first place the structural characteristics of the film prepared by LGIR were investigated using possible methods. In the second place the interface reaction products for three different curing temperatures were studied. The elemental analysis using X-ray photoelectron spectroscopy

and structural analysis using low angle X-ray diffraction were carried out over these interfaces, the results of which are discussed in light of passivating effects of ZnSe on GaAs.

Laser Raman Spectroscopy was used for determination of interface potential between ZnSe and GaAs. Electronic properties of the interface were investigated through C-V diffusion length and photoluminescence measurements. Another very useful interface property of heterojunction is valence band discontinuity. For semiconductor heterojunctions, the fact that the two semiconductors have different energy gaps results in valence and conduction band discontinuities. In turn these offsets play a crucial role in the electrical properties of the heterojunction [1-2] and they can be used in the design of solid state electronic devices. Inspite of significant advances of the past few years many fundamental questions remain [3-6].

Most theoretical treatments of heterojunction band bendings have assumed abrupt lattice matched interface [7]. Likewise, most assume that there is an absolute energy associated with each semiconductor so that the band offset reflects differences in these energies. Experimentally however it has been observed that the electrical properties can be related to the chemical and geometric structure at the interface and can be dictated by deviations from perfection [5,8,9]. In particular, band offset can depend upon such variables as substrate orientations, overlayer crystallinity, the order of deposition and interdiffusion or reactivity. In such cases there is no unique value for the line up and experiments must therefore provide better in sight into structure property correlations for heterojunctions. Photoemission techniques have been applied to study quite a few heterojunction systems. Here we use the X-ray

photoelectron spectroscopy (XPS) for determining the heterojunction band discontinuities. Second half of this chapter reports the results of these.

5.2 THEORETICAL BACKGROUND

5.2.1. Heterojunction Band Discontinuity

The XPS technique for determining heterojunction band discontinuities can be described as follows. In this method, the binding energy difference between a semiconductor core level and the valence band edge can be accurately determined and this is used to estimate the heterojunction band discontinuities. The disruption of a perfect crystal lattice, produced by the presence of either a metal, semiconductor, or vacuum interface is generally accompanied by a deviation of the charge distribution near the interface from that of deeper in the bulk semiconductor. Consequently, Poisson's equations predict a spatially varying electrostatic potential V_{BB}^{x} which bends all of the bands or energy levels by the same amount as a function of distance away from the interface. For semiconductor x in Fig. 1(a) the energy of the core level E_{CL}^{x}, the valence band maximum E_{V}^{x} and the conduction band minimum E_{C}^{x}, are shown in the bulk (b) and at an interface (i) with either a metal, semiconductor, insulator, or vacuum. Binding energy E_B is measured with respect to the Fermi level E_F ($E_B = 0$). The band gap E_G^{x}, position of the Fermi level in the bulk relative to the valence band edge δ^{x} band bending potential V_{BB}^{x} and depletion layer width w are also shown in Fig. 1(a). Given an XPS measurement of the position of the core level E_{CL}^{x} (i) at the interface and the binding energy difference ($E_{CL}^{x} - E_{V}^{x}$) between core level E_{CL}^{x} and the valence band maximum E_{V}^{x}, it follows from Fig. 1(b) that the position of the conduction band minimum at the interface is given by

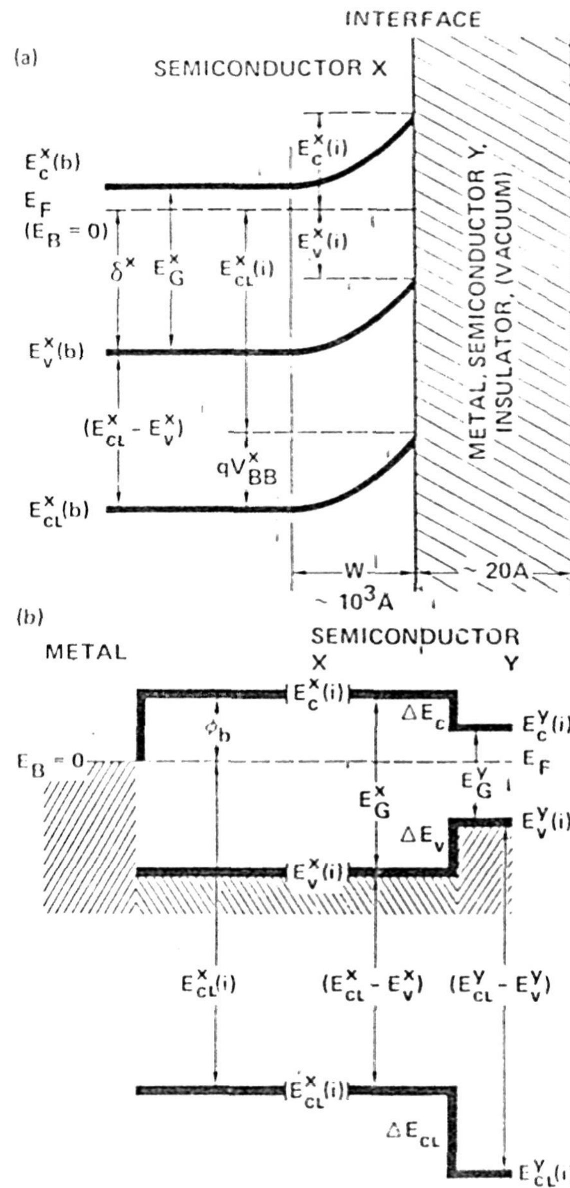

Fig. 1(a) : Generalized energy band diagram at an abrupt interface.

(b) : Schematic flat band diagram at a metal semiconductors (left) or heterojunction (right) interface.

$$E_C^X\ (i) = (E_{CL}^X - E_V^X) + E_G^X - E_{CL}^X\ (i) \qquad 5.1$$

the position of the valence band maximum at the interface is given by

$$E_V^X\ (i) = E_{CL}^X\ (i) - (E_{CL}^X - E_V^X) \qquad 5.2$$

The valence band discontinuity ΔE_V at the the heterojunction interface is given by

$$\Delta E_V = (E_{CL}^Y - E_V^Y) - (E_{CL}^X - E_V^X) - \Delta E_{CL} \qquad 5.3$$

where $\Delta E_{CL} = E_{CL}^Y\ (i) - E_{CL}^X\ (i)$ 5.4

The effect of interface states is to shift the potential within the sampled region on both sides of an interface by the same constant value. Thus any potential shift due to interface states or other sources of band bending cancel.

5.3 EXPERIMENTAL DETAILS

5.3.1 Growth of ZnSe films by Liquid Gas Interface

Thin films of zinc selenide were grown by a simple technique which is based on a double decomposition reaction. The reactants are an (i) aqueous salt solution of zinc, may be zinc acetate or zinc chloride and (ii) aqueous hydrogen selenide, which is generated in-situ by the reaction of a metallic selenide like cadmium selenide or iron selenide with concentrated hydrochloric acid. The reaction is as follows :

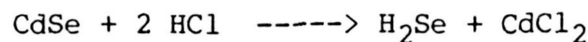

$CdSe + 2\ HCl$ -----> $H_2Se + CdCl_2$

or $FeSe + 2\ HCl$ -----> $H_2Se + FeCl_2$

This $FeCl_2$ reacts with the aqueous zinc salt

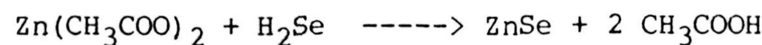

$Zn(CH_3COO)_2 + H_2Se$ -----> $ZnSe + 2\ CH_3COOH$

or $ZnCl_2 + H_2Se$ ------> $ZnSe + 2\ HCl$

The zinc selenide is formed as a thin layer on the surface of the aqueous solution.

The schematic of the experimental set up consists of an air tight dessicator which encloses the reactants. The aqueous solution of zinc acetate is prepared by dissolving about 1 gm of zinc acetate in about 250 ml of deionised water. A drop of acetic acid is added to the zinc acetate solution to make it slightly acidic. The pH of the solution was about 5. This zinc acetate solution was taken in a shallow petridish so that a large surface area of the aqueous solution is exposed for reaction. [An inverted watch glass provided with a hook is placed dipped in this solution. This is to enable one to pick up the film once it forms on the surface and to allow the excess zinc acetate solution to drip down easily]. This zinc acetate solution is enclosed along with a small capsule containing cadmium selenide and concentrated hydrochloric acid. The hydrogen selenide gas generated reacts with zinc acetate and forms a thin film of ZnSe on the surface of the solution. The reaction is allowed to take place for about two minutes. Once the film is formed the reaction stops because there is no more zinc acetate exposed to the hydrogen selenide.

The ZnSe films are then picked with the inverted watch glass and allowed to float on deionised water. This is to get rid of any residual zinc acetate or other adsorbed impurities. The films thus grown can be picked onto any desired substrate.

The films picked on clear slides were allowed to dry. Planar aluminium electrodes were deposited on the film, for measurement of electrical resistivity. For the structural investigations using Transmission Electron Microscopy (TEM) the films were picked over the standard gold mesh provided with TEM. Whereas for the actual purpose of investigation the films were picked over cleaned surface of GaAs wafers. The specimens of GaAs were polished (100) wafers which were

cleaned by etching in $H_2SO_4:H_2O_2:H_2O::4:1:1$ solution just before deposition of ZnSe. The X-ray diffraction of room temperature deposited ZnSe indicated that the films were completely amorphous in nature. In order to improve the morphology of ZnSe, the deposited GaAs wafers were annealed at 100°C and 200°C for 30 min in argon atmosphere.

The analytical instrument which were either used to characterize the passivating film and/or to find the nature of passivation are listed in Appendix I.

5.4 RESULTS

5.4.1. Physical Properties

The ZnSe films grown by this technique were very uniform, whitish in colour and very tenacious. The thickness of the films were measured with Talley's step measurement and was found to range between 400 to 500 A°. Extreme care was taken to see that no water could cause the film to break during the process of drying of the film.

The current voltage plot was obtained to be a straight line and the resistivity was found to be about 10^7 Ωcm; this shows that the films deposited were not highly insulating; but slightly semiconducting. Since the semiconducting films are produced either due to the presence of excess Zn or Se, we recorded X-ray fluoroscence spectrum for confirming this.

5.4.2. X-ray fluoroscence analysis for composition analysis

A typical XFA spectrum of the room temperature grown ZnSe film is shown in Fig.2. The intensity of the ZnK_{α} and SeK_{α} peaks alongwith the corresponding cross section for the X-ray fluoroscence gives the concentration of the species. The ratio of Zn to Se comes out to be nearly one. These results do not indicate any nonstoichiometry within

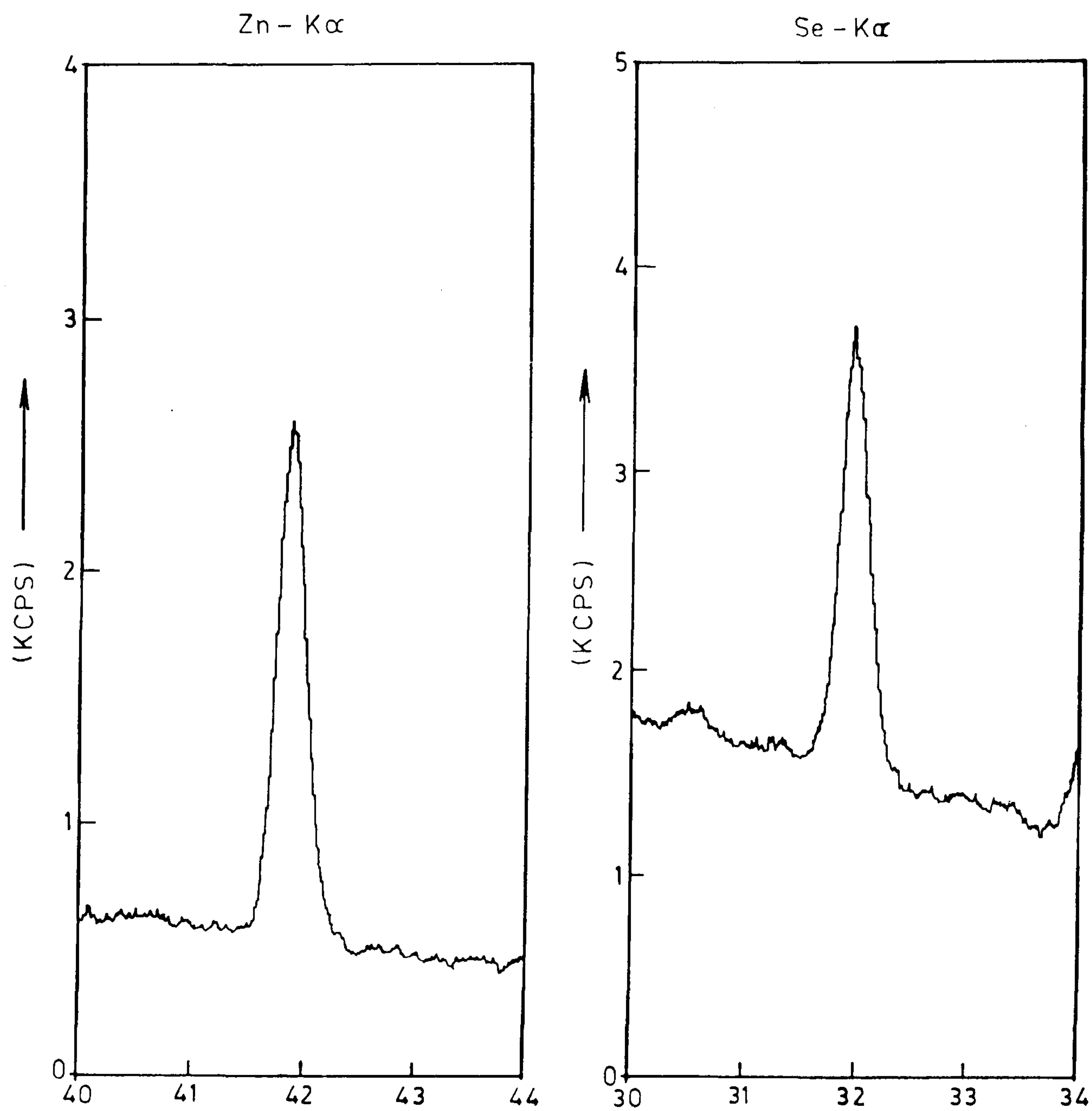

Fig. 2 : XRF spectrum for ZnSe

the experimental accuracy. However due to the low resistivities of the film it can not be even completely ruled out. Further analysis is necessary to confirm this fact, however due to few limitations this could not be performed.

5.4.3. Structural analysis by TEM

The structure of the films grown at RT was totally amorphous as seen by X-ray diffraction. However, crystalline films were grown at higher temperature of the bath. As the growth temperature was increased from about $2^{o}C$ to $80^{o}C$ the corresponding electron diffraction pattern became sharper and well defined resulting in well defined diffraction patterns. Gold was taken as standard to obtain the spectrometer constant. Table 1 gives the observed d values and the literature values for a cubic ZnSe single crystal.

TABLE 1

Radius of ring cm	d_{cal}	d_{lit}	hkl
1.15	1.638	1.635	222
1.45	1.302	1.299	331
1.6	1.17	1.156	422

Figure 3 shows the electron diffraction pattern of ZnSe grown with the temperature of the bath maintained at $2^{o}C$, $30^{o}C$ and $80^{o}C$. This shows that the films produced at higher bath temperatures have better crystalline order.

at 2 °C

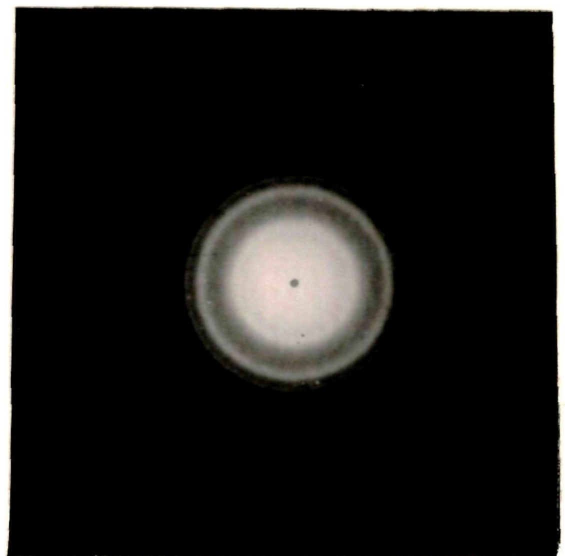

at R.T.

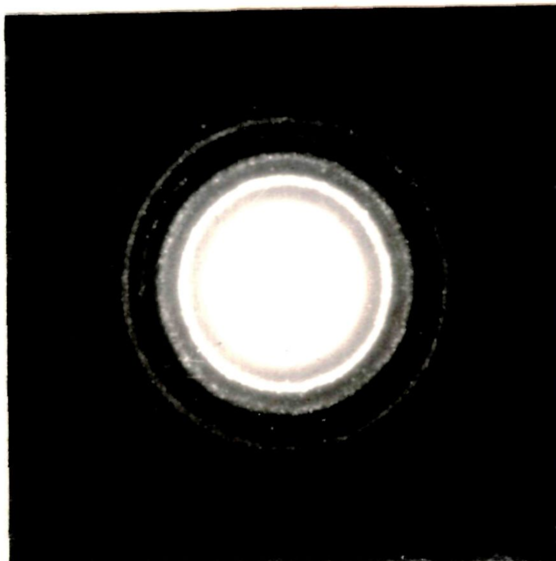

at 80°C

Fig.3: Electron diffraction pattern for ZnSe.

5.4.4. Chemical analysis of GaAs/ZnSe interface using ESCA :

Before drawing any conclusions about the heterojunction and the role of ZnSe as a passivating layer it is necessary to know the reactivity and diffusion in the surface layers of GaAs and the impurities present in the overlayer. Photoemission techniques are most suitable for interface studies because it is possible to determine the composition and electronic structure by depth profiling over the surface by argon ion sputter [10].

Cleaned (100), n-type GaAs samples showed a small amount of carbon and oxygen as the contaminants when examined with XPS, however, repeated cycles of argon ion bombardment removed both carbon and oxygen completely from the surface. Reaction between GaAs and ZnSe at different in-situ annealing temperatures was also studied.

Ga 3d, As 3d, Zn 3d and Se 3d core levels were used to determine the relative concentrations of Ga, As and Zn and deposited on GaAs. These spectra are shown in Fig.4 to Fig.7. Each figure contains the XPS line for the corresponding core level recorded after depth profiling for three sputtering times, and for three annealing temperatures of the sample. Thus Fig.4(A) corresponds to Ga 3d level of room temperature deposited ZnSe for three sputtering timings as indicated in the figure 4 (b) and 4 (c) correspond to samples annealed at 100°C and 200°C respectively. Table 2 gives the data covering the binding energies of the observed peaks. The relative concentrations of the various elements were determined using the formula.

$$\frac{n_1}{n_2} = \frac{I_1}{I_2} \left[\frac{E_{K2}}{E_{K1}} \right]^{0.71} \times \frac{\sigma_2}{\sigma_1}$$

The resulting data is tabulated in Table 4 .

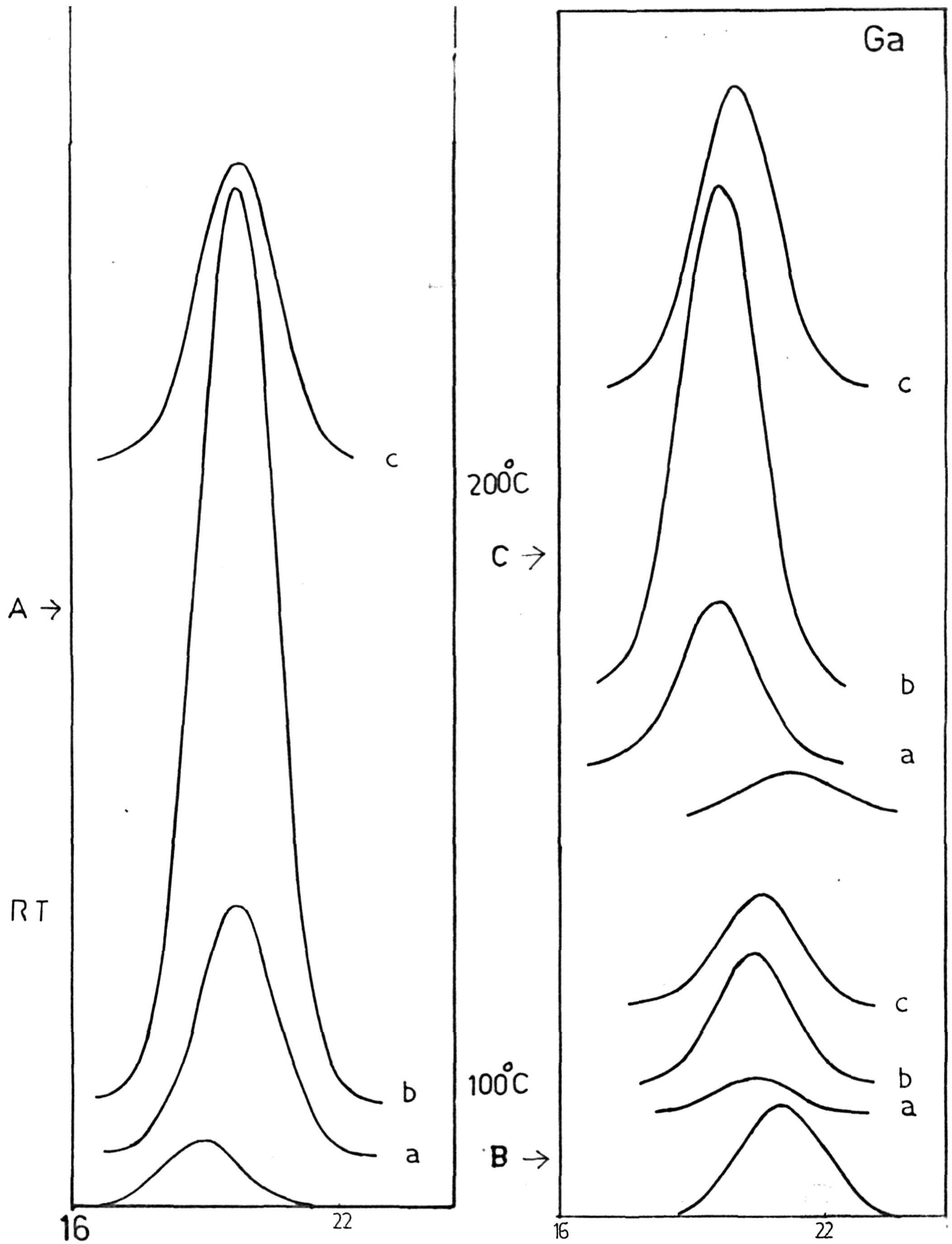

Fig. 4 : XPS spectrum for Ga 3d A (RT), B (100°C), C (200°C)

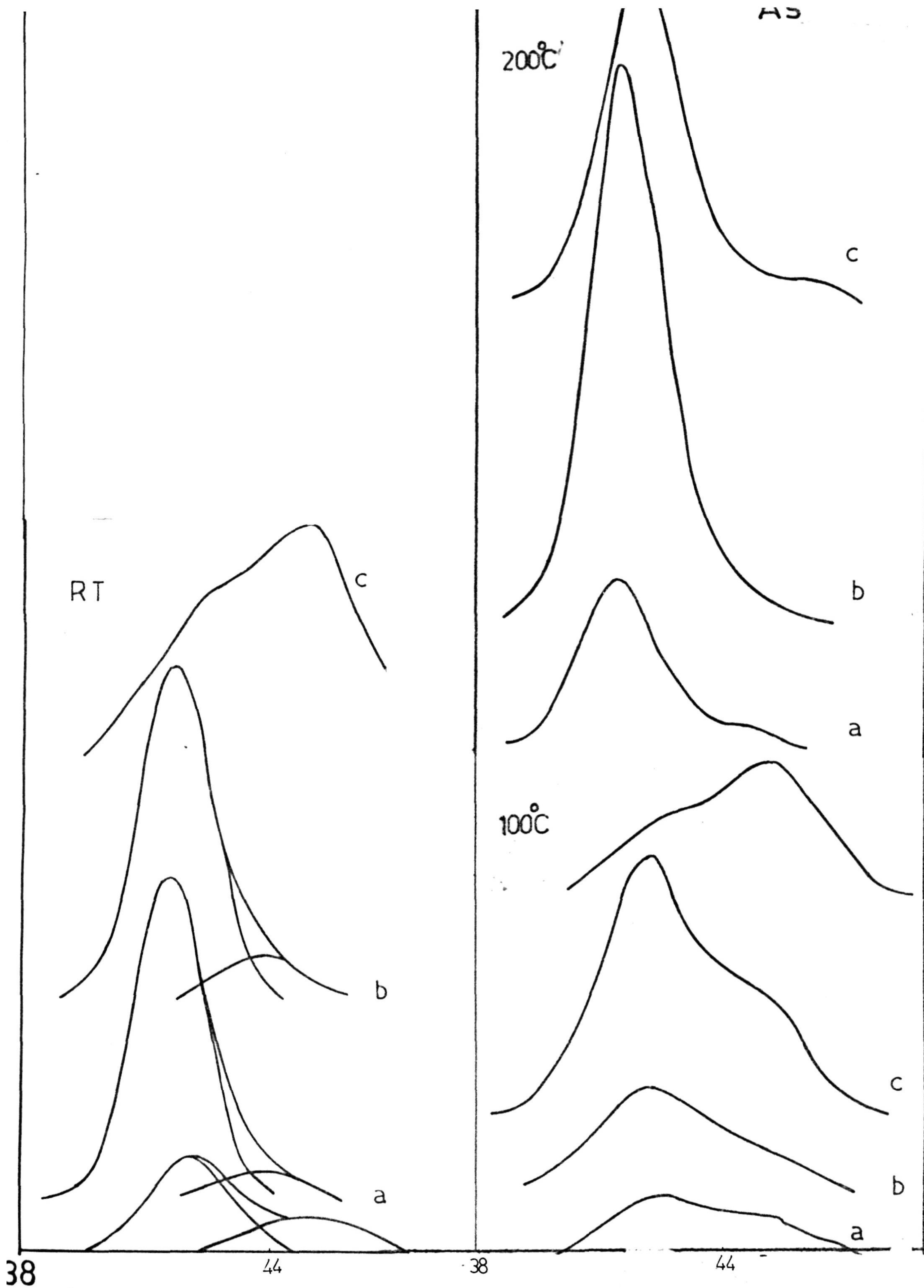

Fig. 5 : XPS spectrum for As 3d A (RT), B (100°C), C (200°C)

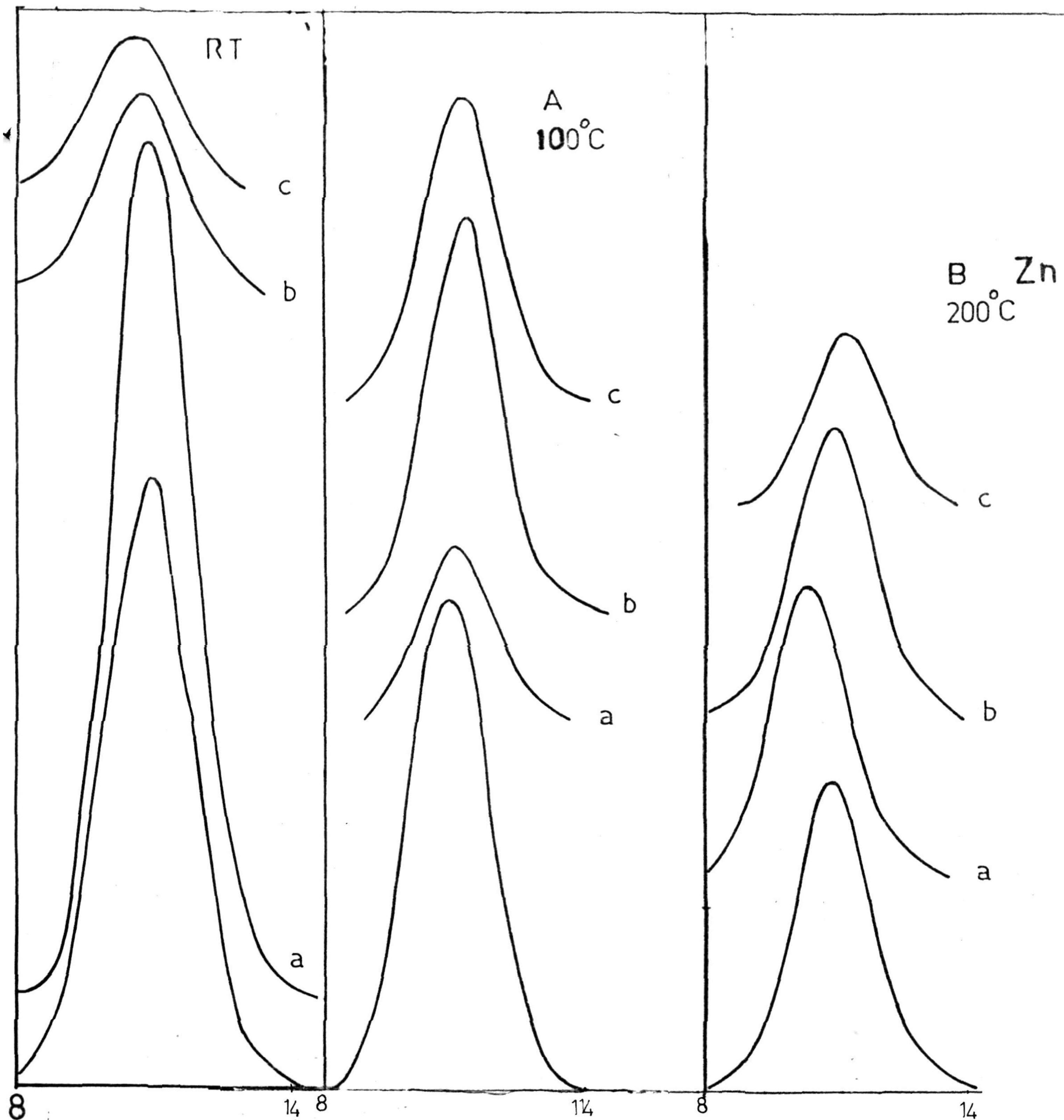

Fig. 6 : XPS spectrum for Zn 3d A (RT), B (100°C), C (200°C)

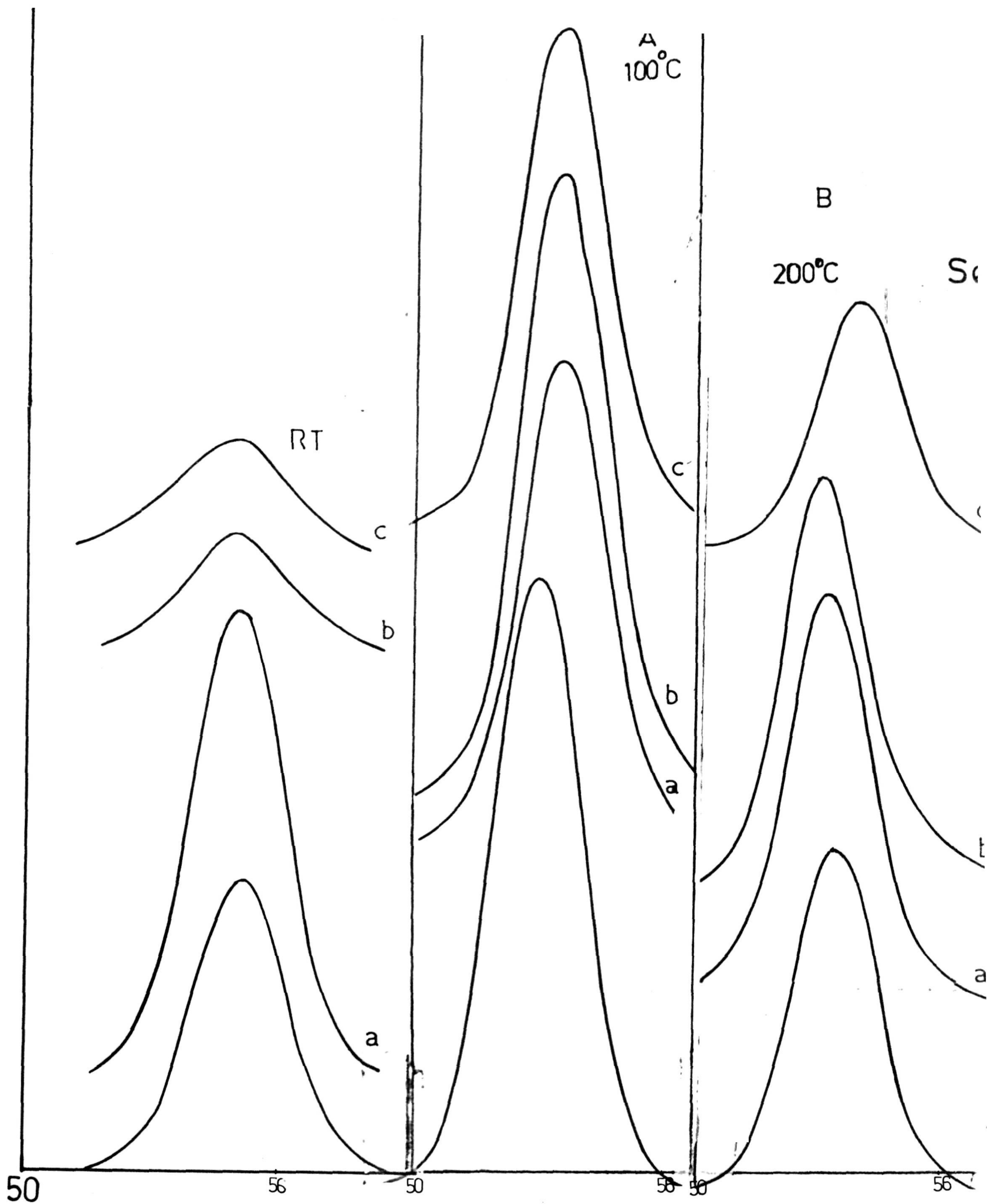

Fig. 7 : XPS spectrum for Se 3d A (RT), B (100°C), C (200°C)

TABLE 2

Binding energies of various elements Ref. Fig. 4 to Fig. 7.

Temp.	Ga	As	Zn	Se
RT	19	-	10.8	54.60
a	19.55	41.1	10.4	54.60
b	19.56	41.24	10.78	54.84
c	19.7	41.52	10.5	54.84
100°C	21	43.2	11.1	55.3
a	20.6	42.24	10.8	54.85
b	20.10	41.90	10.7	54.75
c	20.26	42.00	10.75	55.00
200°C	21.00	42.5	10.95	55.00
a	19.5	41.6	10.5	54.7
b	19.6	41.55	10.7	54.85
c	19.7	41.76	10.7	55.4

When ZnSe is deposited on GaAs (100) substrate at room temperature, rapid changes in the concentration of Ga and Se occur in the first 20 A^{o} of deposition as can be seen in Fig.4. Above 20 A^{o} the Se signal increases and Ga decreases rather slowly. The interaction between Se and Ga from GaAs substrate even at room temperature is very strong as revealed by the Ga 3d and Se 3d spectral line. As can be seen in Fig.4 this peak shows a drastic change in binding energy right from the coverage of ZnSe. At 200 A^{o} ZnSe coverage, the binding energy of the Ga 3d peak is resolved into two. After this, the binding energy change is gradual and then continuously shifts towards the value attaining the Se value of 54.7 eV in ZnSe. Thus interaction between Ga and Se starts as soon as a few molecules of ZnSe are deposited onto the GaAs substrate.

Usually when the interaction between two atoms takes place via the charge transfer process, electrons are transferred from the element with lower electronegativity (in this case Ga with electronegativity of 1.6) to the one with higher value (in the present case Se with an electronegativity value of 2.4) and the core level binding energy of the electron donor atom increases while that of the other decreases. In the case of ZnSe/GaAs interface, we observe binding energy changes for Ga 3d and Se 3d. Ga atoms donate their charge to Se atoms. As the charge on Se is increased, its binding energy decreases. Hence the strong interaction between Ga and Se atoms results into a large increase in the binding energy of Ga, viz. 19.88 eV.

A comparison of binding energy changes in Se 3d levels with depth for a 2000 A^{o} ZnSe layer on GaAs different temperatures is made in Fig.7. These figures indicate that as we increase the annealing

temperature the binding energy even in the top layer increases from 54.8 eV to 55.15 eV for 100°C and 55.16 eV for 200°C. With argon sputtering the binding energy reaches the value of 54.8 eV for room temperature, 55.05 eV for 100°C and 55.16 eV for 200°C at the interface of GaAs/ZnSe. The increasing binding energy at the interface is an indication of stronger bonds with the substrates with annealing temperature. In all the three cases the variation of binding energy with depth also seems to be different.

For the sample at room temperature, the top most layer is ZnSe as indicated by the binding energy values for Zn3d and Se2p respectively. The top surface binding energy values of Zn and Se even for the annealed sample are closer to the ZnSe values indicating that the deposited thickness of ~ 200 A^{o} is nearly sufficient for reaction at the temperature. However, the one certain difference between the 100°C and 200°C annealed samples, viz. between the first few layers for the sample annealed at 100°C shows rapid changes but reaches a steady value thereafter while for the 200°C annealed sample there is a rapid change till nearly double depth and the steady value is attained thereafter. It can also be noted that the interface has become broader by annealing at 100 and 200°C. Although there are differences in the nature of the interfaces in the three cases, limited resolution of the x-ray photoelectron spectrometer does not give the exact phase identification. As will be shown in the next section, different phases can be observed using glancing angle XRD at various temperatures and depths.

5.4.5. X-ray diffraction analysis :

Using the X-ray at glancing incidence very thin surface layers

(~ 50 A^{O}) can be probed. In these investigations an attempt is made to observe the variation in the diffraction pattern by varying the angle of incidence. The diffraction patterns are shown in Fig.8.

As deposited ZnSe films did not show any feature in XRD recorded with a glancing angle of 0.2^{O} and therefore the spectra for room temperature deposited films are not shown. With low angle XRD spectrometer. The film thickness which is viewed by X-rays 0.2^{O} is calculated to be 20 A^{O}. Thus it is clear that there is no interdiffusion of ZnSe and GaAs within this thickness.

However by increasing the angle of incidence to 2^{O} we could observe the phases corresponding to Ga and As. From a comparison of the observed diffraction patterns with the reported values it can be said that even at room temperature Ga_2Se_3 phase is formed with a small inclusion of Ga_2O_3 or As_2O_3.

For the samples annealed at $100^{O}C$ the nature of the ~~nature~~ of the interface becomes completely different. First of all the number of diffraction lines are increased indicating the formation of additional chemical species besides Ga_2Se_3. It is likely due to the migration of As into the deposited layer forming As_2Se_3 at that temperature. Probably at room temperature only limited interaction occurs at the interface but at $100^{O}C$ a number of Ga-As bonds break and these atoms start migrating into ZnSe layer making the interface rather more reactive. Annealing of the ZnSe/GaAs interface at $200^{O}C$ changes the phase predominantly to Ga_2Se_3 as can be seen from Fig.8. In this case the peaks corresponding to As_2O_3 and Ga_2O_3 are absent . This is an indication of the increased width of the ZnSe/GaAs interface.

5.4.6 Growth model for the ZnSe/GaAs interface :

The thin film growth shows a variety of models depending on the

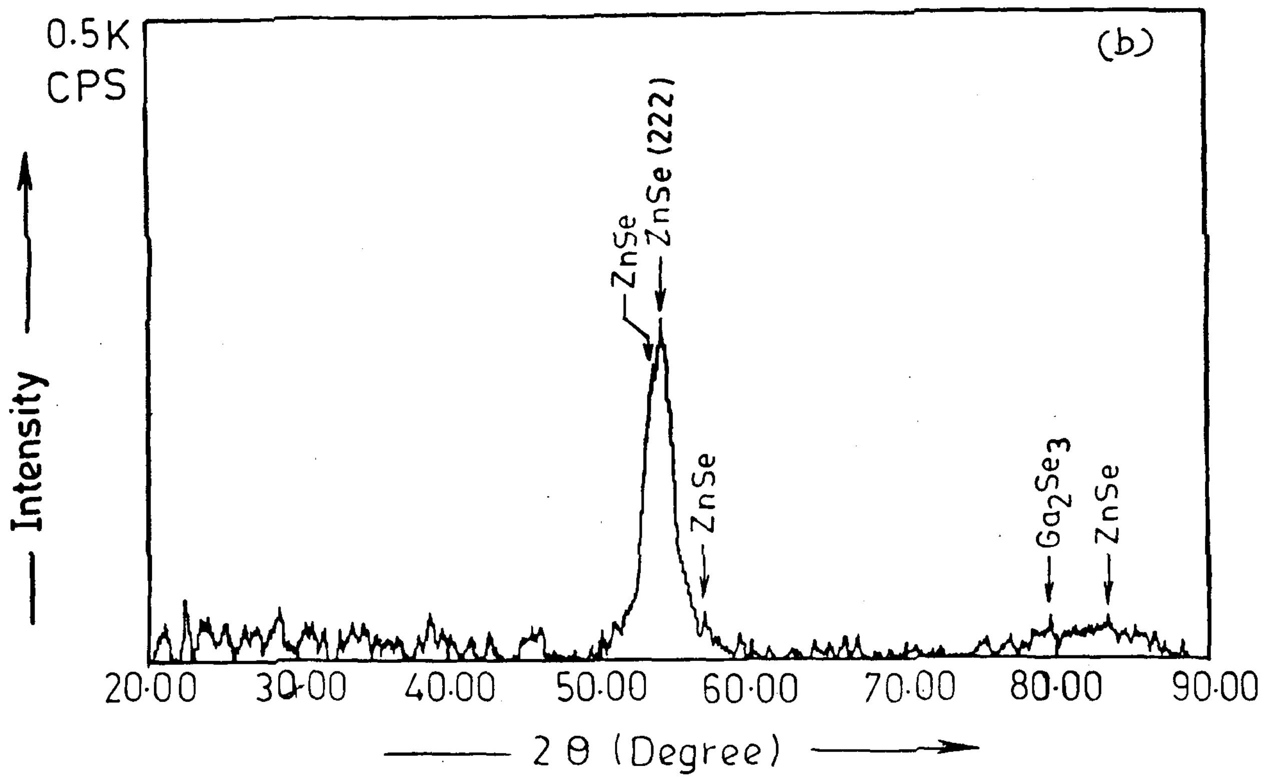

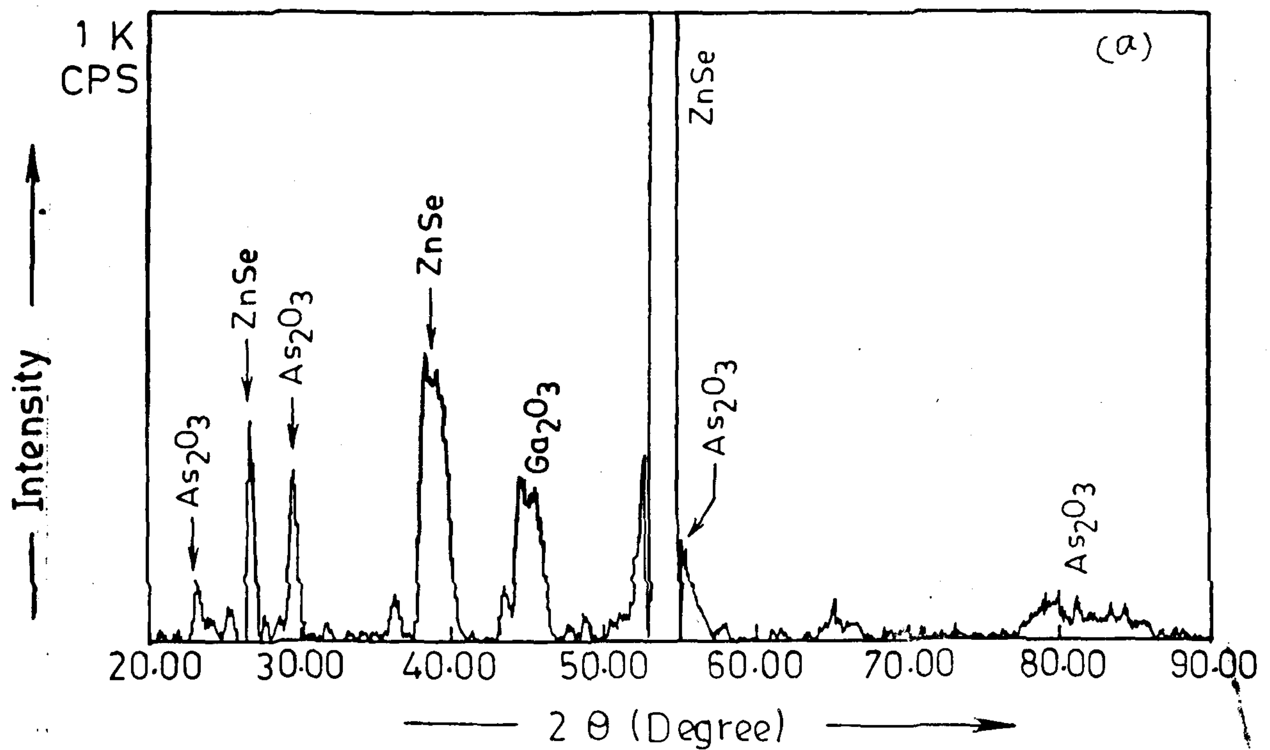

Fig. 8 : XRD of GaAs/ZnSe (a) 100°C (b) 200°C.

materials involved, both the deposit and the substrate, method of preparation (evaporation, sputtering etc) and the condition during the growth. Different growth mechanisms like island growth, layer growth, layer growth followed by island growth or vertical stack growth have been proposed [11]. However, application of a particular growth model even for a particular class of semiconductor - semiconductor has not been possible. Besides, during the initial stages of interface formation, further details like material diffusion, bond breaking mechanism [12] optimum deposition thickness for reaction to occur, etc are quite important.

In the present case of ZnSe/GaAs interface where 200 A^o thick ZnSe is deposited on the GaAs substrate it is possible to discuss the phases from the XRD data at the various temperatures. When ZnSe layer is deposited on the GaAs substrate, the Ga-As bonds at the interface are broken by the charge transfer mechanism. However, the limited diffusivity of Ga at room temperature controls the growth of Ga_2Se_3 formation. In fact, few layer of ZnSe at the top is present even at room temperature as indicated by XPS.

On 100^oC annealing, the XRD pattern indicates the formation of additional chemical species such as As_2Se_3 though it is small in concentration. The XRD also reveals that the interface is widened but graded. The widening is due to the increased Ga migration. The immediate interface with the GaAs substrate is a Ga-rich phase viz. Ga_2Se_3 followed by a mixture of Ga_2Se_3 and As_2Se_3.

With increasing annealing tempeature 200^oC the interface transform into a predominantly Ga_2Se_3 phase followed by a mixture of As_2Se_3 and Zn_3As_2 as evidenced by XRD and XPS data. With a glancing

angle of 2°, no peak corresponding to GaAs appears indicating the widened interface. The nature of the XPS analysed sputter profiles is indicative of differences in the chemical nature of selenides formed. The binding energies show trends of changes with increasing annealing temperatures but the exact nature of the phase formed is more clear from glancing angle X-ray diffraction analysis.

5.4.7. C-V Measurements :

Capacitance (C) voltage (V) plot were obtained for Schottky diodes prepared by deposting silver over the thin film of ZnSe on GaAs. $1/C^2$ versus bias (V) plot is shown in Fig.9 for diodes of virgin GaAs and those with ZnSe overlayers. A remarkable increase in the built in potential progressively from 0.8 eV to 1.8 eV with annealing temperature was observed.

The reduction of surface states on GaAs by bond passivation should ideally decrease the surface potential and therefore the built in potential also. However if there is a thin insulating layer of Ga_2Se_3 at the interface the charge transfer from GaAs is inhibited and thus the potential may show an increase. It is therefore not very clear as to whether the surface is passivated by surface layer of ZnSe or not. Two different junctions may give rise to different capacitors and built in potentials which may add together effectively increasing the net value that is measured. Few more rigorous experiments should therefore be performed in order to draw any definite conclusions.

5.4.8. Photoluminescence Measurements :

As discussed in Chapter 2A PL intensities are directly related to the radiative recombinations and reflect any change in the nonradiative recombination centres. PL spectra for ZnSe deposited GaAs surface for three different samples were recorded.

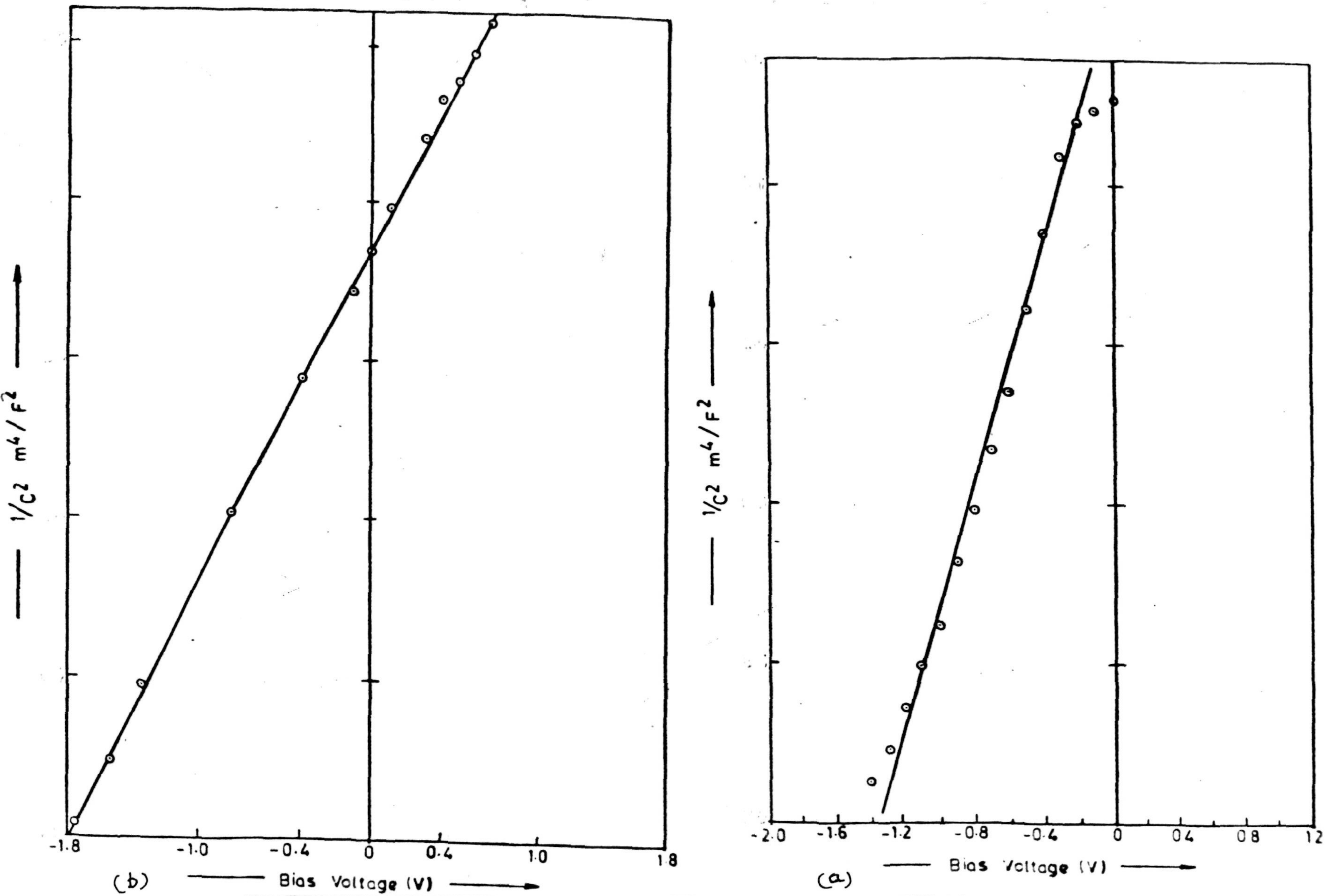

Fig. 9 : $1/C^2$ Vs. plots for n-GaAs/ZnSe/Ag diodes
(a) 100^oC (b) 200^oC.

Fig. 10 gives the PL spectra for (a) virgin (b) as deposited (c) annealed at 100°C and (d) annealed at 200°C. By comparing (a) and (c) it is found that the PL intensity increases by two times when the overlayer is annealed at 100°C. However after annealing at 200°C the intensity has dropped down although still remaining higher compared to that observed in (a).

The photoluminescence has therefore indicated that the overlayer of ZnSe deposited by LGIR technique is effective in passivating apart from providing a good heterojunction. However the PL intensities have not increased to a level which is expected (by orders of magnitude). This may be due to a thin oxide layer present on the substrate while deposition of ZnSe by LGIR technique. Apart from this the interface layer of GaAs might have been disturbed due to seggregation of Zn after annealing. The interface may become more defective and Fermi level still remains pinned due to added defects.

5.4.9. Valence band discontinuity in ZnSe/GaAs Heterojunction

From the XPS data reported in the section 5.4.4 and using the equation 5.3, the band discontinuities for three heterojunctions were calculated. According to this three quantities are required to determine Δ Ev. These are (1) the core level to valence band maximum binding energy difference for GaAs ($E^{GaAs}_{Ga3d} - E_v^{GaAs}$) (2) the core level to valence band maximum binding energy difference for ZnSe ($E^{ZnSe}_{Zn3d} - E_v^{ZnSe}$) and (3) the core level binding energy difference $E_{CL} = (E^{GaAs}_{Ga3d} - E^{ZnSe}_{Zn3d})$.

The first two values are obtained from the measurements on individual semiconductors. Here in absence of the data for ZnSe we have used the reported data for Z_{3d} level in pure ZnSe. It has been

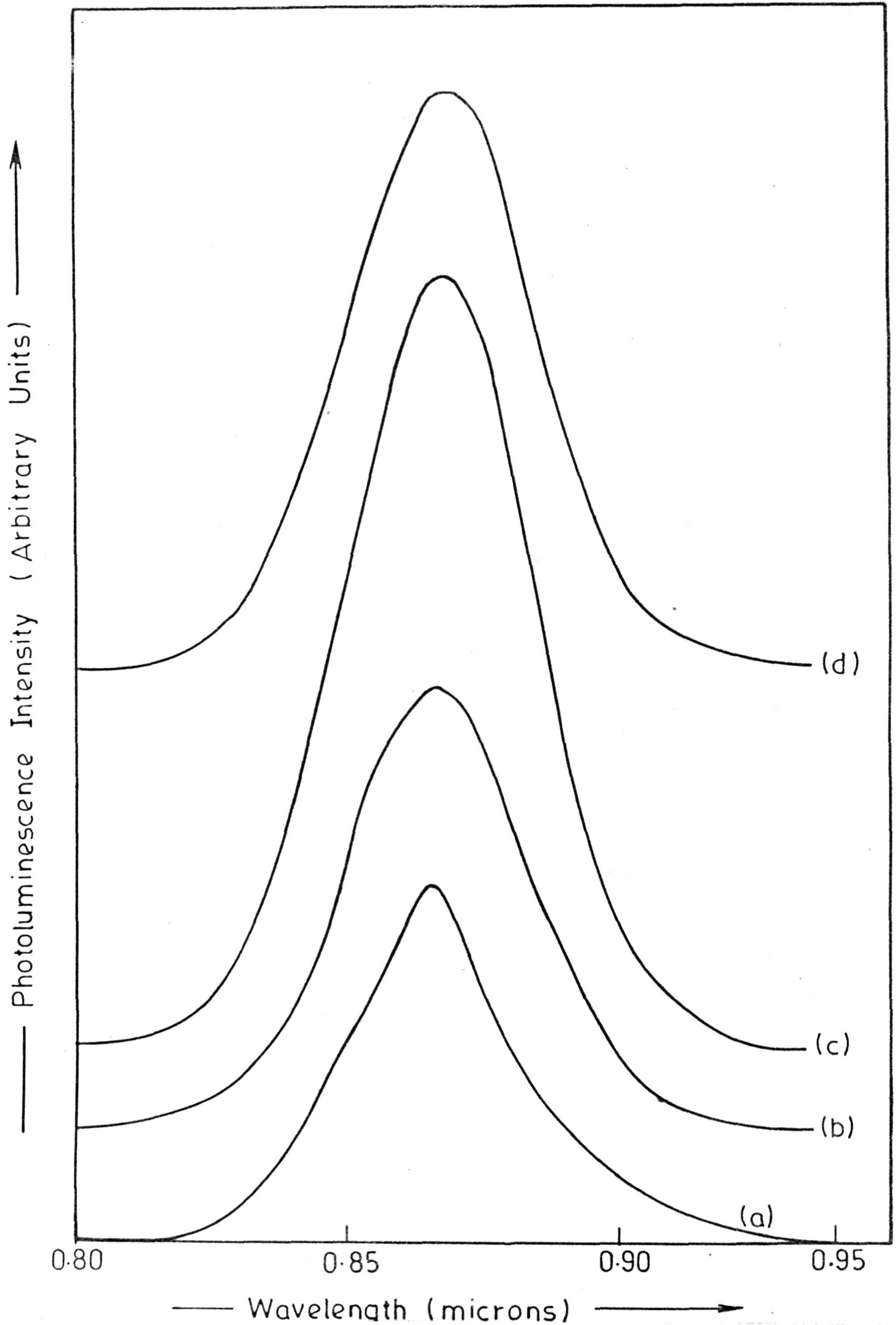

Fig. 10 : Photoluminescence spectrum for (a) n-GaAs (b) n-GaAs/ZnSe (c) n-GaAs/ZnSe (100°C) (d) n-GaAs/ZnSe (200°C).

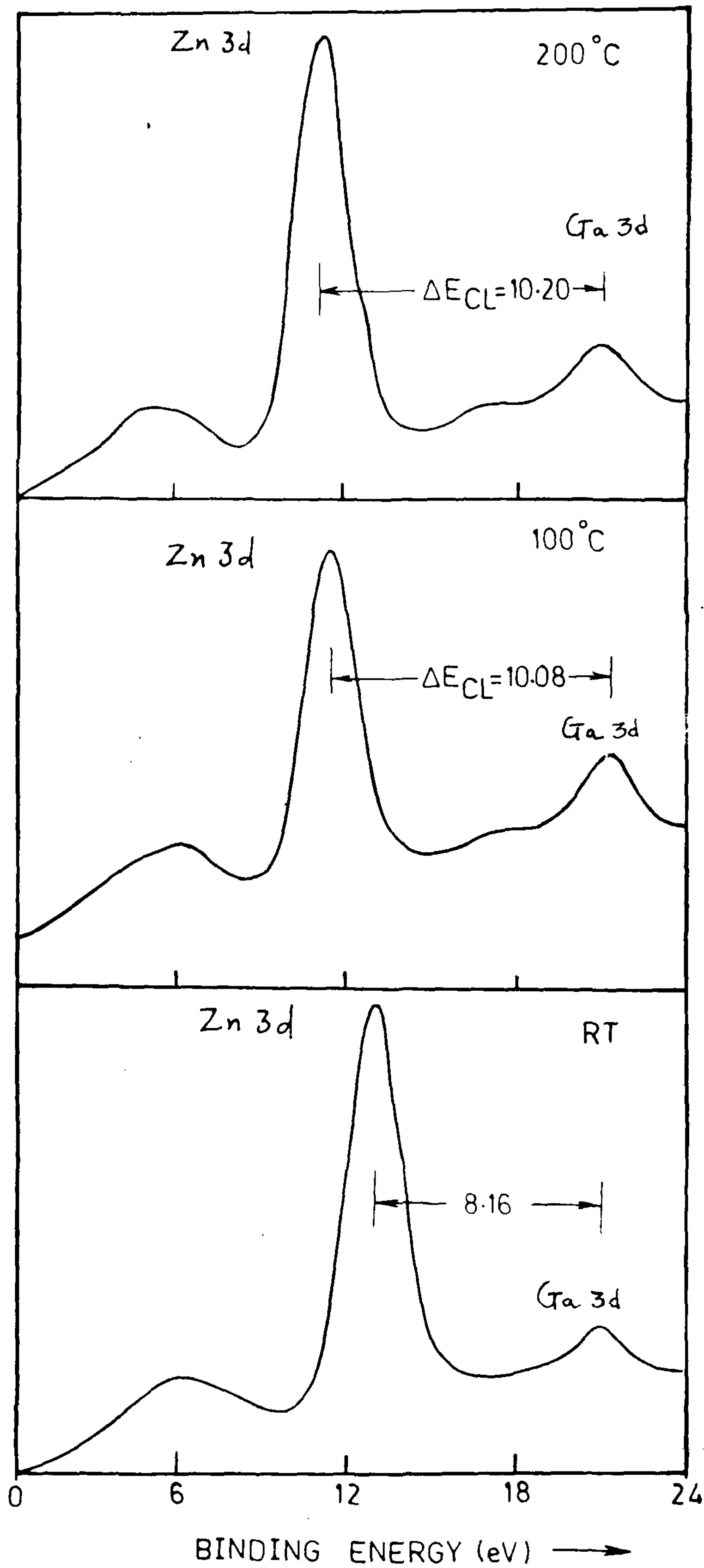

Fig. 11 : E_{CL} calculations for band discontinuity

shown by Kowalczyk et al. by comparing the XPS data with the fitted instrumentally broadened theoretical density of states that E_0 can be considered at spectrometer zero energy value. Thus the data collected from the XPS spectra are and the calculated values of ΔE_V are given in Table 3.

A possible band diagram is presented in Fig. 12 for ZnSe/GaAs interface at room temperature following the results of valence band discontinuity. The position of Fermi level in GaAs was found from the energy position of the spectrometer where the actual zero photoemission is observed. The film of ZnSe was assumed to be totally intrinsic and its Fermi level was taken at the middle. The band bending at the interface is shown on the basis of the values of ΔE_V and ΔE_{CL}.

It is apparent from these calculations that the discontinuity ΔE_V has reduced from 2.02 to 0.10 when the film was annealed and to a value of - 0.02 which is almost equivalent to 0.0 for after annealing at 200°C. This indicates that the band bending has markedly reduced by annealing and effectively the surface states at the interface are largely reduced.

TABLE 3

XPS data used for calculating the Valence band Discontinuity (Reference Fig.11).

$(E^{GaAs}_{Ga3d} - E_V^{GaAs}) = 19.08$ From XPS data.

$(E^{ZnSe}_{Zn3d} - E_V^{ZnSe}) = 8.90$ eV From reported data

Using Fig.11 following data is obtained.

Energy	RT	100°C	200°C
$\Delta E_{CL} = (E^{GaAs}_{Ga3d} - E^{ZnSe}_{Zn3d})$	8.16 eV	10.08 eV	10.2 eV
ΔE_V (Calculated)	2.02 eV	0.10 eV	-0.02 eV

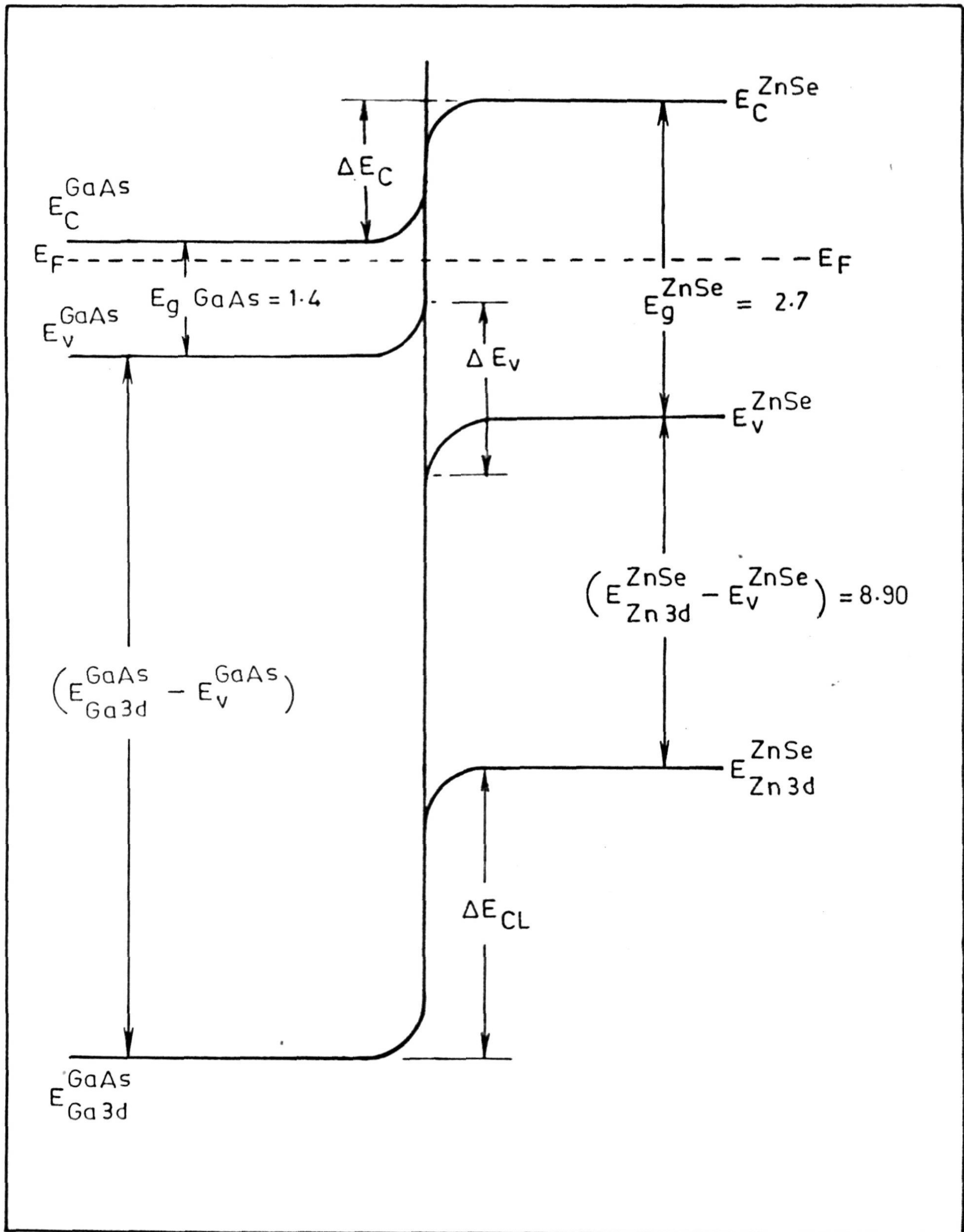

Fig. 12 : Possible band bending diagram for GaAs/ZnSe system

REFERENCES

1. H. Kroemer,

   Surf. Sci. 132, 543 (1983).

2. A.G. Milnes and D.L. Feach,

   Heterojunction and metal semiconductor junctions (Academic, New York, 1972). F. Capasso and G. Margamitondo, heterojunction Band Discontinuities, Physica and device. Applications (North Holland, New York, 1987).

3. G. Marganitondo,

   Surf. Sci. 168, 439 (1986).

4. F. Capasso,

   Surf. Sci. 132, 5217 (1983);

   Surf. Sci. 142, 513 (1984);

   J. Vac. Sci. Techn. B3, 457 (1983).

5. R.S. Baner and H.W. Sang,

   Surf. Sci. 168, 479 (1986).

6. J.A. Vau Vechtew;

   J. Vac. Sci. Tech. B3, 1240 (1985).

7. W.R. Frensley and H. Kroemev,

   Phys. Rev. B15, 2642 (1977).

   A. Munoz, J. Sanchez - Dehisa and F. Flozez

   Phys. Rev. B35, 6468 (1987).

   W.A. Horrison

   J. Vac. Sci. tech. B3, 1231 (1985).

8. J.R. Waldrop, R.W. Grant, S.P. Kowalczyk and E.A. Kraut. J. Vac. Sci. Tech. A3, 835 (1985).

9. S.P. Kowalczyk, E.A. Kraut, J.R. Waldrop and R.W. Grant. J. Vac. Sci. Tech. 4, 482 (1982).

CONCLUSION

Heterojunction of ZnSe/GaAs were successfully prepared following the new technique of LGIR. Various analytical methods were used to study this interface from the viewpoint of a passivating insulating layer and a heterojunction. XRD and TEM have shown that a good lattice matched crystalline layer of ZnSe is obtained by annealing the deposited layer at 200°C. The quality of the film was thus quite satisfactory.

The passivating properties were however not found to be very strongly influential, although band picture showed extensive reduction in band bending after annealing at 200°C. Before comming to any conclusion it is necessary to pursue the work in more details.

6.1 INTRODUCTION

Amorphous III-V films began to be studied after 1970 and their use in various industrial applications has stimulated considerable interest. Most of the electronic systems use crystalline semiconducting materials. Nevertheless, it is to be anticipated that increasing use will be made of amorphous semiconductor films as potential solar photovoltaic energy converters of specific thin film components. For example, considerable research is in progress in the field of amorphous silicon, prepared by glow discharge decomposition of silane [1], dealing with both basic aspects and applications. In comparison, very few investigations are performed on binary amorphous films, particularly amorphous GaAs (a-GaAs) [2-6]. Moreover, the experimental procedures used to obtain films by sputtering or vapourisation of GaAs do not give enough flexibility to enable a deposit to be formed under different experimental conditions.

The delay in the interest in a-GaAs can be attributed to the difficulty in understanding the Physics and Chemistry of crystalline GaAs and III-V compounds in general. The current research on crystalline GaAs (c-GaAs) has reached a stage where the intrinsic material problems have been identified. The search for an excellent material for surface passivation and for use in Metal Insulator Semiconductor (MIS) devices is still in progress. There are at present quite a few candidate materials [7-10] which are being used for the above application. Hence, the attention is now being diverted to the study of amorphous GaAs, which is also capable of exhibiting several interesting properties for future thin film technology.

Such studies on amorphous materials are highly desirable as thin films offer many advantages.

- They can be prepared with larger area as compared to single crystals.
- In thin films, the freedom to deposit stoichiometric proportions enables us to have a fine control over its electrical and optical properties.
- When cooled from the melt, irrespective of the rate of cooling; deposition of thin films is the only method by which such materials can be obtained in the amorphous form.

In the recent past, work has been done on a-GaAs thin films prepared by various techniques. Some of these include hydrogen incorporated rf sputtering to prepare a-GaAs:H [11], Molecular Beam Epitaxy (MBE) [12], combination of plasma decomposition and physical sputtering [13], plasma chemical vapour deposition [14] and sputtering or flash evaporation[15] etc. The over all similarity of the radial distribution functions of these amorphous III-V compounds to those of a-Ge or a-Si, as deduced from X-ray diffraction experiments [16], suggest that, on an average, they retain the same tetrahedral short range order, and that their structure can be well described by the continuous random network models proposed for tetrahedrally co-ordinated amorphous semiconductors [17-19]. Differences in network topology can be expected between amorphous Ge or Si and amorphous III-V compounds even if they contain the same basic tetrahedral unit, since in the latter the bonding is partially ionic [20]. This should in particular, help to prevent the formation of odd-membered rings of atoms, which would necessarily introduce bonds between like atoms.

These amorphous compounds are also susceptible to defects. Some are certainly related to the occurance of unsatisfied or dangling bonds as in a-Ge and a-Si, however, these may rearrange or reconstruct

themselves differently from those in the group IV elements, since, the group V components in particular, can adapt threefold co-ordination. Other defects, specific to compound materials, may be related to the presence of bonds between like atoms or wrong bonds. Even if intrinsic wrong bonds are likely to be inhibited by the partially ionic character of the bonding, the possibility of chemical disorder cannot be discarded in real materials, especially when quenched from the vapour. Recent studies on the X-ray photoelectron spectroscopy of a-GaAs has conclusively proved the presence of As-As wrong bonds [21]. The problem is complicated in real materials by the fact that film stoichiometry is difficult to achieve and control with sufficient accuracy.

Chemical ordering was strongly suggested by photoemission experiments, which in particular, showed no shift and no broadening of the core levels with respect to those of the corresponding crystal [22]. The results of Raman [23] and infrared absorption [24] measurements were more ambiguous, but the possibility of extrinsic defects related to deviations from stoichiometry could not be completely ruled out [25]. EXAFS measurements on a-GaAs revealed different environments for Ga and As atoms, which was interpreted as evidence for the presence of wrong bonds. However, contrary EXAFS results are also reported on flash evaporated a-GaAs forms [26]. The authors from their observations, showed the existence of chemical ordering in their 2000 Å thick samples deposited at room temperature and not annealed. These results strongly suggest a predominance of normal GaAs bonds. If wrong bonds were to exist, both types (Ga-Ga and As-As) should have exactly the same length as the normal bonds. The discrepancy in these two results probably illustrate the structural

differences which are likely to occur between amorphous compound films which are not deposited by the same method.

Our work on amorphous GaAs encompasses deposition of thin films onto substrates at room temperature by the technique of flash evaporation. The structure and morphology of these as-deposited films and the effect of annealing at elevated temperatures on the above mentioned properties are studied by X-ray diffraction (XRD) and Transmission electron microscopy (TEM). The effect of post hydrogen passivation of these films is studied by Fourier Transform Infrared Spectroscopy (FTIR). These results are compared with studies on hydrogenated amorphous gallium arsenide, a-GaAs:H.

6.2 EXPERIMENTAL DETAILS

6.2.1 Deposition of thin films of a-GaAs:

Thin films of a-GaAs were deposited onto various substrates by the technique of flash evaporation. This technique is most suitable when the compound to be deposited is likely to dissociate during evaporation. In our case if the deposition is done by conventional vacuum evaporation or sputtering, GaAs decomposes and arsenic (having a high vapour pressure) escapes out. This results in the deposited film becoming arsenic deficient.

The technique of flash evaporation consists of dropping the compound in the form of a fine powder onto a boat of tungsten heated to a temperature well above that required for the vapourisation of the least volatile component of the source material. An ac vibrator with mechanical chute fixed rigidly to the vibrator is used to feed the finely powdered compound onto the boat. The rate of feed of the powder could be regulated by controlling the vibrator speed. The substrates were placed on a holder held above the source. The deposition was

carried out in dynamic vacuuum conditions using a vacuum coating unit (HIND HIVAC 12A4, INDIA). The background pressure during deposition was 10^{-6} torr or better and the distance between the source and substrate was between 6-8 cms. By optimising the various parameters including the rate of feed of the powder, distance between source and substrates etc. we have obtained thin amorphous uniform films about 2000 Å thick.

6.2.2 Structure:

The thin films of a-GaAs deposited onto cleaned glass substrates were used for X-ray diffraction studies. These films were sealed at a pressure of about 10^{-6} torr in silica capsules. This was done to prevent oxidation due to exposure as well as out diffusion of arsenic, which is possible if the films are annealed in dynamic vacuum conditions. For this purpose silica tubes with diameter about 1.5 cms and length about 6-7 cm were used. They were sealed to standard B26 joints and connected to the vacuum system. These silica tubes were cleaned and dried by the standard procedure. The a-GaAs films deposited on glass substrates were placed inside the capsule and a constriction was made at the neck to make the job of sealing at 10^{-6} torr pressure, easier. The low pressure was realised by an all glass vacuum system. It mainly consisted of a mercury diffusion pump backed by a rotary pump, two liquid nitrogen traps and a McLoid gauge for pressure monitoring. Once the pressure of 10^{-6} torr was attained the silica capsules were sealed at the constriction. These sealed capsules were then placed in a resistive furnace and annealed at different temperatures and for different durations of time. The effect of annealing temperature and duration on the structure of the a-GaAs films were studied by X-ray diffraction (PHILIPS, PW 1730, HOLLAND).

6.2.3 Morphology:

For studying the morphology the same procedure as described above was used for the deposition of a-GaAs, but the substrates were NaCl single crystals. The crystals were cleaned by dipping in deionised water to get rid of any residual adsorbed impurities and then wiped dry. After deposition these films on NaCl crystals were sealed in silica capsules as described above and annealed at the same temperatures. After annealing the films were taken out from the capsule. The NaCl crystal was dipped very slowly into a trough of deionised water so that the a-GaAs film on the top separates out from the crystal and float on the water surface. The film is then picked onto a copper mesh on which a layer of colloid is already present. The GaAs film on the copper mesh is then used for the morphology studies by Transmission Electron Microscopy (TEM-JEOL 1200, EX microscope TOKYO, JAPAN).

6.2.4 Hydrogen passivation of a-GaAs:

The post passivation of the a-GaAs films deposited at room temperature, by hydrogen was achieved by two different techniques. For these passivation studies the substrates used were single crystals of intrinsic silicon. The specifications of silicon used as substrate material were very rigid because the IR studies in the absorption mode necessiated a very low coefficient of reflection which in turn implied that the carrier concentration in the wafers be as low as possible. Hence our choice for intrinsic silicon wafers. The first technique for hydrogen passivation of a-GaAs involved exposing the films to hydrogen plasma for several hours and the second one was subjecting the films to hydrogen ion bombardment for a few minutes before hydrogenation effects would be noticeable.

Th. 9309

6.2.4A Hydrogen plasma passivation:

The system for hydrogen plasma passivation of a-GaAs consisted of a cylindrical tube with two horizontal parallel plates made of copper which also served as the electrodes for plasma excitation. The plates were rectangular in shape about 3 cm x 2 cm area and about 1 mm thick. The separation between the plates was about 2 cm. The a-GaAs films were deposited on the single crystals of intrinsic silicon wafers by the same technique of flash evaporation. Prior to deposition of a-GaAs the silicon wafers were chemically cleaned by etching in HF acid and rinsed in deionised water. These fil ms of a-GaAs on silicon were placed on the lower plate. The system was evacuated to a low pressure using a diffusion backed by rotary vacuum pump and hydrogen was flushed into the system. The pressure of about 0.5 Torr of hydrogen was maintained in the system with the help of a precision controlled needle valve. The plasma was excited between the plates by a 13.56 MHz rf generator. The plasma hydrogenation was carried out in dynamic vacuum conditions for different durations of time. The effect of this hydrogen plasma treatment on the absorption spectra of a-GaAs was studied by Fourier Transform Infrared spectroscopy (FTIR-NICOLET 60 SXB).

Th. 9309

6.2.4B Hydrogen ion bombardment:

In this method the films were subjected to high energy (2.3 keV) hydrogen ion bombardment. The system consisted of an rf ion source made of a 6 cm diameter quartz tube and an aluminium extractor. The plasma was excited by a capacitive coupling using external ring type electrodes at a frequency of 10 MHz. Hydrogen was introduced into the chamber with the help of a thermomechanical leak valve. During extraction the ion beam was also focussed by appropriate magnetic

field. The ion current was monitored by a Faraday collector. The a-GaAs films were bombarded with an ion current of about 700 uA. The effect of this hydrogen ion treatment on the a-GaAs was studied by FTIR.

6.3 RESULTS AND DISCUSSIONS:

6.3.2 X-ray diffraction (XRD):

Fig.1 gives the XRD results of thin films of a-GaAs deposited on glass substrates. It reveals that the films in the as-deposited condition are amorphous or non crystalline. Atleast, the grain size was so small, and the disorder within the grains so great, that no specific diffraction lines could be detected. Comparison of the very broad maxima in Fig.1(a) for the as deposited films with the peaks in Fig.1(d) for a fully annealed film shows the existence of a rough correlation of the Bragg angles for the two sets of diffraction patterns, which is anticipated for non-crystalline and crystalline material of the same composition. In Fig. 1(b) one can observe crystallisation to some extent after annealing at 300°C for 2 hours and progressively the appearance of a pattern characteristic of well defined crystalline material at about 400°C (Fig. 1(c)). The sharpening of the peaks observed after an anneal at 500°C for 2 hours is indicative of better crystalline order, reduced microstresses and a large grain size. Table 1 gives the diffraction peak positions obtained from the film annealed at 500°C compared with those reported [27] from a random powder sample. All of the possibly identifiable diffraction peaks were observed, and matching of the intensities between the two sets of peaks indicates that the annealed film was almost totally free of any preferred orientation to a degree that rarely occurs in thin films regardless of their mode of deposition.

TABLE 4

Relative concentrations of various elements at different temperatures of annealing, for three depths of sputtering.

Temp.	As received	a	b	c
		Ga/Se ratio		
R.T.	0.15	0.30	4.2	6.26
100°C	0.36	0.5	0.4	0.4
200°C	0.07	0.71	2.27	2.27
		As/Se ratio		
R.T.	-	0.39	3.78	3.81
100°C	0.08	0.1697	0.23	0.29
200°C	0.06	0.512	1.65	1.88
		As/Zn ratio		
R.T.	-	0.18	2.74	3.73
100°C	0.02	0.18	0.13	0.14
200°C	0.09	0.28	0.95	0.94

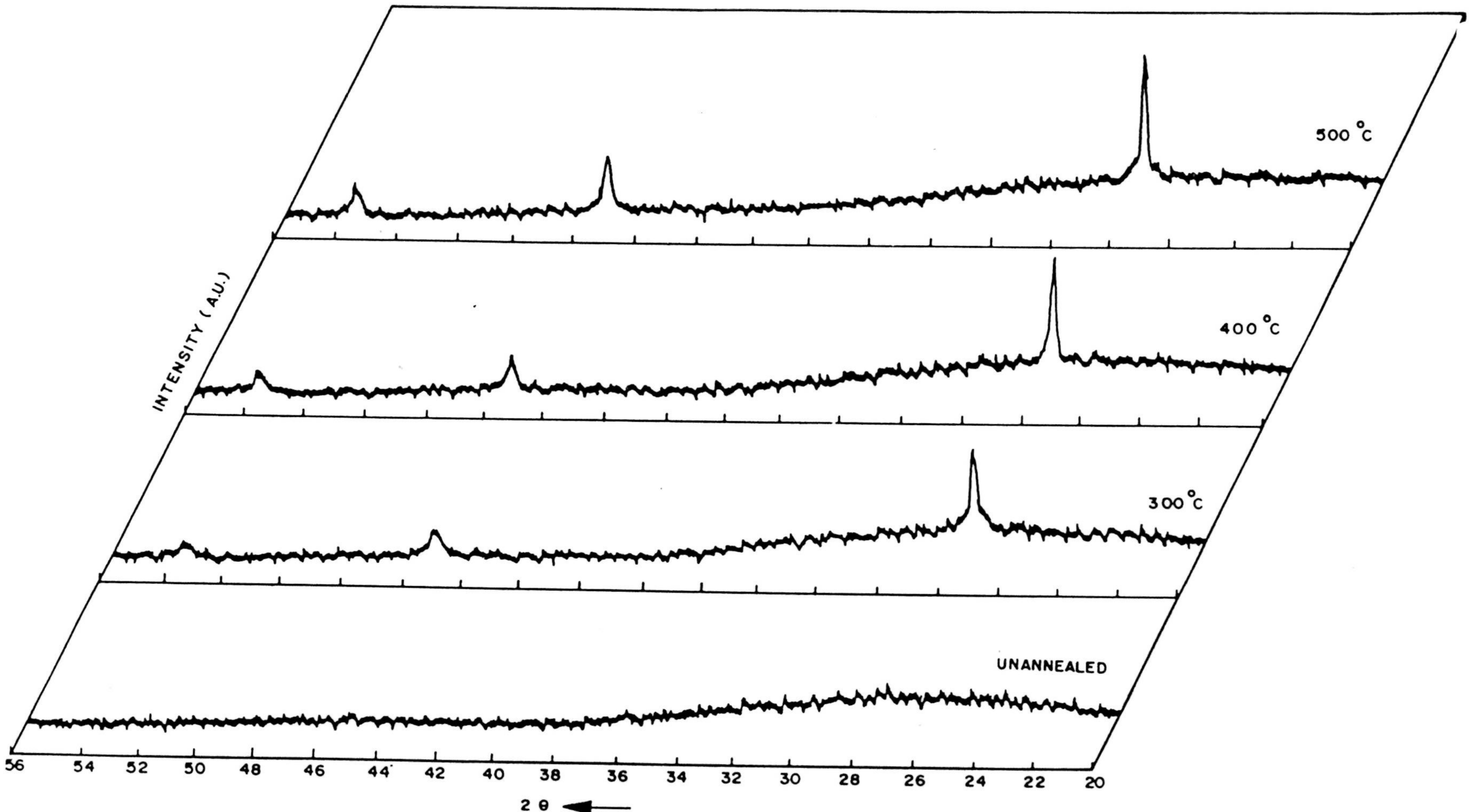

Fig.1. X-ray diffraction pattern of a-GaAs
(a) as deposited; (b) annealed at 300°C;
(c) annealed at 400°C; (d) annealed at 500°C.

TABLE 1 : XRD DATA ANNEALED a-GaAs

20	d	I/I_o	d (reported)	I/I_o (reported)	hkl
27.3	3.26	100	3.27	vs	111
45.3	2.00	54	2.00	s	220
53.7	1.70	18	1.70	ms	311

vs:very strong

s :strong

ms:medium strong

The average grain size is also calculated from the XRD data using the Sherrer formula [28],

$$d = \frac{\beta^{1/2} \lambda}{2 \cos \theta}$$

where d : grain size

λ : wavelength of the X-rays

β : FWHM of the particular peak in radians

θ : Angle at which the peak appears.

This comes out to be about 30-50 nm for the fully annealed sample.

6.3.3 Transmission Electron Microscopy (TEM):

The above X-ray information is nicely supplemented by the observation made by TEM. The results are presented in Fig.2. For the as deposited samples the TEM micrograph does not reveal any structure, while the electron diffraction pattern, shows only a broad halo characteristic of any amorphous material, in agreement with the X-ray results. After 2 hr anneal at 200°C and 300°C the results indicate crystallisation of a small order corresponding to very faint continuous diffraction rings and the formation of microcrystalline films. Other TEM results presented in the figure show a continuous transition at temperatures between 300°C and 500°C to the structure corresponding to the diffraction pattern characteristic of micro crystalline nature. Fig.2(d) shows the TEM micrograph for the film annealed at 500°C for a couple of hours and this indicates crystallinity corresponding to the formation of larger grains, which is further confirmed by continuous diffraction rings. The micrograph indeed shows that the GaAs film is fine grained with an average size of about 30-50 nm which compares well with that calculated from the XRD data.

(a)

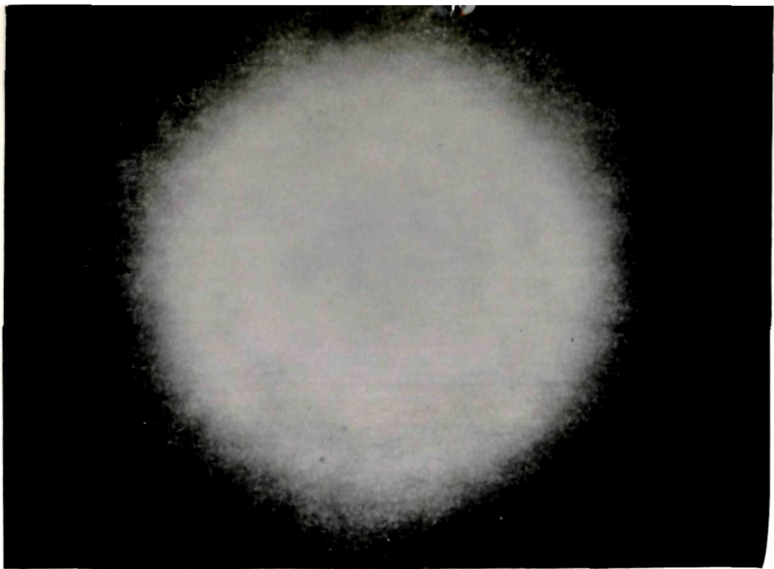

(b)

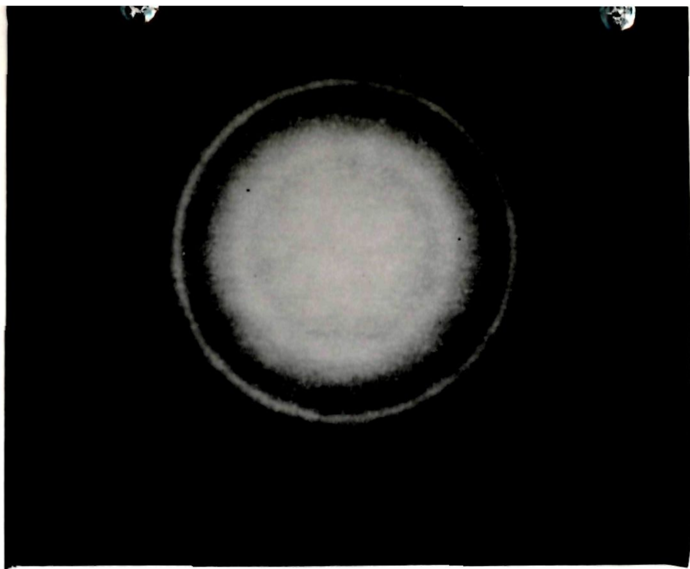

(c)

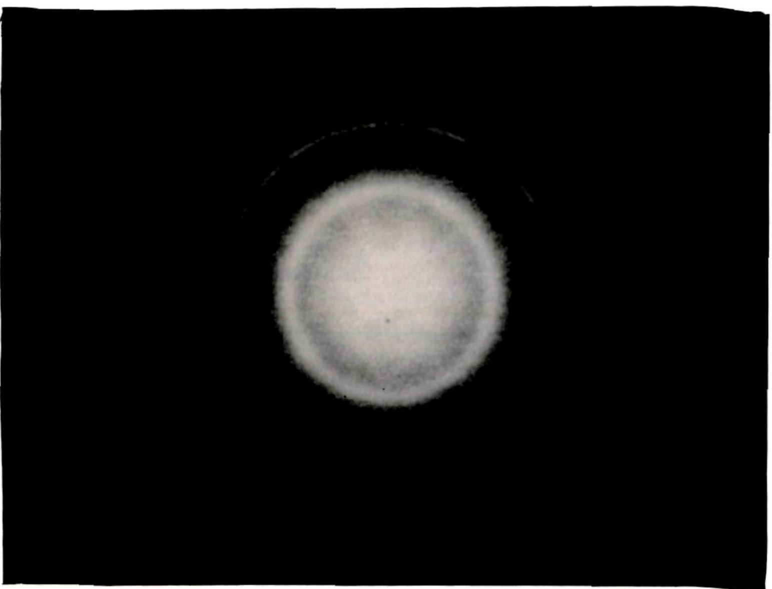

(d)

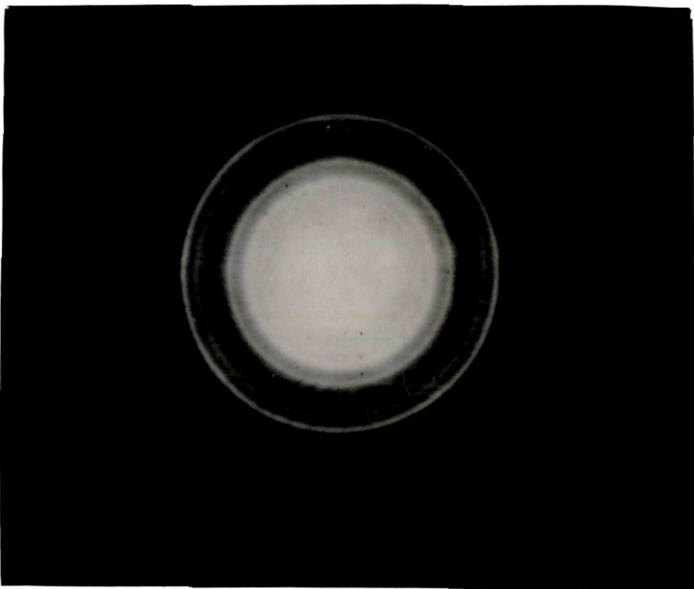

Fig.2- Transmission electron micrograph of a-GaAs
(a) as deposited; (b) annealed at 300°C;
(c) annealed at 400°C; (d) annealed at 500°C.

(a)

(b)

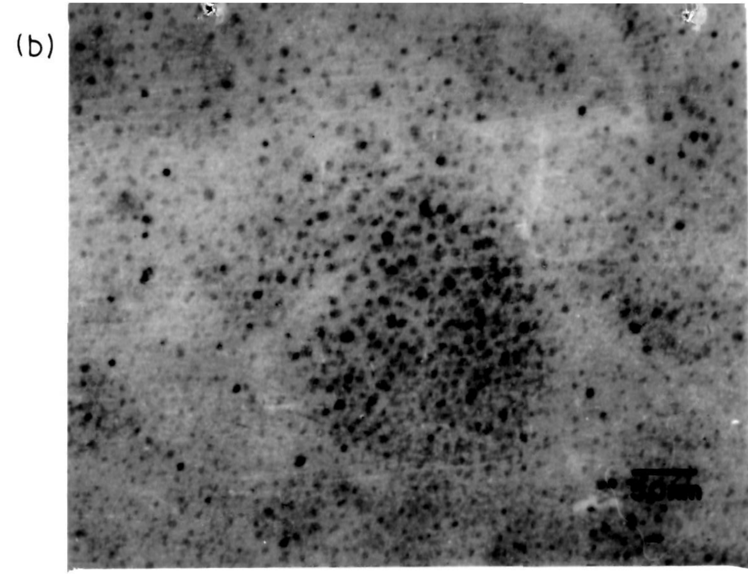

(c)

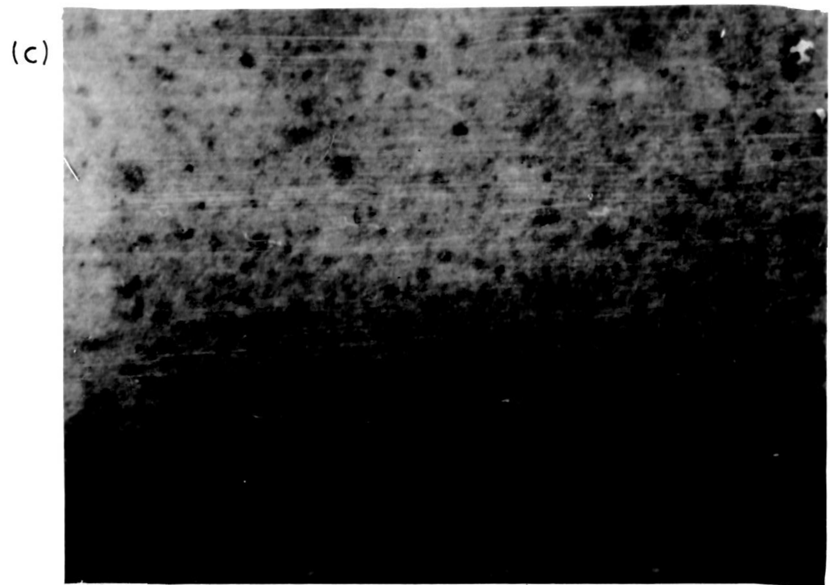

(d)

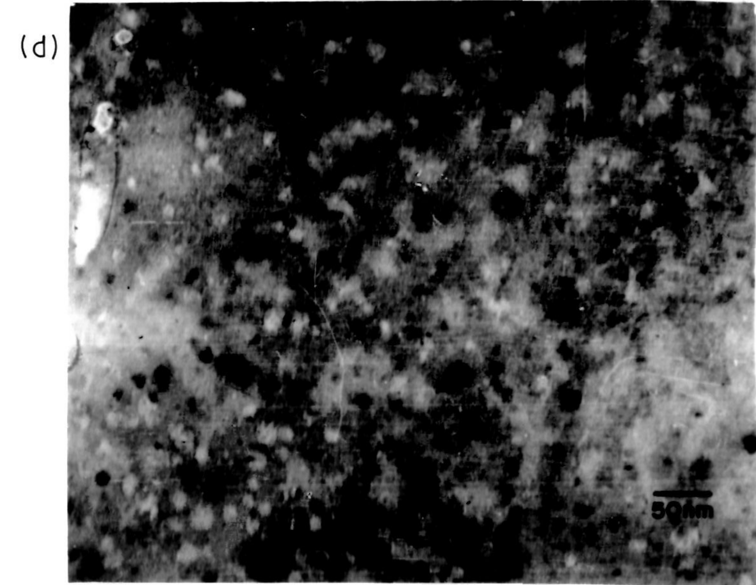

Fig. 2 : Electron diffraction patterns of a-GaAs
(a) as deposited ; (b) annealed at 300°C ; (c) annealed at 400°C ; (d) annealed at 500°C.

6.3.4 Fourier Transform Infrared Spectroscopy (FITR):

6.3.4A

Fig.3 shows the FTIR spectrum of unpassivated a-GaAs deposited on intrinsic silicon substrate. There are no peaks observed in this absorption spectrum. To observe any change in the FTIR spectra necessiated nearly eight hours of continuous hydrogen plasma treatment. Figs.4 and 5 show the FTIR absorption spectra of a-GaAs subjected to different durations of hydrogen plasma. The spectra clearly show changes in the lower wavenumber region. It is also evident that there is not much difference in the FTIR spectrum of Figs. 4 and 5 for the 4 and 8 hours hydrogen plasma treated a-GaAs films respectively. Only the peaks become more well defined in the latter as compared to the former where they appear as spikes.

There is experimental evidence for the theoretical calculations of the localised vibrational modes, but these are restricted to the high frequency region. Theoretical calculations also suggest vibrational modes due to GaH_2, As-H and AsH_2 in the low frequency region. Our studies on post hydrogenation of GaAs also show the presence of these modes. The spectra also reveal better resolved peaks especially in the low frequency region.

The broad band appearing around 510-540 cm^{-1} in Fig.5 has been assigned to Ga-H-Ga bridging bonds. This type of bridge bonding has been reported for GaP:H and GaSb:H [29] as well. This has also been predicted for GaAs:H [30] by theoretical calculations and which is now proved by our experimental observations. The existence of this type of hydrogen bridges has been suggested for a-Si:H [31]. But as yet no evidence for such bridging hydrogens has been provided for a-Si:H or a-Ge:H. These have been found in a number of aluminium compounds (Al-

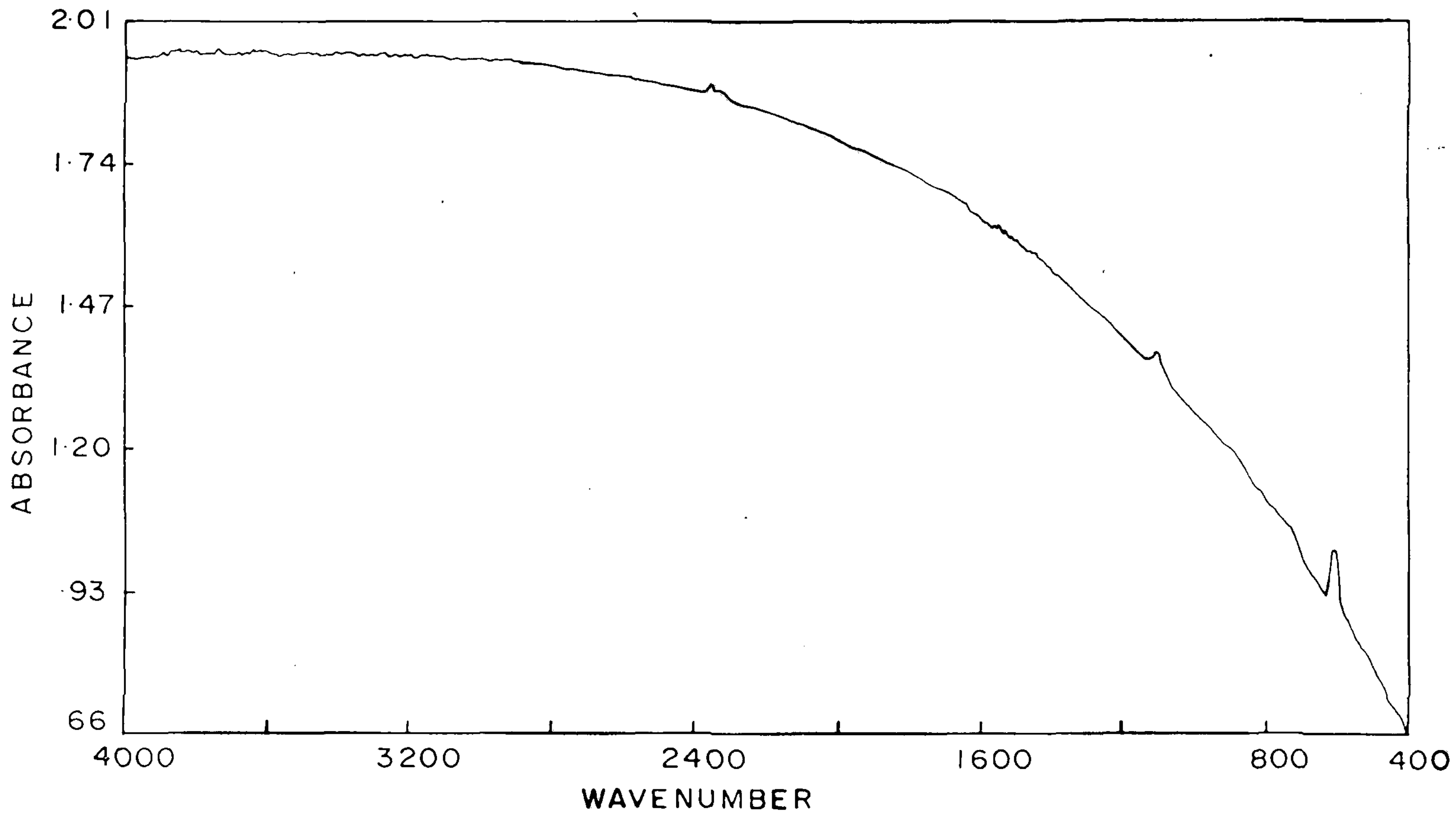

Fig.3. FTIR spectrum of unpassivated **a-GaAs.**

H-Al bridges). The distinguished features of such bridging bonds are, their appearance at lower frequencies as compared to single bonds. The monomer bonding Ga-H appear at about 650 cm^{-1} which is higher than the bridging Ga-H-Ga bond at about 510-540 cm^{-1}.

Apart from this, there are clear peaks at about 700 cm^{-1} and 560 cm^{-1} which have been attributed to GaH_2 bending and twisting modes respectively and a small spike at about 620 cm^{-1} due to AsH_2 wagging. At about 1460 cm^{-1} there is a dip similar to the one reported by Wang et al. and designated as due to the Ga-H-Ga stretching mode. Table 2 gives the vibrational frequencies with the associated complex and reported values also, for comparison. Figs. 4 and 5 also show some clear modes in the lower wavenumber region of the spectra which have not been observed by earlier workers. At the moment we have no concrete evidence to assign any particular species to the various peaks.

6.3.4B

The FTIR spectrum of hydrogen ion implanted amorphous gallium arsenide is shown in Fig.6. This spectrum is quite different from the hydrogen plasma treated a-GaAs. In this case there are sharp peaks at about 530 cm^{-1}, 565 cm^{-1} and 670 cm^{-1}. It is clearly seen from Fig.5 that there is a small peak at about 670 cm^{-1} in the hydrogen plasma treated a-GaAs which is more prominent in the ion bombardment induced hyrogenation case. There is no reference to this peak in any of the earlier work on hydrogenated a-GaAs.

Fig.7 shows the FTIR spectrum of a-GaAs subjected to hydrogen ion bombardment with the substrates maintained at about $100^{o}C$. The effect of sample heating is clearly seen by the peak at about 620 cm^{-1} due to As-H bonding becoming very intense. It is also seen that the 530 cm^{-1}

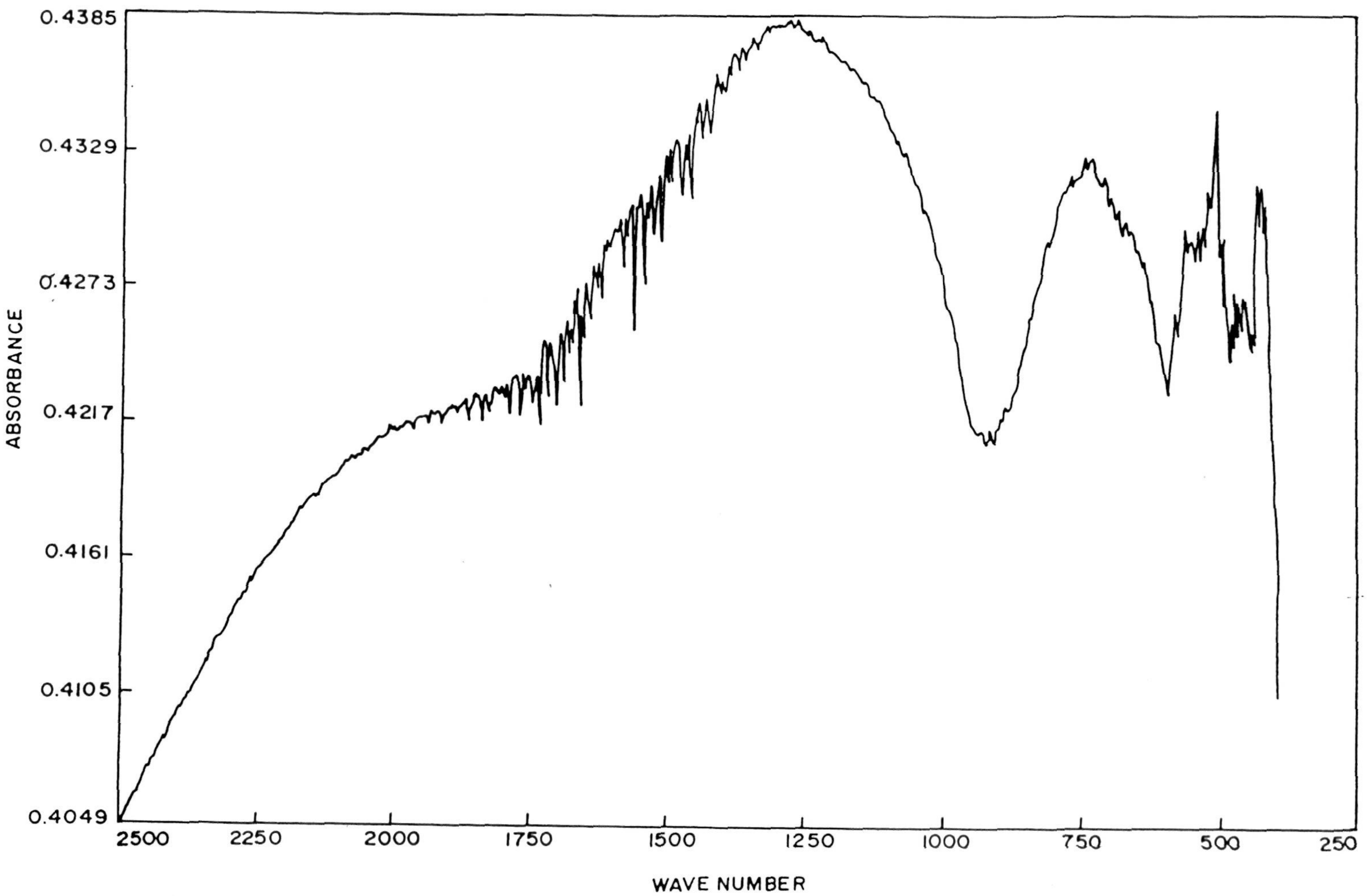

Fig.4. FTIR spectrum of a-GaAs subjected to hydrogen plasma for 4 hours.

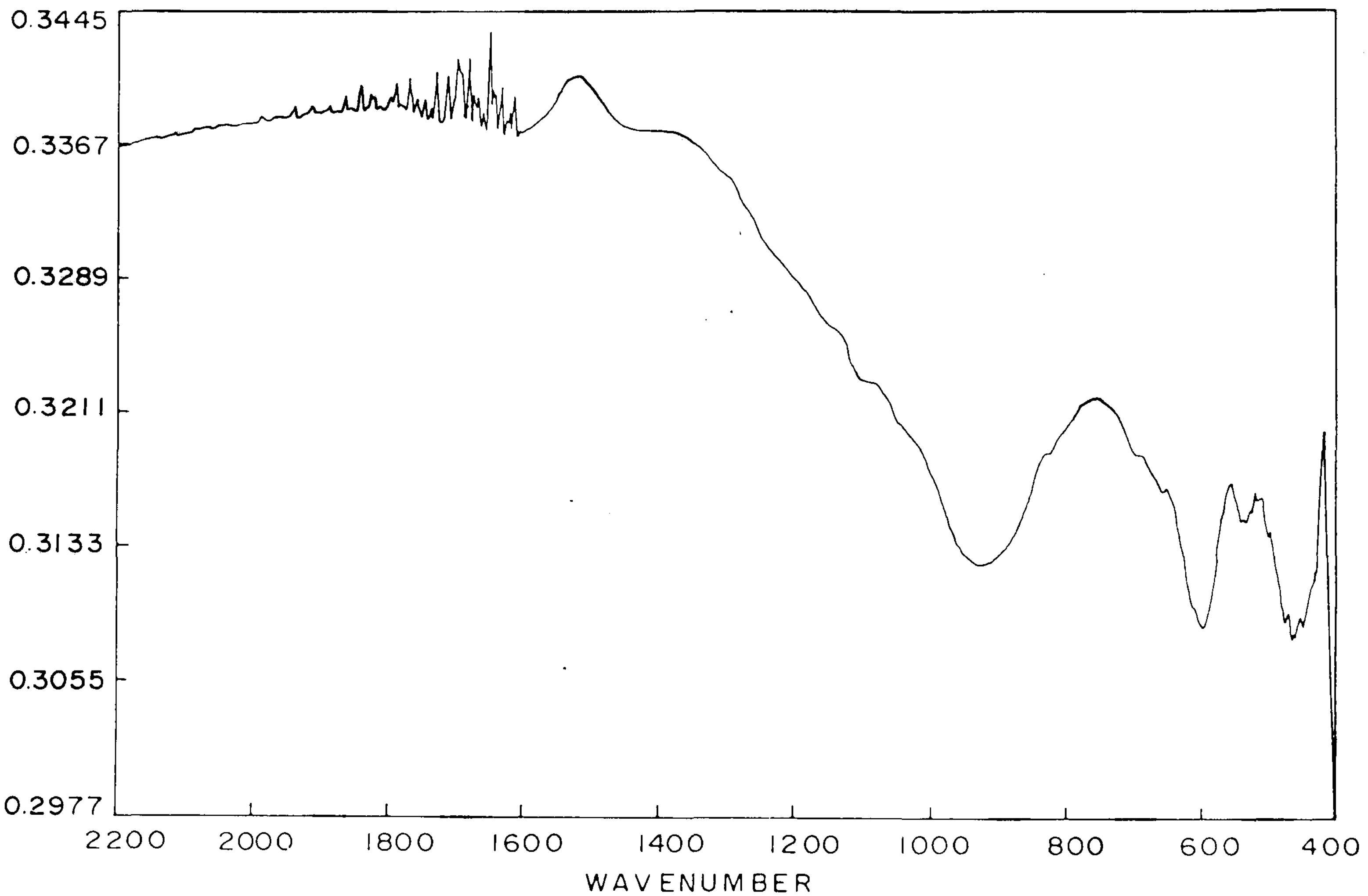

Fig.5. FTIR spectrum of a-GaAs subjected to hydrogen plasma for 8 hours.

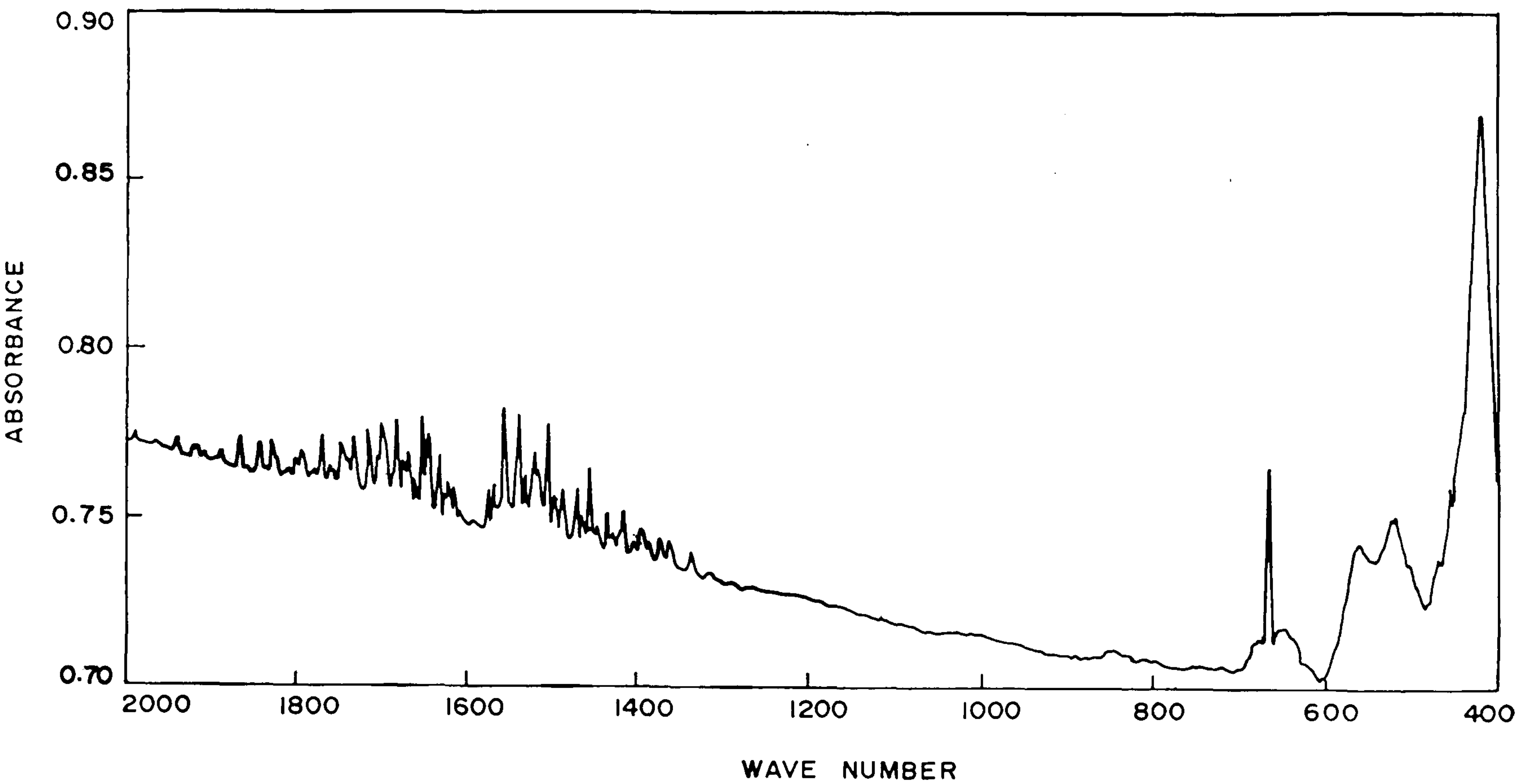

Fig.6. FTIR spectrum of a-GaAs subjected **to 2 keV hydrogen** ion treatment for 10 minutes.

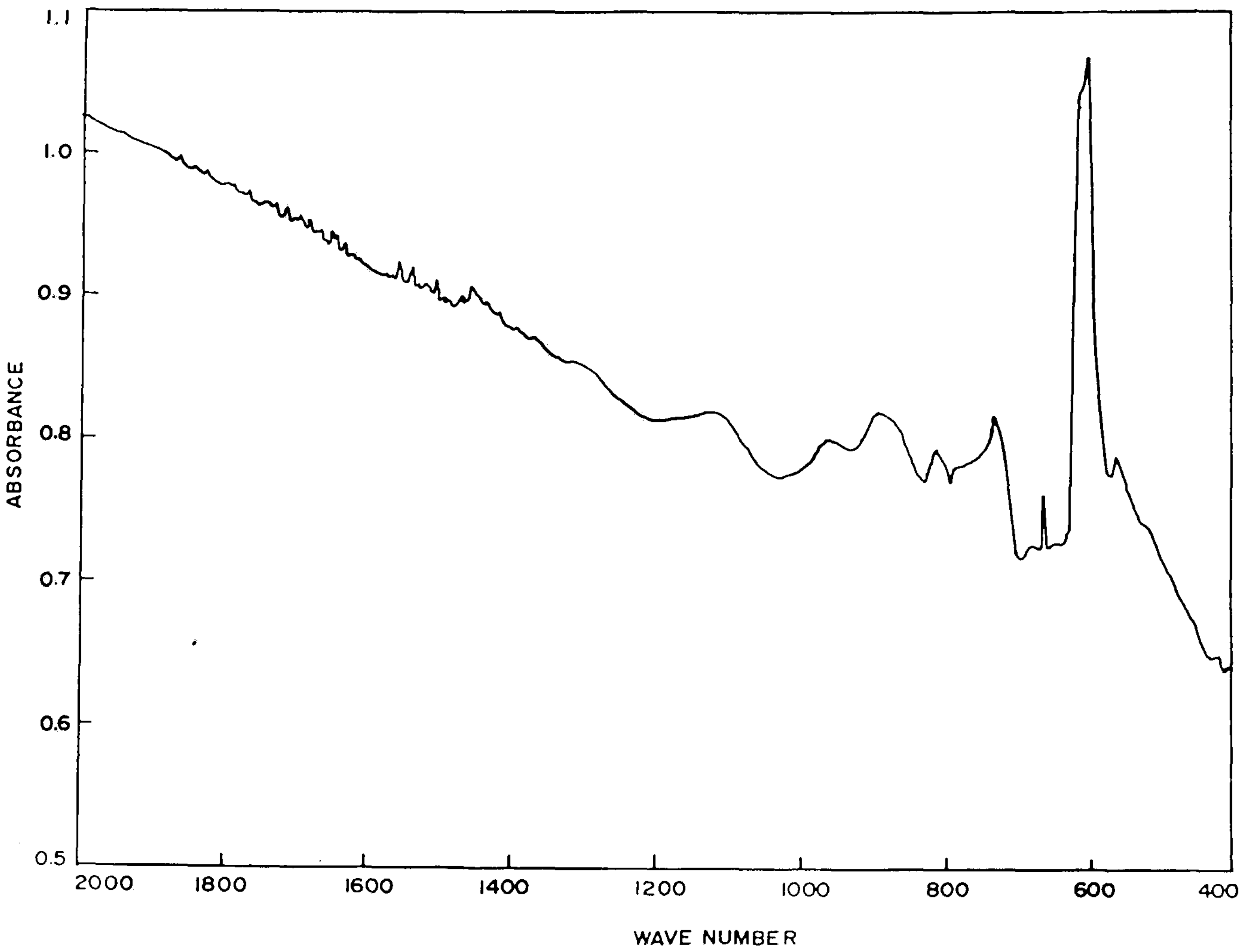

Fig. 7. FTIR spectrum of a-GaAs subjected to **2 KeV hydrogen** ion treatment with sample at 100°C.

TABLE 2 : VIBRATION MADE FREQUENCIES OF THE HYDROGEN PLASMA TREATED a-GaAs.

Wave number cm^{-1}	Mode	
510-540	Ga-H-Ga	wagging
565	Ga-H	wagging
620	As-H	wagging
700	GaH_2	Bending
840	As-H	Bending

TABLE 3 : VIBRATION MODE FREQUENCIES OF THE HYDROGEN ION BOMBARDED a-GaAs WITH SAMPLE AT 100°C

Wavenumber cm^{-1}	Mode	
570	Ga-H	wagging
610	$As-H_2$	twisting
620	As-H	wagging
700	GaH_2	Bending
980	AsH_2	Bending

peak which is due to Ga-H bridging bond disappears completely and the one at about 670 cm^{-1} becomes very weak and shows itself just as a sharp spike. The wavenumber corresponding to the stretching mode due to Ga-H-Ga bridging is reported to be around 1460 cm^{-1}. This is clearly seen in this particular case. There are some more peaks at about 900, 970, 1125 and 1300 cm^{-1} which could not be correlated to any known species. These appear only in this particular case of hydrogen ion bombardment. These could be due to species formed because of the sample heating and at the moment we have no concrete evidence to draw any definite conclusions about them.

CONCLUSIONS :

Our results indicate that the procedure we have standardised and adapted for deposition of gallium arsenide gave us amorphous films which crystallised into a polycrystalline film with no preferred direction when annealed in vacuum at about 300-400°C. This data is well supported by the electron diffraction patterns which show the rings becoming clearer and well defined as the crystallisation increases.The TEM pictures also corroborate with these studies.

The FTIR studies on the post hydrogen passivation of the a-GaAs films clearly show the presence of various hydrogen-gallium and hydrogen-arsenic species.

REFERENCES:

1. B. Despax, K. Aguir and Y. Segui
Thin Solid Films, **145**, 233 (1986).

2. W. Paul, T.O. Moustakas, D.A. Anderson and P. Freeman
Proc. 7th Int. Conf. on Amorphous semiconductors Edinburgh, p.426, (1977).

3. L. Alimoussa, H. Carchano and J.P. Thomas
J. Phys. (Paris). Colloq. C4-42, 683 (1981).

4. K.L. Narsimhan and S. Guha
J. Non-Cryst. Solids, **16**, 143 (1974).

5. A. Gheorghiu and M.L. Theye
Amorphous and liquid semiconductors,
W.E. Spear (Ed.) Stevenson, Sundei, 462 (1977).

6. J.J. Hauser
Int. Conf. on the Physics of Non-Crystalline Solids, Clausthal-Zellefeld, G.H. Frischat (Ed) Trans-Tech., Aldermannsdorf p. 230, (1977).

7. V.J. Rao, Vardhireddy Manorama and S.V. Bhoraskar
Appl. Phys. Lett. **54**, 1799 (1989).

8. D.J. Olego, R. Schacter and J. Baumann
Appl. Phys. Lett., **45**, 1122 (1984).

9. L.A. Farrow, C.J. Sandroff, M.C. Tamargo
Appl. Phys. Lett., **51**, 1931 (1987).

10. E. Yablonovitch, B.J. Skromme, R.Bhat, J.P. Harbison and T.J.Gmitter,
Appl. Phys. Lett., **54**, 555 (1989).

11. L. Alimoussa, H. Carchano and J.P. Thomas
J. Phys. Paris, **10**, C4-686 (1981).

12. N. Matsumoto and K. Kumabe
Jpn. J. Appl. Phys., **19**, 1583 (1980).

13. B. Despax, K. Aguir and Y. Segui
Thin Solid Films, **145**, 210 (1986).

14. J.C. Knights and R.A. Lujan
J. Appl. Phys. **49**, 1291 (1978).

15. A. Gheorghiu and M.L. Theye
Phil. Mag. **44**, 285 (1981).

16. N.J. Shevchik and W. Paul
J. Non-Cryst. Solids **13**, 1 (1973/74).

17. D.E. Polk,
J. Non-Cryst. Solids, **5**, 365 (1971).

18. D.E. Polk and D.S. Boudreaux
Phys. Rev. Lett. **31**, 92 (1973).

19. G.A.N. Connell and R.J. Temkin
Tetrahedrally bonded amorphous semiconductors, M.H. Brodsky, S. Kirkpatrick and D. Wearie (Ed). AIP Conf. Proc. No.20 (New York) p. 192 (1974).

20. J.S. Blakemore
J. Appl. Phys.**53**, 10 (1982).

21. K.J. Chen, Z.Y. Yang, R.L. Wu
J. Non-Cryst.Solids, **77**, 1281 (1985).

22. N.J. Shevchik, J. Tejeda and M. Cardona
Phys. Rev. B. **9** 2627 (1974).

23. M. Whil, M. Cardona and J. Tauc
J. Non-Cryst. Solids, **8-10**, 172 (1972).

24. W. Prettl, N.J. Shevchik and M. Cardona
Phys. Stat. Sol. (b) **59**, 241 (1973).

25. J.S. Lannin
Tetrahedrally bonded amorphous semiconductors
M. Brodsky, S. Kirkpatrick and P. Wearie (Ed) AIP Conf. Proc. No.20, p. 260 (1974).

26. M.L. Theye, A. Gheorghiu and H. Launois
J. Phys. C 13, 6569 (1980).

27. Ph.D Thesis of Prabhat Singh, NCL Pune-411008.(Poona University)

28. H.P.Klug and L.E.Alexander
X-ray Diffraction Procedures for Polycrystalline and Amorphous Materials, p.491. John Wiley, New York; Chapman and Hall, London.

29. Z.P. Wang, L. Ley and M. Cordona
Phys. Rev. B, 26, 3249 (1982).

30. B.K. Ghosh, B.K. Agarwal
J. Phys. C. Solid State Phys., 19, 7157 (1986).

31. R. Fisch, D.C. Licciardello
Phys. Rev. Lett. 41, 889 (1978).

Appendix

Thermally Stimulated Exoelectron Emission

This part of the thesis deals with the setting up of a simple experimental facility to study the surface and near surface defects in solids by the technique of Thermally Stimulated Exo-Electron Emission (TSEE). Exo-emission is a fairly new phenomenon which involves the emission of electrons from surface defects. The method is not fully explored and needs further investigation, for application to solve the real problems. In the context of the surface states in semiconductors and specially in the present context of pinned surfaces of GaAs, it may serve as a supplementary tool. Since experimental results on GaAs are not reported here, the work on TSEE is added to the thesis as an appendix.

INTRODUCTION:

Not long ago it was found that not only photons but also low energy electrons are emitted in the process of irradiation and subsequent thermal stimulation as in Thermoluminescence (TL). This phenomenon is known as Thermally Stimulated Exoelectron Emission (TSEE). The curve obtained of the electron emission intensity as a function of sample temperature is referred to as the TSEE spectrum. In the thermodynamic sense exo-electron emission is a result of relaxation of various perturbations applied to the material. There have been quite a few reports in recent times, on studies of TSEE on different systems like metal oxides [1], metallic glasses [2,3], abraded surfaces [4-7], gases adsorbed on clean metal surfaces [8] etc. TSEE especially from alkali halides is being extensively studied as it provides a prototype for research in understanding the exact mechanism of exoelectron emission. Alkali halides have been well studied by techniques like thermoluminescence, thermally stimulated

conduction, temperature dependence of absorption and electron spin resonance, whereas, in comparison TSEE is not so well studied.

The intensity of the exoemission peak gives information about the defect concentration, whereas the kinetic energy of the emitted electrons tells us about the energy gained in the process of its liberation from the trap. The delocalisation of electrons from traps during thermally stimulated emission is a multiphonon process. Exoelectron energy measurements become complicated due to the strong electron phonon interaction and the transport conditions to the surface, and hence it is difficult to gather information directly about the energies of the electrons delocalised from traps. Electron energies are also strongly dependent upon electric fields in the surface layer of the solid. They vary during electron emission measurement with respect to time and position. Thus it is difficult to determine the energy distribution of the emitted electrons. Especially, exoelectron emission from alkali halides is known to be influenced by many factors, such as irradiation conditions, perturbation of the sample and existance of impurities.

Section Al of this chapter reports the results of the prototype TSEE experiments on γ-irradiated alkali halides. Alkali halides are chosen, since the defects in them are well studied by other techniques.

The determination of the kinetic energy of the emitted exoelectrons from these γ-irradiated alkali halides, KBr and LiF, using a 127° cylindrical deflector analyser is discussed in section A2.

A1: TSEE FROM - IRRADIATED ALKALI HALIDIES.

A1.1 EXPERIMENTAL DETAILS:

A1.1.1 Experimental setup:

The schematic of the experimental setup used for measuring the TSEE intensity is as shown in Fig.1. It mainly consists of a Channel Electron Multiplier (CEM) (Model : Galileo 4700) used as a detector and also for amplifying the exoemission intensity. A sample holder was fabricated with an inbuilt arrangement for heating the sample and a thermocouple for temperature monitoring. The CEM is operated in the pulsed mode and the amplified signal is fed to a charge sensitive preamplifier. (Model: AMP-TEK 225-206) whose output is measured in terms of counts on a frequency meter or a ratemeter. The CEM and the sample holder are mounted on two opposite flanges in a cylindrical stainless steel chamber. The arrangement is such that the specimen placed on the sample holder comes very close to the front electrode of the CEM. The whole assembly is evacuated to a pressure of about 10^{-6} Torr using a diffusion backed by rotary vacuum pump. The sample temperature was raised at a constant rate of about 0.015^{o}/Sec. using a resistive heater.

A1.1.2 : Samples:

The samples of single crystal KBr and LiF were chosen as the specimens for our experiments. These samples were initially heated to about 350°C in vacuum to get rid of the adsorbed impurities and water vapour, which are known to greatly influence the TSEE spectr um. These samples were then subjected to γ-irradiation in a ^{60}Co source with a dose rate of 4.79×10^{3} rad/min. The irradiation was carried out at room temperature. After irradiation the samples were mounted on the sample holder and the TL and TSEE experiments were independently

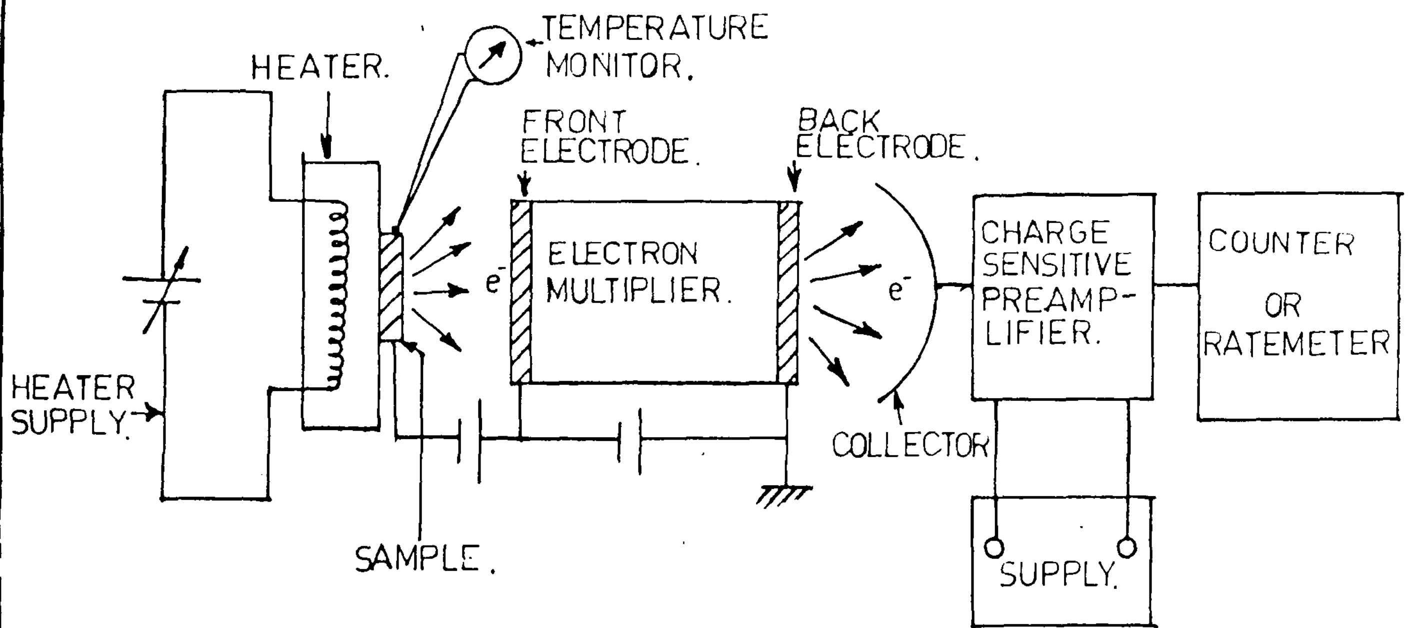

Fig.1. Schematic of the experimental setup used for measuring the TSEE intensity.

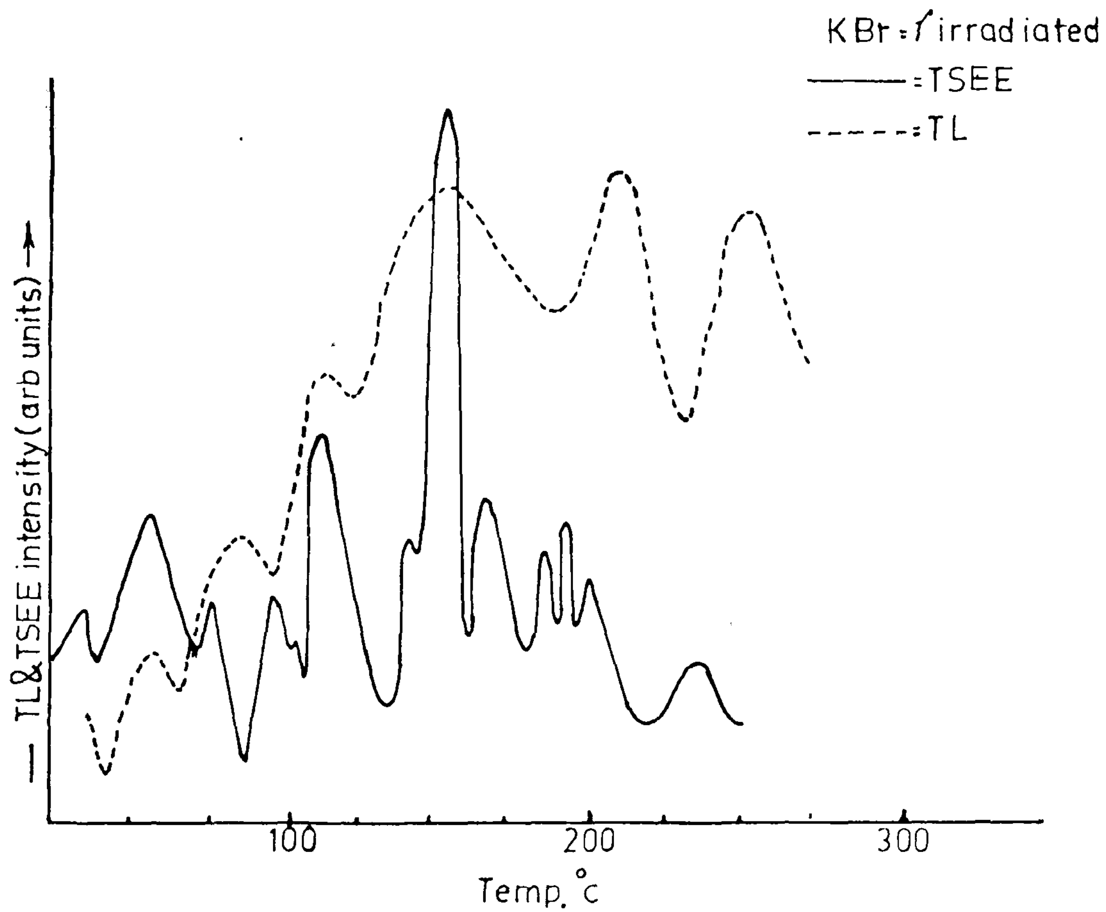

Fig.2. TL and TSEE spectra of γ- irradiated KBr.

performed.

A.1.1.3 : Experimental Procedure:

In the first part of the experimentation both TL and TSEE intensities were meaasured from room temperature to 300°C in the sample of KBr subjected to a dose of 6×10^6 rads of γ-irradation. The TL studies were performed at atmospheric pressure using the same arrangement as described for TSEE measurements except for the Photo-Multiplier Tube (PMT) instead of the CEM. In the second part of our experimentation single crystals of LiF were subjected to γ-irradiation of different doses and the TSEE studies were performed to study the effect of dose on the TSEE peak position and intensity. The same sample was also subjected to a pretreatment of annealing at 400°C before being exposed to the γ-irradiation and its effect on the TSEE spectrum was also studied.

A1.2 Results:

Figure 2 shows the TL and TSEE spectra of γ-irradiated KBr. The TL spectrum clearly shows that the noise level continuously increases as the sample temperature is raised. This is because, as already mentioned, the TL experiments were performed at atmospheric pressure conditions. This is not observed in the TSEE spectra as the experiments were performed under high vacuum conditions. This distinction in the experimental conditions was because of inadequate experimental facilities. The spectra clearly indicate that there are peaks around 35°C, 55.5°C, 110.5°C and 153°C which are common to both the spectra. The TL spectrum also shows peaks at 85°C, 200°C, 260°C and the TSEE at 190°C, 240°C. There is also a downward going peak at 85°C in the TSEE spectrum. The peak at about 153°C is the major one in both the spectra. This peak in the TL spectrum is quite broad and

probably encloses one or two smaller peaks around it.

Figure 3 gives the TSEE spectra of single crystal LiF exposed to γ-rays of different doses (9×10^5 rad, 18×10^5 rad, 52×10^5 rad). It shows that as the dose of irradiation is increased the peak appearing at 100°C increases in intensity and the one at about 200°C diminishes. There are a few more peaks which do not show any consistent effect.

Figure 4 shows the effect of pretreatment on the TSEE of irradiated LiF single crystal. It is clearly seen that if the sample of LiF is heated at 400°C for 1 hour and then irradiated, the 100°C peak increases in intensity and the 200°C peak disappears totally.

A1.3 Discussion:

As seen in Fig.2 the TSEE spectrum of γ-irradiated KBr shows more peaks as compared to the TL spectrum. This suggests the creation of more defects on the surface than in the bulk, because, it is well known that the TL is predominantly a bulk phenomenon and the TSEE a surface sensitive effect. It could also be that there are defects created by the irradiation for which only TSEE is sensitive and which are not detected by TL. This is valid, because the mechanism of exoelectron emission and luminescence are not the same.

Earlier work [9] on TL of γ-irradiated KBr showed two peaks at 57°C and 152°C. The present 55.5°C and 153°C peaks presumbly correspond to the above two. The second peak is known to appear only for larger irradiation doses as suggested by Murti et al. [10]. As expected, in our studies also, this 153°C peak appears most predominantly in both the TSEE and TL spectra, because our sample was subjected to a dose of 7×10^5 rad of γ-irradiation which is quite high.

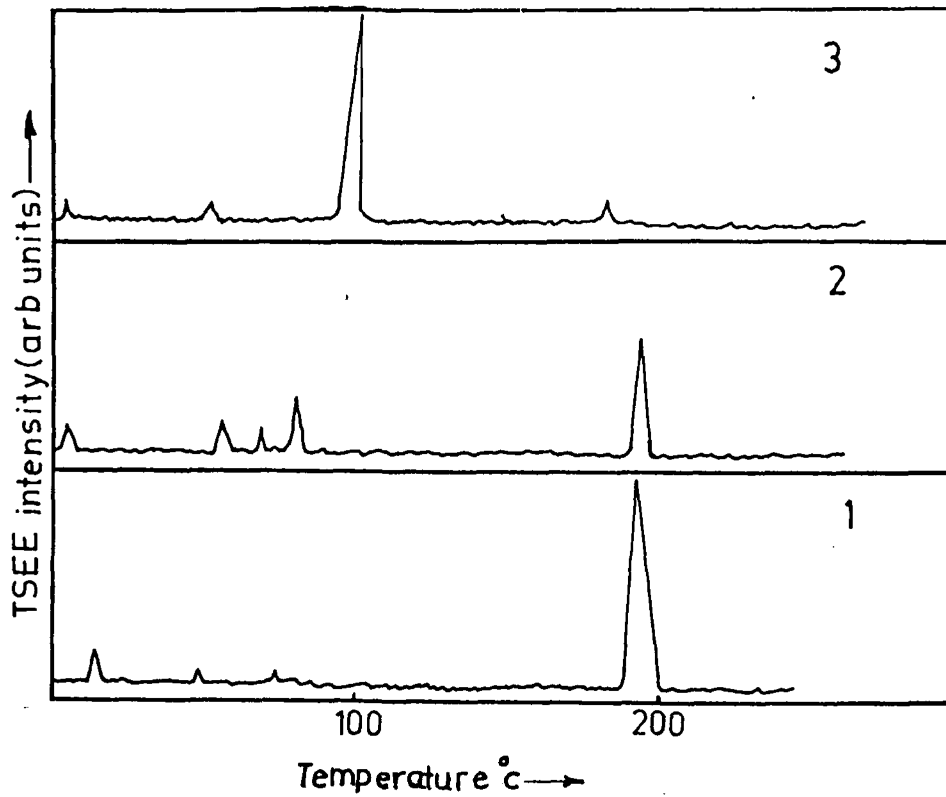

Fig.3. TSEE spectra of single crystal LiF exposed to rays for different doses. (1) 9 x 10^5; (2) 18 x 10^5; (3) 52 x 10^5.

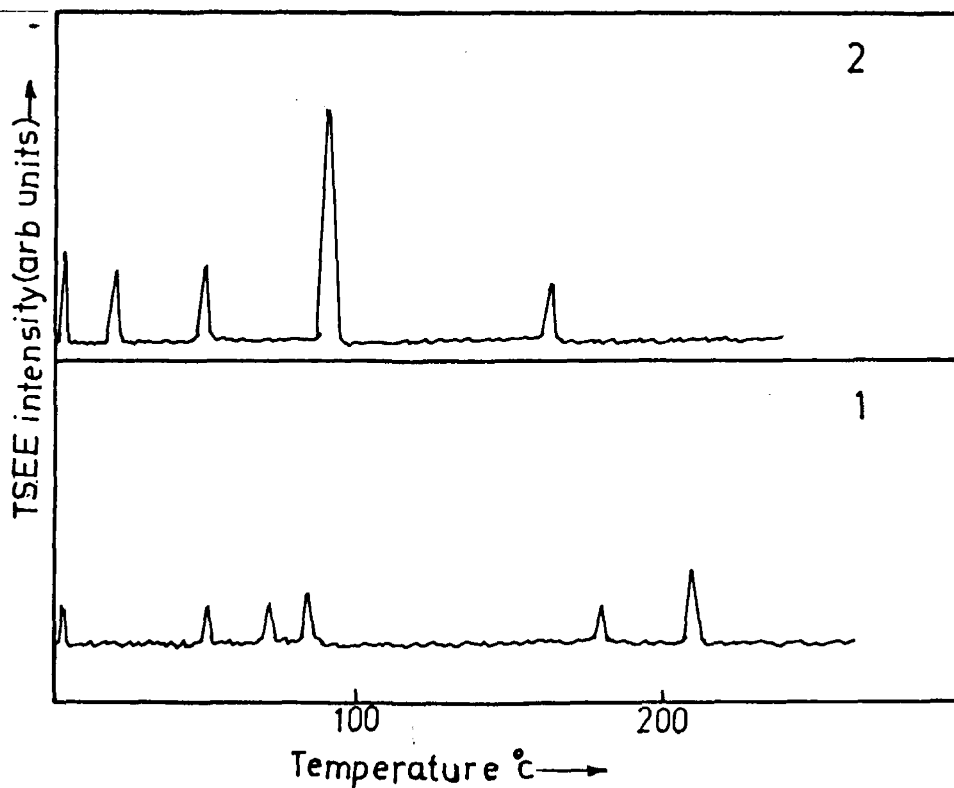

Fig.4. TSEE spectra of single crystal LiF.
(1) γ- irradiated; (2) heated at 400°C for one hour and γ- irradiated.

The 85°C and 153°C peaks [10,11] in both the TL and TSEE spectra correspond to the 90°C and 150°C peaks already observed in case of TL of irradiated KBr.The authors attributed these glow peaks to the first and second stage F centres respectively following the work of Jain and Mahendru [12] on KCl. The 85°C peak in the TL spectrum consistently appeared as a negative going peak in the TSEE spectrum suggesting that the noise level of the detecting system is decreasing below its average value. This can be possible if some positive species are liberated from the sample surface at this temperature. Any definite conclusion would require further experimentation. The TSEE peaks which have no counterpart in the TL spectrum may be attributed to the surface imperfections present in the crystal which fall below the detection level of TL.

The effect of dose of irradiation and pretreatment on the TSEE has been studied and from Fig.3 it is clear that the increase in dose has the effect of increasing the 100°C peak and simultaneously reducing the 200°C peak intensity. This suggests that the defect density corresponding to the 200°C peak is decreasing and that corresponding to 100°C increasing. This may possibly be related to the rearrangement of defects corresponding to these two peaks. There are a few more sharp peaks appearing in the low temperature region which do not show any consistent change with the irradiation dose. These may be due to some unintentionally present impurities in the sample.

Figure 4 shows that annealing at 400°C for one hour prior to the irradiation has the effect of enhancing the 100°C peak relative to the 200°C peak. The 400°C annealing restores a previously irradiated sample to its pre irradiation state, allowing repeated use of the same sample.Similar work [13] on the correlation of TSEE and TL of X-

irradiated LiF showed a similar spectrum. All their samples underwent the 400°C annealing treatment. Their TL spectrum above 0°C was composed of five very weak peaks or shoulders while the TSEE glow curve showed a relatively intense peak near 100°C, a weak peak near 200°C and an abrupt rise above 250°C.

According to Gordon and Scharmann [14] the TSEE peak in LiF at 100°C is caused by surface centres such as adsorbed atmospheric constituents or surface lattice imperfections. Our results show that this peak is mainly related probably not to adsorbed atmospheric constituents but to some surface lattice imperfections. This is because these surface imperfections increase as the dose is increased which is clearly seen in Fig.3 by the increase in the 100°C peak intensity with the dose of irradiation. The peak at 200°C may be attributed completely to the presence of surface impurities or adsorbed atmospheric constituents, because this 200°C peak disappears completely by the 400°C annealing treatment prior to the irradiation. This 200°C peak is also observed to be strong only in the unannealed sample exposed to a low dose of irradiation (9×10^5 rad) as shown in Fig.3. Holzapfel [15] observed TSEE peaks in Ar^+ ion bombarded LiF at about 190-200°C which vanished on reheating which he attributed to surface centres. He proposed that these are due to the presence of adsorbed layers, whose nature he could not identify. From all these observations it can be positively concluded that in case of LiF the surface lattice imperfections are reflected in the 100°C peak and the surface adsorbed constituents are seen by the 200°C peak.

A2 : ENERGY ANALYSIS OF THE THERMALLY STIMULATED EXOEELCTRONS USING A 127° CDA:

During the last decade the phenomenon of exoelectron emission has been widely studied. It has proved to be a powerful tool in the study of the defects created by various ionising radiations in alkali halides [13-16], phase changes in metallic glasses [3], fracture and fatigue in metals [8,17], etc. However there has not been adequate work on the energy analysis of the exoelectrons. Although several attractive models for exoelectron emission have been proposed, none of these seems to have been clearly explained. With a view to provide necessary data, the present work on TSEE of single crystals of LiF and KBr was carried out. The TSEE spectrum provides valuable information regarding the nature of the trap sites induced dur to perturbation. These trap sites appear to be a characteristic of the nature of the perturbation and of the surface. While the exoemission peak energy gives the trap depth and the intensity of the same measures its concentration. The energy of the emitted electrons is just the energy gained in the process of their liberation from the trap. The delocalisation of electrons from the traps during their stimulated emission is a multiphonon process. Exoelectron energy measurements become complicated due to the strong electron phonon interaction which in the main controls the mechanism of the transport of the trapped electron to the surface.

The resulting electron energies are strongly dependent upon the electric fields operating in the surface layer of the solid substrate. They vary with position and probably with aging. Thus it is difficult to determine the real energy distribution of the emitted electrons. Exoelectron emission from irradiated alkali halide crystals is known

to be affected by additional factors, such as energy and dose rate of the irradiation used to cause the initial perturbation in the sample, and the presence of impurities [18]. We present here results of our determination of the kinetic energy of the thermally stimulated exoelectrons from γ-irradiated lithium fluoride and potassium bromide crystals using a 127° Cylindrical Deflection Analyser (CDA).

Electrostatic energy analysers for charged particles have been widely used in both electron and ion spectroscopy in surface sciences. Especially the cylindrical deflector analyser has been found to be best suited in high resolution electron loss spectroscopy (EELS). The production or acceptance of a beam with rectangular cross section is well adapted for the present experiment, where a larger sample area can be covered by the entrance slit. Moreover its simple geometry makes its construction easier and its alignment less critical.

A2.1 Experimental details:

The 127° CDA with a mean radius of 6.5 cm was designed and built on the lines proposed by Oshima et al [19] and gave a resolution of 0.8%. Single crystals of LiF and KBr were cleaved, chemically polished, dried and annealed to remove memory effects due to any residual trapping of defect centres. The exoemission peak positions were first determined as explained in the previous section, before carrying out the energy analysis with the CDA. The schematic of the experimental setup used for the energy analysis of the TSEE peaks is shown in Fig. 5 The basic calibration equation which relates the pass energy E_0 to the potential difference ΔV between the 127° cylindrical electrodes of the CDA is

$$E_0 = (e\ \Delta V/2)\ (\ln R_2/R_1)$$

where R_2 and R_1 are the radii of the outer and inner electrodes

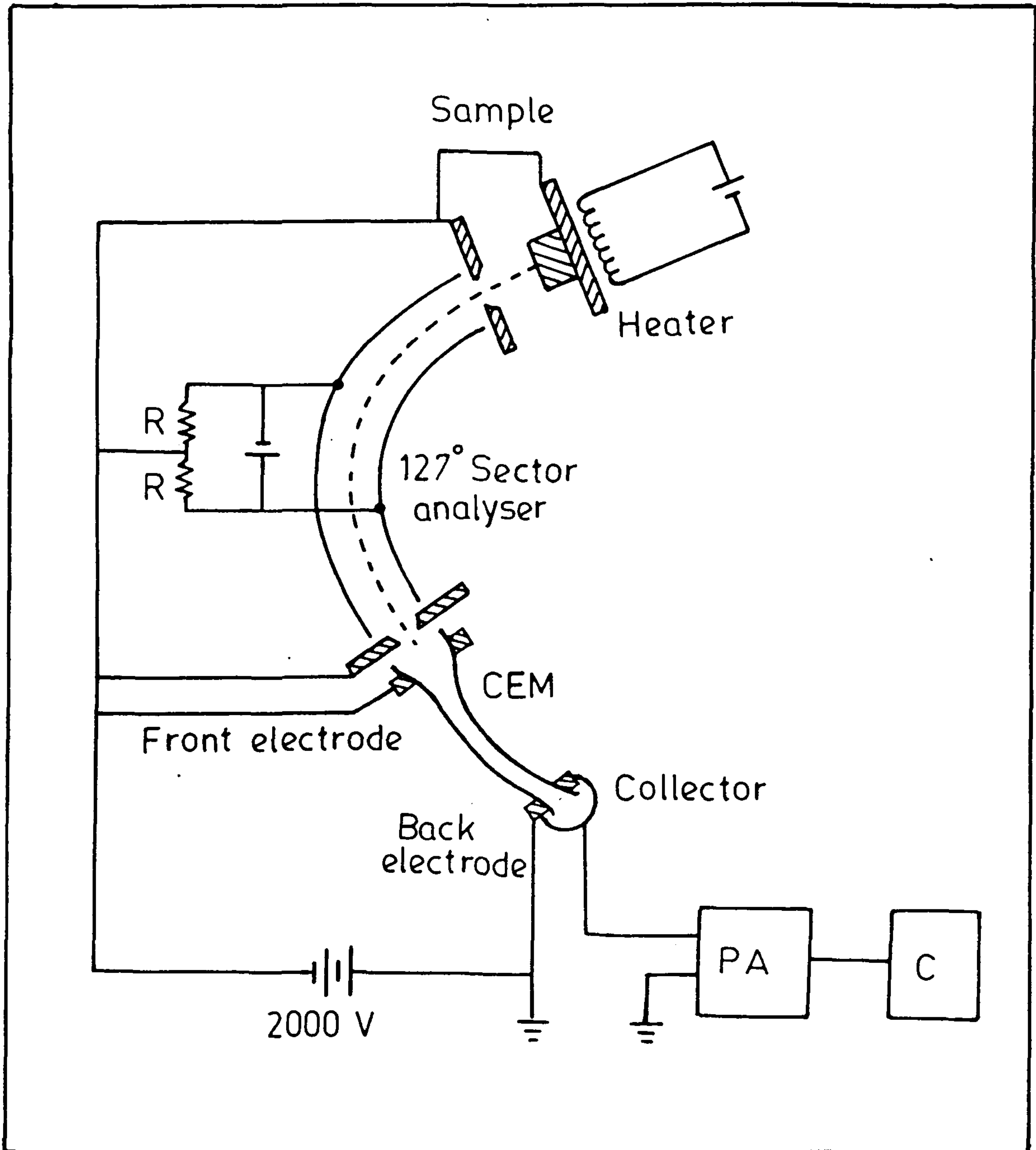

Fig.5. Schematic of the experimental setup used for the energy analysis of the TSEE peaks.

respectively and e is the electronic charge. In the present case R_2 was 7 cm and R_1 6 cm giving

$$E_o = 3.24 \quad e\,\Delta V. \qquad (2)$$

An accurate experimental calibration of the CDA was carried out before using the same for analysing the TSEE spectrum.

The energy analysis experiment consisted of maintaining the sample at a particular temperature as determined in the previous section and then applying a ramp voltage between the cylindrical electrodes of the CDA as shown in Fig. 5 and measuring the counts on the ratemeter.

RESULTS AND DISCUSSIONS:

The spectra showing the energy distribution of exoelectrons for LiF at 163° and for KBr at 150°C are shown in Figs. 2 and 3 respectively. Following were the dominant peaks for LiF and KBr.

Crystal	TSEE peak position/°C	Energy of EE/eV
LiF	163	1.8, 2.9
KBr	150	3.5

The reproducibility of the energy distribution was confirmed by repeated experiments of similar kind, carried out with each crystal. The emission intensity for KBr crystal was always about 2 to 2.5 times the intensity of the LiF emission.

Although some energy analysis of the exoelectron emission have been reported on alkali halides, no satisfactory mechanism has been advanced to explain the observed high energy (of about 3 eV) of the exoelectrons. Earlier workers (Drenckhan et al 1970, [20]), have tried to explain the emission of the high energy exoelectrons as due to (i) Auger emission (ii) Local space charge and (iii) High energy radiation recombinations.

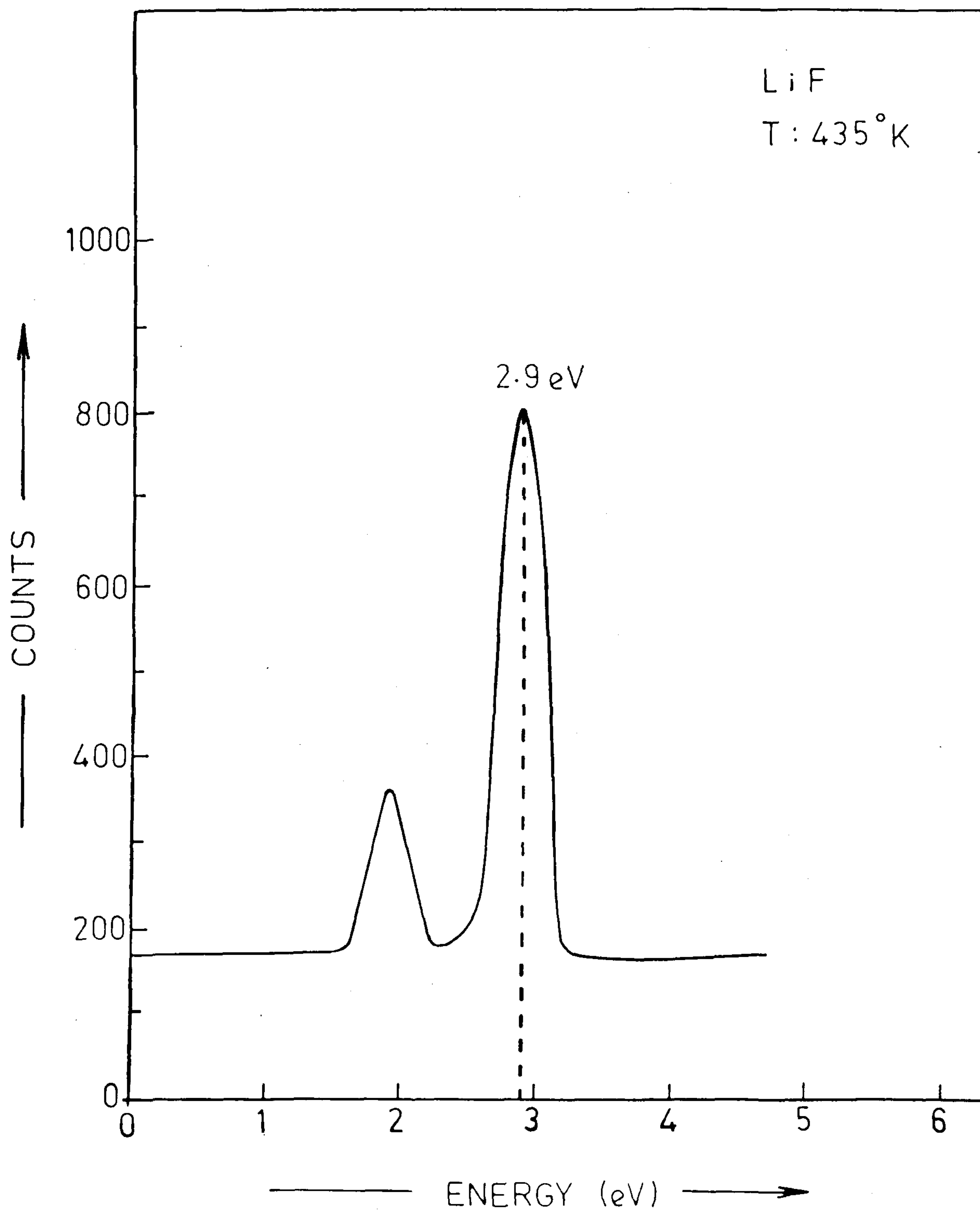

Fig.6. Energy distribution of exoelectrons for LiF at 163°C.

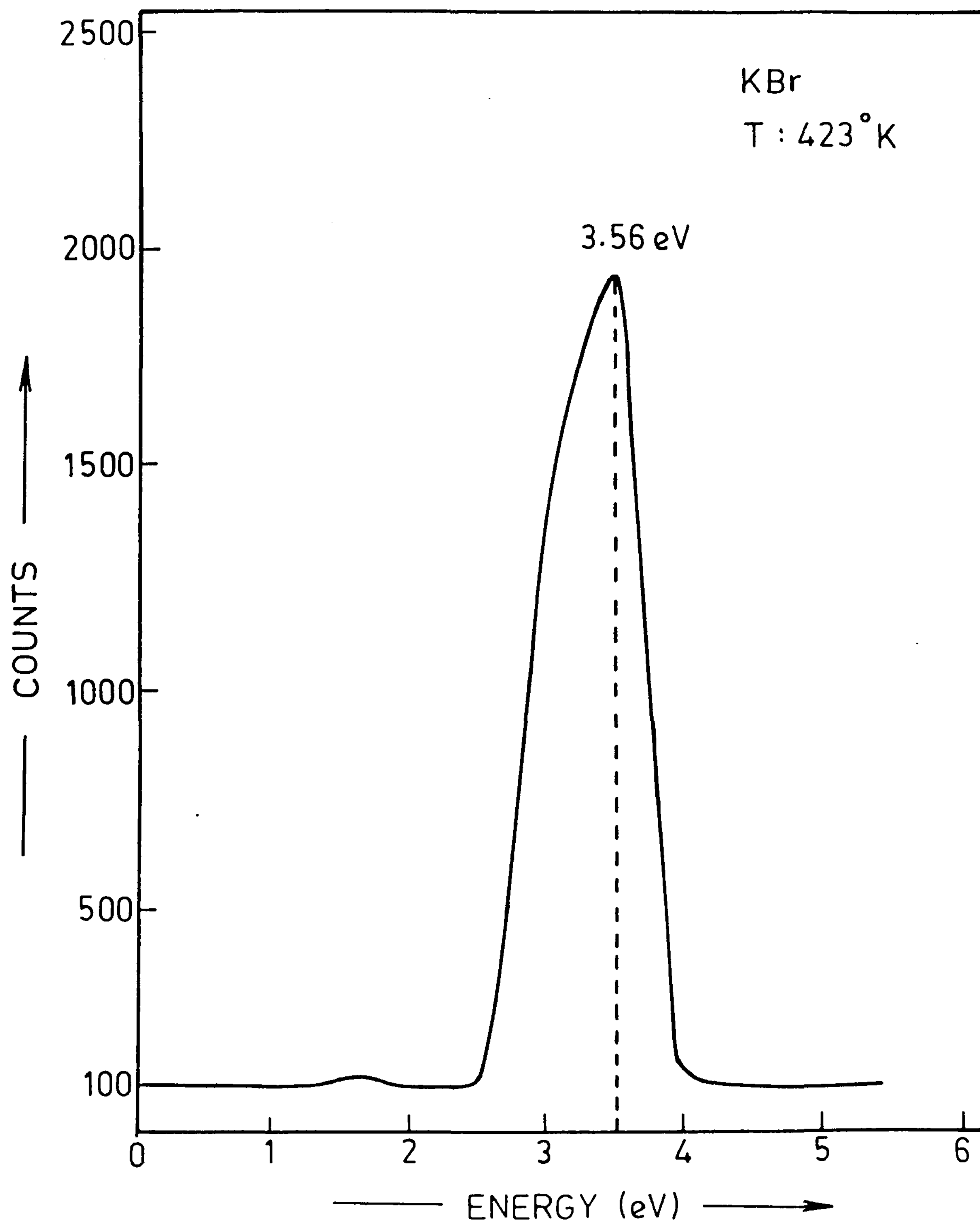

Fig.7. Energy distribution of exoelectrons for KBr at $150^{o}C$.

The data available do not permit us to make a clear choice between these alternative mechanisms, but we are proposing the following as a probable explanation of the above observations in γ-irradiated alkali halides.

The irradiation of the alkali halides with γ-rays results in the formation of some free electrons and holes. A fraction of these electrons get trapped at appropriate vacancy sites giving rise to F centres. These centres have a large cross section for the capture of an additional electron to form F^- centre (Mathison et al 1989, [21]).

When thermally activated some of the trapped electrons are delocalized, they drift in the conduction band from where they de-excite to an intermediate energy level and subsequently recombine with holes or are recaptured at F centres radiatively. The energy released in this process can only be around 3-4 eV appropriate for the release of the exoelectrons from the perturbed surface .An alternative mechanism involves,

1. The formation of interstitials as X, and X_2^- in the room temperature irradiated alkali halides (Crawford 1968, [22]). Their concentrations have been reported to be as high as 0.1 to 0.6 times the vacancy pairs created initially during irradiation (Hacskaylo et al 1953, [23]). This phenomenon can be thought of as similar to internal photoemission.

$$X^- \text{ (lattice)} \xrightarrow{h\nu} X + e^- \qquad (3)$$

The electron drifts in the conduction band and later is captured in an anion vacancy to form an F centre which imparts colour to the crystal.

2. A fraction of trapped electrons, given by the Boltzmann's distribution are assumed to have sufficient energy to overcome the barrier and react with X giving

$$\cdot X + e^- \longrightarrow (X^-)^* \qquad (4)$$

3. The excited species deexcite by emitting thermoluminescence

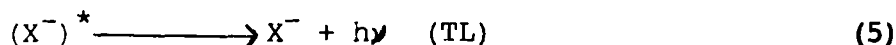

$$(X^-)^* \longrightarrow X^- + h\nu \quad (TL) \qquad (5)$$

4. Alternatively, or in addition, one of the $\cdot X$ produced in the process (3) slips into an interstitial position and combines with a lattice ion forming $\cdot X_2^-$.

$$\cdot X + X^- \longrightarrow \cdot X_2^- \qquad (6)$$

Such a specie is known to be in a metastable state. On warming upto around 200°C the metastable species breaks by the emission of an exoelectron leaving behind the species like $\cdot X .. X \cdot$

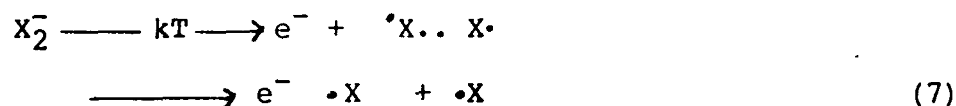

$$X_2^- \text{ --- } kT \longrightarrow e^- + \cdot X .. X \cdot$$
$$\longrightarrow e^- \ \cdot X + \cdot X \qquad (7)$$

Evidence for the presence of free chlorine atoms is provided by the observed characteristic special chemical reactivity (Hacskaylo et al 1953), for example the reaction with o-tolidine.

CONCLUSIONS:

Emission of exoelectrons was observed from γ-irradiated single crystals of KBr and LiF on thermal stimulation over the temperature range of 100-200° C. The energies of the TSEE peaks were measured with a CDA, and were found to be in the range of 2 to 4 eV. Alternative mechanisms have been suggested to explain the relatively large energy of the emitted electrons.

REFERENCES:

1. R.Huzimura, S.Miyagawa, Y.Ato, M.Kawanishi
Jap. J. Appl. Phys. **24**, 53 (1985).

2. B. Sujak, M. Dus-sitek, Y. Olszewski, B. Wyslocki
Jap. J. Appl. Phys. **24**, 122 (1985).

3. T. Gorecki, C. Gorecki
Jap. J. Appl. Phys. **24**, 27 (1985).

4. H. Shigekawa, Y. Fujiwara
Jap. J. Appl. Phys. **21**, 1279 (1982).

5. H. Shigekawa, S. Hyodo
Jap. J. Appl. Phys. **22** , 42, 1493, 1627 (1983).

6. H. Shigekawa, S. Hyodo
Jap. J. Appl. Phys. **23** 1146 (1984).

7. H. Shigekawa, Y. Fujiwara, Y. Ando, A. Kumagai, S. Hyodo
Jap. J. Appl. Phys. **24**, 122 (1985). .

8. J.A. Ramsey
Jap. J. Appl. Phys. **24**, 32 (1985).

9. L.F. Heckelsberg, F. Daniels
J. Phys. Chem. **61**, 414 (1959).

10. Y.V.G.S. Murti, K.R.N. Murthy, C. Ramasastry
J. Phys. C: Solid Phys. **4**, 1606 (1971).

11. P.C. Mahendru and S. Radhakrishna
J. Phys. C: Solid State Phys. **2**, 796 (1969).

12. S.C. Jain, P.C. Mahendru
Phys. Rev. **140** A, 957 (1965).

13. A. Tomita, N. Hirai, K. Tsutsumi
Jap. J. Appl. Phys. **15**, 1899 (1976).

14. Garden, Scharmann
Z. Phys. **217**, 309 (1968).

15. G. Holzapfel, Z. Engew
Phys. **29**, 107 (1970).

16. N.I. Konyushikina, I.V. Krylova, V.N. Opekunou, A.A.Predvoditelev
Phys. Stat. Sol. (a), **43**, 639 (1977).

17. I. Oshima, Y. Momose, K. Kawafune
Jap. J. Appl. Phys. **24**, 190 (1985).

18. M. Kamada, K. Tsutsumi
Jap. J. Appl. Phys. **24**, 15 (1985).

19. C. Oshima, R. Sauda, M. Aono, Y. Ishizawa
Rev.Sci. Instrum. **56**, 227 (1985).

20. J. Drenckhan, H. Gross, H. Glafeke
Phy. Stat. Sol. (a) **2**, K51 (1970).

21. J.P. Mathison, S.C. Langford, J.T. Dickinson
J. Appl. Phys. **65**, 1923 (1989).

22. J.H. Crawford (Jr)
Adv. Phys. **17**, 93 (1968).

23. M. Kacskaylo, D. Otterson, P. Schwed
J. Chem. Phys. **21**, 1434 (1953).

APPENDIX II

TABLE GIVING THE NAMES OF THE INSTRUMENTS USED IN THE THESIS

Sr.No.	Purpose	Name and make
1.	I-V Characteristic	Tecktronix
2.	C-V characteristics	Lock-in-Amplifier EG and G 5204
3.	Low angle X-ray Diffraction	Rigaku
4.	Transmission Electron Microscopy	TEM - JEOL TOKYO, JAPAN
5.	Infra red spectra	FTIR Nicolet 60 SXB
6.	SEM-EBIC for diffusion length and SRV.	Cambridge model 9000
7.	X-ray photoelectron spectroscopy (XPS)	V.G. Scientific ESCA MK-II system
8.	X-ray fluorescence Analysis for stoichiometry.	
9.	Talley's step measurement for thickness determination.	

CONCLUDING REMARKS AND SCOPE FOR FURTHER WORK :

The work encompassed in the thesis was started with the aim of finding a suitable solution to the GaAs surface passivation. Having embarked on this study we tried several candidate materials with a fair amount of success.

Our attempt to passivate the GaAs surface by a polymer deposited by the technique of plasma polymerisation is the first venture of its kind. This polythiophene/GaAs system has been completely characterised and it has been proved to be a sufficiently good passivating element. Our next aim is to use this polythiophene as the insulation in Metal Insulator Semiconductor (MIS) configuration. We are now developing procedures necessary to develop MIS-FETs using this polymer. We could also see the possibility of using the ion implantation and ion beam mixing techniques for making the channel in the MIS-FET.

The growth of ZnSe on GaAs by the technique described above and the study of its surface and interfacial properties has been undertaken for the first time. We have studied this system in all aspects and arrived at some fascinating results. We have studied the ZnSe/GaAs system as a prototype of the II-VI/III-V heterostructure. Our technique of deposition gave us very good stoichiometric films of ZnSe. By similar method and other improvements we are now going into the field of ZnS_xSe_{1-x}/GaAs which is more lattice matched than ZnSe/GaAs system. The exact percentage composition of S and Se in the film has to be critically controlled.

We have also attempted hydrogen passivation of a-GaAs deposited by flash evaporation. This was on the lines of hydrogenated amorphous silicon, a-Si:H. We could explore the possibilities of using a-GaAs:H

taking hints from all the studies already done and now well established in a-Si:H technology. Although this part of investigation was not extended further by us, our studies may find base for the future development in microelectronics.

Finally, the technique of thermally stimulated exoelectron emission to study defects in solids can be applied to the study of defects in GaAs as well.

LIST OF PUBLICATIONS

1. Passivation of pinned n-GaAs surfaces by plasma polymerised thin films.
   V.J.Rao, Vardhireddy Manorama, S.V.Bhoraskar,
   Appl.Phys.Lett. **54**, 1799 (1989).

2. Interfacial properties of n-GaAs and polymer deposited by plasma CVD.
   Vardhireddy Manorama, S.V.Bhoraskar, V.J.Rao, S.T.Kshirasagar.
   Appl.Phys.Lett. **55**, 1641 (1989).

3. Nearly ideal interfacial properties of organic sulphide coated n-GaAs surfaces.
   V.J.Rao, Vardhireddy Manorama, S.V.Bhoraskar.
   Presented at the International conference on Semiconductor Materials (ICITC), New Delhi, December 1988.

4. Ion beam mixing at S/GaAs interface : An ESCA study
   Vardhireddy Manorama,, A.P.Malshe, S.V.Bhoraskar, V.J.Rao, S.Badrinarayan and A.B.Mandale.

5. Hydrogen passivation of amorphous gallium arsenide films deposited by flash evaporation
   Vardhireddy Manorama, S.V.Bhoraskar, V.J.Rao.
   Paper communicated to Journal of Applied Physics

6. Defect studies by TSEE in γ-irradiated alkali halides
   Vardhireddy Manorama, S.V. Bhoraskar
   Paper presented at the 2nd National Seminar on defects in insulating solids, IIT Madras, February (1988).

7. Energy measurement of thermally stimulated exoelectrons using a 127° cylindrical deflector analyser.
Vardhireddy Manorama, S.K. Pawar and S.V. Bhoraskar
Paper communicated to Journal of Physics D : Applied Physics.

8. EBIC measurements on amorphous and crystalline silicon
Vardhireddy Manorama
Presented at the 4th Annual Seminar for Research students, University of Poona, February, 1988.

9. Effect of reduction of PLZT on carrier lifetime determined by EBIC
J.C. Maurya, A.V. Dixit, Vardhireddy Manorama, S.V. Bhoraskar
Solid State Communications, Vol. 64, No.9 (1987) p. 1235.

.0. Chemical and Electronic Structure of ZnSe/GaAs Heterointerfaces
V.J.Rao,S.Badrinarayan,S.D.Sathaye,A.B.Mandale,G.N.Chaudhari, Prabhat Singh,Vardhireddy Manorama,R.S.Bhide,S.V.Bhoraskar
Paper presented at Third National Seminar on X-ray spectroscopy and allied areas Oct. 1989. Regional Engineering College, Srinagar,Kashmir.